Radiometric dating ($^{40}Ar/^{39}Ar$ and ^{14}C), compositions, and erupted volumes of volcanoes of the Valle de Santiago area (Michoacán-Guanajuato Volcanic Field, Mexico)

Elizabeth Rangel-Granados*[,1], Claus Siebe[1], Juan Enrique Suárez-Jiménez[2], Mélida Pilar Schliz-Antequera[1], Nanci Reyes-Guzmán[3], Marie-Noëlle Guilbaud[1], Sergio Salinas[4], Daniel Paul Miggins[5]

[1]Departamento de Vulcanología, Instituto de Geofísica, Universidad Nacional Autónoma de México, Ciudad Universitaria, Coyoacán 04510, CDMX, México.

[2]Servicio Geológico Colombiano, Diagonal 53, Nº 34-53, Bogotá, D.C., Colombia.

[3]Department of Geology and Environmental Earth Science, Miami University, Oxford Ohio, 45056, USA.

[4]Colegio de Geografía, Facultad de Filosofía y Letras, SUAyED, Universidad Nacional Autónoma de México, Ciudad Universitaria, Coyoacán 04510, CDMX, México.

[5]College of Earth, Ocean, and Atmospheric Sciences, Oregon State University, Corvallis, OR 97331-5503, USA.

*Corresponding author: *elizrangel@gmail.com* Twitter: @elizabethrangel61

June 24, 2024

ABSTRACT

The Valle de Santiago (VS) area is located in the Michoacán-Guanajuato Volcanic Field (MGVF), within the Trans-Mexican Volcanic Belt (TMVB). Based on geological mapping of a ~2,800 km^2 quadrangle, $^{40}Ar/^{39}Ar$ and radiocarbon dating, morphometry, and whole-rock chemical and petrographic analyses of the volcanic products, we established the stratigraphy and eruptive history of the VS area. A total of 118 volcanic landforms was identified, including 61 scoria/spatter cones, 21 phreatomagmatic volcanoes, 20 medium-sized shield volcanoes, 8 lava domes, and 8 fissure-fed lava flows and plateaus. Volcanic activity in the VS area began ~8 Ma ago, persisting until the Late Pleistocene, ~11 ka ago. During the Pliocene to Middle Pleistocene, volcanism was distributed throughout the VS area, and was predominantly effusive, giving rise to voluminous medium-sized shield volcanoes (e.g., Cerro Grande, Cerro Culiacán, and Picacho-Cerro Prieto). In the Late Pleistocene, phreatomagmatic eruptions dominated the western sector of VS along an NNW-SSE-oriented stripe. This phreatomagmatism was facilitated by fractured aquifers on the slopes of shield volcanoes and the humid climatic conditions that existed during the Late Pleistocene, which guaranteed water-saturated conditions. Erupted products are mainly basaltic andesites/basaltic trachyandesites, followed by andesites, basalts/trachybasalts, trachyandesites, and rhyolites. Furthermore, their chemical affinity shifted over time, transitioning from solely sub-alkaline to both, sub-alkaline and alkaline by the Late Pleistocene. The VS area holds one of the largest phreatomagmatic clusters in the TMVB, offering an excellent opportunity to study the conditions favoring phreatomagmatism and providing records of intense volcanic activity during the Plio-Pleistocene in the MGVF.

Keywords: Valle de Santiago, Michoacán-Guanajuato Volcanic Field, monogenetic volcanism, morphometry, phreatomagmatism, radiocarbon dating, Ar-Ar dating

INTRODUCTION

Distributed volcanic fields are an important type of volcanic landscape, where a large number of volcanoes (from tens to hundreds) within a defined age range, are clustered and/or aligned within a certain area. Most of these volcanoes are monogenetic and produced by single eruptive episodes before becoming extinct. Hence, they are typically short-lived ($\leq 10^2$ years) and usually of small eruptive volumes (≤ 1 km^3 magma) (Connor and Conway, 2000; Németh, 2010; Le Corvec et al., 2013; Németh and Kereszturi, 2015; Valentine and Connor, 2015; Smith and Németh, 2017), although some can originate from more complex and longer-lasting eruptions (e.g., Németh and Kereszturi, 2015; Luhr and Simkin, 1993; Abrams and Siebe, 1994; Guilbaud et al., 2011; Chako-Tchamabé et al., 2015, 2016, 2020). Furthermore, these volcanoes can be the product of a wide variety of eruptive styles, which in turn depend on the physical-chemical properties of the magma (composition, volatile content, rheology) as well as the geological conditions of the region (type of substrate, hydrogeology, regional and local stress fields) (Valentine and Gregg, 2008; Kereszturi and Németh, 2012a; Németh and Kereszturi, 2015; Martí et al., 2016). Thus, landforms found in monogenetic volcanic fields can include scoria cones with or without associated lava fields, lava domes, spatter cones/ramparts, medium-sized volcanic shields, fissure-fed lava flows or lava plateaus, maars, tuff rings, tuff cones, and even stratovolcanoes (e.g., Hasenaka, 1994; Ownby et al., 2007; Guilbaud et al., 2012; Osorio-

Ocampo et al., 2018; Reyes-Guzmán et al., 2018; Avellán et al., 2020; Jácome-Paz et al., 2022). The distribution of the volcanic vents is controlled by regional and local tectonic conditions and mechanical heterogeneities of the substrate (Martí et al., 2016).

Distributed (monogenetic) volcanic fields occur in almost any tectonic setting, but most commonly in extensional and convergent tectonic settings (Le Corvec et al., 2013; Valentine and Connor, 2015; Cañón-Tapia, 2016) and can be active for millions of years (Németh, 2010; Kereszturi et al., 2013). Erupted magmas are usually basaltic (with a compositional range ≤52 wt.% in SiO_2; Valentine and Connor, 2015), although they can also be of other compositions (e.g., andesitic, rhyolitic, etc.; Jaimes-Viera et al., 2018; Sosa-Ceballos et al., 2021; Torres-Sánchez et al., 2022).

The Michoacán-Guanajuato Volcanic Field (MGVF), located within the Trans-Mexican Volcanic Belt (TMVB) in central Mexico (see inset map in Figure 1), stands out as the largest monogenetic volcanic field on Earth associated with a subduction setting and represents a natural laboratory for in-depth studies of monogenetic volcanism. In the northeastern sector of the MGVF lies the Valle de Santiago (VS) area (Figure 1). This region hosts a noteworthy ensemble of volcanic structures produced by various eruptive styles that include both magmatic (effusive and explosive) and phreatomagmatic activity, whose products are sub-alkaline and alkaline in composition (Losantos et al., 2017). In fact, the VS area has the highest concentration of alkaline volcanic rocks (Losantos et al., 2017; Torres-Sánchez et al., 2022) and hosts the largest number of phreatomagmatic volcanoes in the entire MGVF (Figures 1, 2, and 3). This cluster of phreatomagmatic craters and the lakes in their interiors have motivated many investigations of different topics for more than a century. Several of these studies have focused on environmental, paleoenvironmental, and ecological issues (Brown, 1984; Green, 1986; Metcalfe et al., 1989, 2000; Alcocer et al., 2000; Escolero and Alcocer, 2004; Park, 2005; Armienta et al., 2008; Kienel et al., 2009; Park et al., 2010; Holmes et al., 2016; Domínguez-Vázquez et al., 2019). Other studies have addressed the stratigraphy, geochronology, petrography, and geochemistry of some of the volcanic structures in order to establish their eruptive dynamic (Ordóñez, 1900, 1906; Murphy, 1986; Puente-Solis, 2004; González-Becerra, 2005; Oviedo-Padrón, 2005; Rincón-Herrera, 2005; Uribe-Cifuentes, 2006; Luhr et al., 2006; Cano-Cruz and Carrasco-Núñez, 2008; Aranda-Gómez et al., 2013; Aranda-Gómez and Carrasco-Núñez, 2014; Losantos et al., 2017; Suárez-Jiménez, 2022). Additional studies have been based on petrological and geochronological analyses of xenoliths aimed at knowing the nature of the local basement (Urrutia-Fucugauchi and Uribe-Cifuentes, 1999; Ortega-Gutiérrez et al., 2014), and on geophysical surveys intended to learn about maar-diatreme systems (Yutsis et al., 2014).

Despite numerous studies conducted in the VS area, a comprehensive spatio-temporal analysis of the volcanic structures, including information about their chemical composition, petrography, and morphology, has not yet been carried out. This results in a significant information gap that hinders our understanding of the formation and evolution of the volcanoes in this area. The present study aims to address this gap by providing a detailed investigation into the volcanic evolution of the VS area, utilizing a range of methodologies including detailed field descriptions (via the construction of stratigraphic columns), morphological assessments, volume calculations, $^{40}Ar/^{39}Ar$ and ^{14}C radiometric dating, and analysis of the petrography and geochemistry of the juvenile volcanic products.

TECTONIC AND GEOLOGIC BACKGROUND

The TMVB is a continental volcanic arc active since the early Miocene that is related to the subduction of the Rivera and Cocos oceanic plates underneath the southern boundary of the

North American continental plate along the Middle America trench (Nixon, 1982; Pardo and Suárez, 1995; Ferrari et al., 2012; see inset map in Figure 1). It has an oblique strike with respect to the trench, forming an angle of ~16°, stretching across central Mexico for ~1000 km in a preferred E-W orientation (Johnson and Harrison, 1990; Pardo and Suárez, 1995; Gómez-Tuena et al., 2007). The TMVB comprises at least ten monogenetic volcanic fields, including Los Tuxtlas (Sieron et al., 2021; Rodríguez-Elizarrarás et al., 2023), Xalapa (Rodríguez-Elizarrarás et al., 2010; Jácome-Paz et al., 2022), Serdán-Oriental (Chédeville et al., 2020; Carrasco-Núñez et al., 2021), Apán-Tezóntepec (García-Palomo et al., 2002), Sierra Chichinautzin (Martin Del Pozzo, 1982; Siebe et al., 2004; Arce et al., 2019), Valle de Bravo (Aguirre-Díaz et al., 2006), Los Azufres (Arce et al., 2012, 2021), Michoacán-Guanajuato (Hasenaka and Carmichael, 1985a), Mascota (Carmichael et al., 1996; Ownby et al., 2008), Colima-Cántaro (Luhr and Carmichael, 1981), and the Ceboruco graben (Sieron and Siebe, 2008).

The MGVF, located in the central sector of the TMVB, encompasses an area of ~40,000 km^2 (Hasenaka and Carmichael, 1985b). In this area, ~1400 volcanic structures were produced, including abundant scoria/spatter cones with or without associated lava flows, medium-sized shield volcanoes ("Mexican shields"; Hasenaka, 1994), lava flows and domes, scarce phreatomagmatic volcanoes (maars, tuff rings, and tuff cones), and only two extinct stratovolcanoes (Patambán and Tancítaro; Ownby et al., 2007) (Figure 1).

The distribution of the eruptive vents within the MGVF is proposed to be dictated by the tectonic configuration of the region (e.g., Bolós et al., 2020; Gómez-Vasconcelos et al., 2020, 2023), which is characterized by three normal fault systems. The older fault systems have NNW-SSE and NW-SE trends and are associated with the Taxco-San Miguel de Allende (Alaniz-Álvarez et al., 2002) and the Chapala-Oaxaca faults systems (Johnson and

Harrison, 1990), respectively. The NNW-SSE faults are predominantly located in the northeastern region of the MGVF, whereas the NW-SE faults mostly affect the southwestern area. In contrast, the younger fault system trends ENE-WSW and is linked to the Morelia-Acambay fault system (Garduño-Monroy et al., 2009). These faults chiefly cut the volcanic rocks that are in the central part of the MGVF, developing horst-and-graben structures that result in basins often occupied by wide but shallow lakes (e.g., Cuitzeo, Pátzcuaro, Zacapu; Figure 1).

The chemical composition of the volcanic products in the MGVF is predominantly andesitic, exhibiting SiO_2 contents spanning from 47 to 63 wt.% (Torres-Sánchez et al., 2022). Silicic compositions (dacites and rhyolites) are present in smaller proportions, accounting for approximately 10% of the volcanic products (Sosa-Ceballos et al., 2021). The onset of the volcanism in the MGVF has been dated at ~7 Ma (Avellán et al., 2020), and it is still active with the historic eruptions of Jorullo (AD 1759-1774) and Parícutin (AD 1943-1952) volcanoes (Luhr and Carmichael, 1985; Luhr and Simkin, 1993; Guilbaud et al., 2011), and several seismic swarms that occurred in 1997, 1999, 2000, 2006, 2020, and, 2021 in the Tancítaro-Parícutin area, which could be the precursors to the birth of a new monogenetic volcano (Legrand et al., 2023).

THE VALLE DE SANTIAGO (VS) AREA

General Features

The VS area is located ~380 km from the Middle America Trench within the El Bajío basin, occupying mainly its central and southeastern parts (Figure 1). This basin is a broad fluvio-lacustrine plain (with an average elevation of ~1720 masl), elongated in an NW-SE orientation, which was developed as a semi-graben by the El Bajío fault during the Oligocene (Botero-Santa et al., 2015).

The VS area encompasses a surface of ~2,800 km^2 and is surrounded by mountainous terrains, including the Sierra Codornices to the north, the Sierra de Piñícuaro to the south, the Apaseo and Agustinos calderas (Aguirre-Díaz, 2001) to the east, and some scoria cones, lava flows, medium-sized shield volcanoes, and rhyolitic complexes to the west (Pasquarè et al., 1991) (Figure 1). The typical volcanic landforms that are hosted in the VS area include eroded and well-preserved scoria/spatter cones with or without associated lava flows (e.g., Peña Colorada, Santa Teresa, Cerro Cupareo, La Batea, Cerro Las Silletas), medium-sized shield volcanoes (e.g., Cerro Comaleros, Cerro Grande, Cerro Culiacán, Cerro Santiago, El Picacho), phreatomagmatic volcanoes (e.g., Sanabria tuff ring, and Joya Rincón de Parangueo, Joya Cíntora, and Joya de Yuriria maars), fissure-fed lava flows and plateaus (e.g., Cerro Sanabria, Paredones, La Cumbita), and lava domes (e.g., La Mina, Palo Blanco, El Colloncle) (Figures 2 and 3). The volcanic products within the VS area exhibit a dominant mafic to intermediate composition, varying from basaltic to andesitic, with only a few rhyolitic exceptions, such as the Joya Estrada tuff ring (Cano-Cruz and Carrasco-Núñez, 2008) and La Mina dome (Aranda-Gómez and Carrasco-Núñez, 2014) (Figure 3). Moreover, many of these volcanic products display alkaline affinities, while a minor proportion is sub-alkaline (Murphy, 1986; Ortega-Gutiérrez et al., 2014; Losantos et al., 2017). A feature that stands out in the VS area is the unusual abundance and diversity of xenoliths of crystalline rocks found within the pyroclastic products of certain phreatomagmatic volcanoes, such as Joya Rincón de Parangueo, Joya Cíntora, Joya de Álvarez, and Magdalena de Araceo. These xenoliths have been characterized as gabbros, metanorthosites, mafic and felsic granulites, and charnockites by Urrutia-Fucugauchi and Uribe-Cifuentes (1999) and Ortega-Gutiérrez et al. (2014).

According to the work carried out by Murphy (1986) and the ages obtained by Hasenaka and Carmichael (1985b), Ban et al. (1992), Rincón-Herrera (2005), Peñaloza-Turrubiates (2005), Cano-Cruz and Carrasco-Núñez (2008), and Aranda-Gómez et al. (2009) for some volcanic structures in the VS area, it is inferred that the volcanic activity in the region began during the Miocene and persisted until the Late Pleistocene, between approximately 7 Ma and younger than 70 ka. Furthermore, Murphy (1986) divided the volcanic activity in the VS area into two periods. The first period occurred between the Late Miocene (6.9 Ma) and the Pliocene (2.1 Ma; Ban et al., 1992) and consisted of basaltic and andesitic volcanism, resulting in the formation of the medium-sized shield volcanoes and some of the scoria cones. The second period occurred during the Pleistocene (between 1.2 Ma and <73 ka) and included the formation of the phreatomagmatic volcanoes and the other scoria cones.

From a structural point of view, the rocks within the VS area are not significantly affected by important geological faults, nevertheless, some structural features stand out. One of these features is the NNW-SSE alignment defined by the phreatomagmatic volcanoes (Murphy, 1986). This alignment stretches approximately 52 km from the southern outskirts of Irapuato to Yuriria and probably forms part of the regional NNW-SSE Tzitzio-Valle de Santiago fault system, which in turn is part of the Taxco-San Miguel de Allende fault system (Uribe-Cifuentes and Urrutia-Fucugauchi, 1999; Uribe-Cifuentes, 2006; Garduño-Monroy et al., 2009) (Figure 1). In addition, there are some E-W, NE-SW, and NNW-SSE trending normal faults that mainly affect the oldest rocks in the VS area (Figures 2 and 3).

Regional Stratigraphy

The oldest rocks in the VS area correspond to a Mesozoic marine volcano-sedimentary succession that experienced low-grade metamorphism (greenschist facies) and shortening.

These rocks are exposed in the eastern part of the Sierra Codornices (SC) (Figures 1 and 2), which is an elevated plateau situated north of the VS area and forms part of the southern end of the Mesa Central physiographic province (Alaniz-Álvarez et al., 2002; Nieto-Samaniego et al., 2005; Del Pilar-Martínez et al., 2021). Some of the xenoliths found within the pyroclastic deposits from Joya Rincón de Parangueo (e.g., metamorphosed charnockites in granulite facies) also suggest the presence of Mesozoic (~67 Ma) rocks beneath the VS area (Ortega-Gutiérrez et al., 2014). Unconformably on top of the Mesozoic marine rocks are Paleogene and Neogene rocks. The oldest of the Paleogene rocks are Eocene continental clastic sedimentary rocks (sandstones, conglomeratic sandstones, conglomerates, and calcareous breccias) interbedded with volcanic rocks and granitic intrusions (Aranda-Gómez and McDowell, 1998; Alaniz-Álvarez et al., 2002; Nieto-Samaniego et al., 2005; Del Pilar-Martínez et al., 2021). These Eocene rocks crop out scarcely in the SC. Unconformably overlying the Eocene rocks are Oligocene effusive (lava flows and domes) and explosive (pyroclastic and ignimbrite deposits) volcanic rocks of basaltic, andesitic, and rhyolitic composition (Echegoyén-Sánchez et al., 1970; Cerca-Martínez et al., 2000; Alaniz-Álvarez et al., 2002; Nieto-Samaniego et al., 2005; Del Pilar-Martínez et al., 2021). These volcanic sequences make up a significant part of the SC (Figure 2). Unconformably covering the Oligocene rocks are Miocene rocks. The Miocene record comprises continental sedimentary rocks (conglomerates and sandstones), as well as effusive and some explosive volcanic rocks of mafic, intermediate, and silicic composition (Pasquarè et al., 1991; Nieto-Samaniego, 1990; Cerca-Martínez et al., 2000; Nieto-Samaniego et al., 2005). These rocks crop out extensively in the SC (Figure 2) and around the VS area, particularly towards the east (in the Apaseo and Los Agustinos caldera complexes, and Querétaro basalts; Pasquarè et al., 1991; Aguirre-Díaz, 2001; Alaniz-

Álvarez et al., 2002) and south (Villa Morelos basalts; Pasquarè et al., 1991). Volcanic rocks probably from the Pliocene and Late to Middle Pleistocene are distributed mainly to the south (in the Sierra de Piñícuaro) and west of the VS area (Figure 1). These rocks were formed by both effusive and explosive activity, forming medium-sized shield volcanoes and scoria cones (Pasquarè et al., 1991). Finally, Quaternary fluvio-lacustrine sediments with clasts of volcanic origin and >40-m-thick are found mainly filling the central part of the El Bajío basin.

METHODOLOGY

Fieldwork

This study gathers information from many strenuous fieldwork campaigns that have been carried out in the VS area since 2015. The work in each campaign has focused on the detailed description and sampling of pyroclastic, lava, and paleosol exposures to characterize each of the magmatic and phreatomagmatic structures of the VS area and establish the stratigraphic relationships between them. The exposures are situated on the slopes of the different volcanic structures, in road cuts, in the internal crater walls of the phreatomagmatic volcanoes, and in gullies. At each exposure, we described parameters such as color, bed/unit thickness, contacts, texture (e.g., massive, stratified, grading, degree of induration), constituents (e.g., vesiculated and non-vesiculated juvenile fragments, accidental lithics, crystals), soil maturity, sorting, sedimentary structures (e.g., planar-and-cross bedding, dunes), grain size, syn-depositional deformational structures, and clast texture (e.g., color, shape, mineralogy, vesicularity).

The collected samples, which include juvenile material, pyroclastic deposits, lava flows, and paleosols, were used for different analyses such as grain-size distribution, componentry, $^{40}Ar/^{39}Ar$ and radiocarbon geochronology, petrography, and whole-rock composition.

Geological Map

Based on preliminary geological cartography, fieldwork observations, morphological features, and $^{40}Ar/^{39}Ar$ and radiocarbon dates, a detailed geological map of the VS area was constructed using ESRI ArcMap and Adobe Illustrator computer programs (Figures 2 and 3). The outline-contours of each volcanic structure in the VS area were drawn over a shaded digital elevation model with the aid of Google Earth satellite images and 1:50,000 scale topographic information from the Instituto Nacional de Estadística, Geografía e Informática (INEGI). The shaded digital model was built from high-resolution Light Detection and Ranging (LiDAR) data with 5 m of horizontal resolution, and from elevation data at 10 m resolution (when 5 m data were not available), both downloaded from the INEGI webpage.

$^{40}Ar/^{39}Ar$ Dating

Twenty-four samples were collected for $^{40}Ar/^{39}Ar$ dating (Table 1). For this purpose, fist-sized samples without alteration crust were sent to the Argon Geochronology Laboratory at Oregon State University, USA. Samples were crushed, sieved, washed, and dried using standard mineral separation techniques. Groundmass splits were obtained for the sample, rinsed with cold water then dried in a drying oven at 55 °C. Once the samples were dried, they were sieved to 250-150 µm. Special care was taken to remove any alteration material by using an intensive acid leaching procedure using a combination of HCl (1Normal and 6Normal) and HCO_3 (1Normal and 3Normal) at different acid strengths (Koppers et al., 2000). A final separation of groundmass was obtained using a binocular microscope. Any visible alteration or adhering crystal phases were carefully removed before packaging and irradiation of the sample.

$^{40}Ar/^{39}Ar$ ages (Table 1) were obtained by incremental heating methods using the ThermoFisher Scientific ARGUS-VI mass spectrometer and data collection using internal lab software ArArExperiments version 4.4.0. The samples were irradiated for 6 hours (Irradiation 22-OSU-02 in the CLICIT position in the Oregon State University's TRIGA nuclear reactor). Samples were irradiated with the Fish Canyon Tuff sanidine (FCT-2-NM sanidine) with an age of 28.201 ± 0.023 Ma, 1σ flux monitor (Kuiper et al., 2008).

Individual J-values for each sample were calculated by polynomial extrapolation of the measured flux gradient against irradiation height and typically give 0.06-0.12% uncertainties (1σ). The $^{40}Ar/^{39}Ar$ incremental heating age determinations were performed on a multi-collector ARGUS-VI mass spectrometer at Oregon State University that has 5 Faraday collectors fitted with one ion-counting CuBe electron multiplier (located in a position next to the lowest mass Faraday collector). All the Faraday collectors are fitted with two 10^{12} Ohm resistors for argon masses ^{41}Ar and ^{40}Ar and three 10^{13} Ohm resistors for masses ^{39}Ar, ^{38}Ar, and ^{37}Ar. This configuration allows us to measure simultaneously all argon isotopes, with mass 36 on the multiplier and masses 37 through 40 on the four adjacent Faradays. Furthermore, it provides the advantage of running in a full multi-collector mode while measuring the lowest peak (on mass 36) on the highly sensitive electron multiplier (which has an extremely low dark noise and a very high peak/noise ratio). Irradiated samples were loaded into Cu-planchettes in an ultra-high vacuum sample chamber and incrementally heated by scanning a Synrad Firestar 20Watt defocused 30W CO^2 laser beam in pre-set patterns across the sample, to release the argon evenly. Each heating step is 62 seconds. After heating, reactive gases were cleaned up using four SAES

Zr-Al AP10 getters for 3 minutes: two operated at 450 °C and two operated at room temperature (20 °C). All ages were calculated using the corrected Steiger and Jäger (1977) decay constant of 5.530 ± 0.097 x 10^{-10} 1/yr (2σ) as reported by Min et al. (2000). For all other constants used in the age calculations we refer to Table 2 in Koppers et al. (2003). Incremental heating plateau ages and isochron ages were calculated as weighted means with $1/\sigma^2$ as the weighting factor (Taylor, 1997) and as YORK2 least-square fits with correlated errors (York, 1968) using the ArArCALC v2.6.2 software from Koppers (2002) available from the http://earthref.org/ArArCALC/website.

Argon isotopic results are corrected for system blanks, radioactive decay, mass discrimination, reactor-induced interference reactions, and atmospheric argon contamination. Decay constants reported by Min et al. (2000) are used for age calculation. Isotope interference corrections as determined using the ARGUS VI are: $(^{36}Ar/^{37}Ar)_{Ca}$ = 0.0002703 ± 0.0000005; $(^{39}Ar/^{37}Ar)_{Ca}$ = 0.0006425 ± 0.0000059; $(^{40}Ar/^{39}Ar)_K$ = 0.000607 ± 0.000059; $(^{38}Ar/^{39}Ar)_K$ = 0.012077 ± 0.000011. Ages were calculated assuming an atmospheric $^{40}Ar/^{36}Ar$ ratio of 298.56 ± 0.31 (Lee et al., 2006). Data reduction and age calculation were processed using Ar-Ar Calc 2.7.0 (Koppers, 2002). Plateau ages include >50% of the total ^{39}Ar released with at least three consecutive steps, where the $^{40}Ar/^{39}Ar$ ratio for each step agrees with the mean at the 95% confidence level. In some cases, only a mini-plateau age is given, where a mini-plateau <50% of the ^{39}Ar released.

Representative age spectra and inverse isochron plots are shown in Figure 4. The remaining age plots can be seen in Figure S1.

Radiocarbon Dating

Sixteen paleosol samples were radiocarbon-dated using the accelerator mass spectrometry technique at Beta Analytic Inc., Miami, Florida (Table 2). The samples were collected from the upper 2-3 cm of each paleosol, close to contact with the different pyroclastic sequences emitted by some of the phreatomagmatic and magmatic structures of the VS area (Figure S2). They were then dried in an oven at 55 °C for 24 hours. Beta Laboratories processed the samples as organic sediments and pretreated them with acid washes. The obtained dates (conventional radiocarbon ages) were corrected for isotopic fractionation effects, calibrating them to calendar years using the CALIB 7.1 and BetaCal 4.20 computer programs, employing the IntCal13 and IntCal20 databases for the northern hemisphere radiocarbon age curves (Stuiver and Reimer, 1993; Reimer et al., 2020) and the high probability density range method (HPD; Bronk-Ramsey, 2009). A detailed stratigraphic context of the paleosols used in radiocarbon dating is presented in Figure S2.

Morphometric Analysis

The morphometric analysis of the volcanic structures in the VS area involved the calculation of several parameters proposed by Porter (1972), Wood (1980), and Graettinger (2018). For shield volcanoes and lava domes, we measured the height (Hco) and basal diameter of the structure (Wco), as well as the average slope of the external flanks of the volcano (S_{ave}) (Figure 5A and B). Scoria cones were analyzed using the same parameters, in addition to the crater diameter (Wcr) and depth (Dcr) (Figure 5C). For phreatomagmatic volcanoes, we calculated the Hco, Wco, and S_{ave} of the tephra ring, as well as the Wcr and Dcr of the phreatomagmatic crater (Figure 5D). We also measured the major (Max CrD) and minor (Min CrD) axes of the craters and the lowest elevation of the crater floor (Figure 5D). Max CrD values were used to measure the elongation (EL) of the phreatomagmatic crater through the following equation: $EL = A/ [\pi \text{ (Max CrD/2)}^2]$, where A is the area encompassed by the crater rim (Graettinger, 2018). Elongation values of 1 indicate circular-shaped craters, while values <1 indicate craters with elongated shapes (Graettinger, 2018).

Finally, for fissure-fed lava flows, elevation profiles perpendicular to the flow direction were traced to obtain an average thickness value.

Hco was calculated by taking the average of each structure's maximum (Hco max) and minimum (Hco min) heights. These height values were obtained by subtracting the maximum and minimum elevations of the bases and summits (Figure 5) (e.g., Kereszturi and Németh, 2012b; Becerra-Ramírez et al., 2022). This approach was necessary because most of the structures in the VS area are built on uneven and/or sloping topographic surfaces, which resulted in differing base and summit elevations. To determine Wco we measured the distance between two points that marked the change in slope between the structure and the surrounding terrain (Figure 5). S_{ave} was determined by measuring the inclination of the external flanks of each volcanic structure, considering the sloping surface between the highest point of the structure and its base (Figure 5). Wcr was calculated by measuring the distance between the edges of the crater, Dcr was obtained by taking the difference between the highest elevation of the crater rim and the lowest elevation of the crater floor (Figure 5).

For calculating the aforementioned parameters, we made use of contour line data with 10 and 5 m intervals, along with measurements gathered from four elevation profiles that were delineated for each structure with the aid of Google Earth. These elevation profiles were oriented along E-W, N-S, NE-SW, and NW-SE directions, except for elongated structures, for which two profiles were traced parallel to the major and minor axes of the structure and the other two at a 45° angle to these axes. The resulting values of each elevation profile were averaged to obtain a final value for each parameter (except for Dcr). The results of these analyses are reported in Table S1.

Area and Volume Calculations

The area (A) and volume (V) of all the volcanic structures in the VS area were calculated in ArcMap 10.6.1 using the method of difference of two triangulated surface models (TIN; triangulated irregular network). This method employs the contour lines of the study area (for our case we used contour lines with 10 m intervals) and the polygons that define the surface of each structure. In general, the method involves the creation of two TIN models, one including the contour lines of the volcanic structure and the other excluding it. The difference between these two TINs yields the area and volume of the structure. The procedure and the results of these calculations are shown in Appendix 1, Table 3, and Table S1.

Volumes reported in this study have not been recalculated to dense rock equivalent, because the percentage of empty spaces in the lavas and pyroclastic products of each volcano is unknown. Area measurements correspond to the base of the volcanic structure. In the case of phreatomagmatic volcanoes, the area corresponds to the surface covered by the tephra ring. Another important consideration for the calculation of morphometric parameters and volumes in the VS area is that the morphology of the volcanic landforms is influenced by various primary eruption-related factors (e.g., changes in eruptive style, shape, or migration of the volcanic conduit) as well as secondary syn- and/or post-eruptive erosion-related processes (e.g., structure breaching, anthropogenic, and tectonic activity). The above, together with the overlapping nature of most structures, hinders the precise determination of morphometric parameters and volumes, especially when the structures are in advanced states of degradation. Under such circumstances, only the morphometric parameters and volumes allowed by the remaining structure were calculated, and therefore, some of the parameters must be taken with caution.

Petrographic and Geochemical Analyses

Petrographic thin sections were prepared at the Taller de Laminación de Suelos y Sedimentos of the Instituto de Geología, UNAM, Mexico City, and at Mann Petrographics, New Mexico, USA. The thin sections correspond to representative juvenile samples such as lavas, scoria clasts, and volcanic bombs from representative magmatic and phreatomagmatic structures of the VS area. Mineral and textural identifications were done using a polarizing microscope.

Chemical analyses, including major, trace, and rare-earth elements, were conducted on whole rock samples at two different laboratories, using multiple techniques. Some samples were analyzed at Activation Laboratories Inc., Ancaster, Canada, using fusion-inductively coupled plasma (FUS-ICP), instrumental neutron activation analysis (INAA), total digestion-inductively coupled plasma (TD-ICP), and fusion-mass spectrometry (FUS-MS). Major elements and certain trace elements, such as Ba, Sr, V, and Y, were measured using the FUS-ICP technique, while the other techniques were used to measure the remaining trace elements and the rare-earth elements. Other samples were analyzed at the GeoAnalytical Lab of the School of the Environment of Washington State University, USA. X-ray Fluorescence (XRF) was used to measure major elements and ICP-MS to determine trace and rare-earth elements. The analytical results are reported in Table S2.

RESULTS

Morphology and Morphometry of the Volcanic Landforms

Within the VS area, across a surface of ~2,800 km^2, 118 individual volcanoes were identified with the aid of satellite images and digital elevation models, in conjunction with field observations. This total includes 61 scoria and spatter cones with or without associated lava flows (5.6 vol.%), 21 phreatomagmatic volcanoes (1.8 vol.%), 20 shield volcanoes (90.6 vol.%), 8 lava domes (0.7 vol.%), and 8 fissure-fed lava flows (1.3 vol.%) (Figure 6;

Table S1 and Figure S3). In general, these volcanic landforms exhibit complex morphologies, which have been influenced by various factors such as changes in their eruptive style (ranging from explosive to effusive, magmatic to phreatomagmatic, or vice versa) and/or in the location of the eruptive vent throughout their eruptive history, the formation of younger volcanic structures that either covered or partially destroyed older structures, tectonic activity (faulting), erosion, and/or anthropic activity (quarrying and urbanization). The following section presents a comprehensive description of the morphological features and the morphometric parameters of the different types of volcanic landforms identified in the VS area. A summary of this information is presented in Table S1.

Scoria and Spatter Cones

The predominant volcanic landforms found in the VS area are cone-type monogenetic volcanoes. These cone-type volcanoes are mainly scoria cones (e.g., La Batea), while a smaller number are spatter cones (e.g., La Alberca spatters-1 and 2, Los Molina) (Table S1). These cones are scattered throughout the VS area without showing a discernible alignment pattern, and they can commonly be found in the El Bajío fluvio-lacustrine plain (e.g., Las Jícamas scoria cone), on the flanks of shield volcanoes (e.g., El Tule-II, El Sombrero scoria cones), and over lava plateaus (e.g., Scoria cone-4, San Miguelito scoria cones) (Figure 2; Figure S3). These cones can be associated (or not) with lava flows. Lava flows have lengths that range from ~1 to ~6.8 km and average thicknesses that vary between 14 and 108 m (Table S1). Only a few of these lava flows have preserved surface morphological structures, such as levees (e.g., Cerro Las Silletas, Cerro Poruyo, Cerro Juan Diosdado, Cerro Prieto-III; Figure S3).

Regarding their morphological characteristics (see Table S1), most cones in the VS area have asymmetrical shapes and lack distinct craters. However, some cones exhibit elongated (e.g., Cerro Colorado scoria cone), breached (e.g., Buenavista scoria cone), and symmetrical forms (e.g., Cerro Poruyo scoria cone). Furthermore, there are cones with closed, circular-shaped craters (e.g., La Batea scoria cone) and open craters with horseshoe shapes (e.g., San Andrés scoria cone). Also, some scoria cones without craters exhibit craggy summits (e.g., Cerro Cupareo, Blanca scoria cones), which are likely composed of spatter-type deposits (Figure 2; Figure S3).

In general, most cones in the VS area are affected by anthropic activity (quarrying and urbanization) and erosion to varying degrees. As a result, many of these cones are partially or almost completely degraded (e.g., Las Antenas, Santa Teresa, Cerro Guantecillos, Viejo scoria cones), show smooth morphologies (e.g., El Diezmo, Cerro Sotelo scoria cones), and/or are cut by drainage (e.g., La Batea, El Copalar scoria cones) (Table S1, Figure S3).

Cone-type volcanoes in the VS area exhibit diverse morphometric parameters. Their average height (Hco) ranges from 6.4 to 251 m, with La Batea scoria cone attaining the greatest height. The average base diameter (Wco) spans from 0.21 to 2.64 km, while the Hco/Wco ratio varies between 0.013 and 0.187 (Table S1), following a proportional pattern with the average slope angles (Figure 7A). In general, most of the cones in the VS area have gentle slopes with average slope angles ranging from 4 to 15°. However, some cones have steeper slopes (15-22°), with Cerro Prieto-III, Blanca, and El Bonete scoria cones showing the highest values of 19.9, 21, and 21.6°, respectively (Figure 7A; Table S1). Considering the estimated volumes for the cones, a wide range from 0.0006 to 1.32 km^3 is observed, though the majority have volumes below 0.13 km^3 (Table 3; Table S1). The Cerrito Colorado scoria cone displays the lowest values in both height and volume, attributed to extensive quarrying that has left only a few remnants. Conversely, cones with the highest volume values are those associated with lavas, where the volume estimation includes the cone and the lava flow (Table S1).

Shield Volcanoes

Hasenaka (1994) coined the term "Mexican shields" to classify the MGVF shield volcanoes. Despite sharing similar morphometric parameters with the Icelandic shield volcanoes (medium-sized with heights ranging from 100 to 1000 m, basal diameters between 2 and 12 km, and volumes spanning from 0.5 to 10 km^3), the Mexican shields are distinguished by having steeper slopes (5-15°), more evolved compositions (basaltic andesite to andesite), and occasional scoria cone crowning. Shield volcanoes within the VS area generally keep Mexican shield characteristics, although with a few exceptions. In general, these volcanoes have average heights (Hco) ranging from 140 to 1080 m, average basal diameters (Wco) spanning from 2.2 to 19.4 km, Hco/Wco ratios ranging from 0.034 to 0.105, volumes varying from 0.1 to 47 km^3, slightly steeper slopes with average slope angles ranging from 4.4° to 15.4°, and intermediate compositions that vary from basaltic andesite-basaltic trachyandesite to andesite-trachyandesite (Table S1). Among the shield volcanoes, Buena Vista, El Tule, and San Guillermo display the smallest height, basal diameter, and slope values, respectively, while Cerro Culiacán, Cerro Grande, and El Tule show the largest values for these parameters. It is noteworthy that the volume parameter displays a wide range. Shield volcanoes such as El Tule, Cerro Tendido, Buena Vista, San Guillermo, Cerro Chapín, and La Angostura have the smallest volumes, with values <0.5 km^3. In contrast, El Picacho-Cerro Prieto, Cerro Culiacán, and Cerro Grande shield volcanoes have the largest volumes, with 15.4, 19.8, and 46.7 km^3, respectively. However, the majority of shield volcanoes within the VS area exhibit volumes with values ranging from 0.7 to 2.9 km^3 (Table 3; Table S1). The relatively small volumes (<0.5 km^3) for some shield volcanoes can be explained by various factors: 1) emplacement on inclined terrains (flanks of larger shield volcanoes), limiting lava accumulation and thickness development (e.g., El Tule and Cerro Chapín); 2) being covered or cut by younger volcanic structures or deposits (e.g., El Tule, Cerro Tendido, and Cerro Chapín); 3) having relatively low average heights and small average basal diameters (e.g., Buena Vista, San Guillermo, La Angostura, Cerro Chapín, and El Tule). These factors contribute to underestimated volume measurements.

The shield volcanoes in the VS area can be grouped based on their average slope angles and Hco/Wco ratios (Figure 7B). Group 1 is characterized by gentle slopes (4.4° to 7.3°) and low Hco/Wco ratios (0.034 and 0.048) (Figure 7B), indicative of broad but low-height volcanoes. Shield volcanoes included in this group are Cerro Grande, Cerro Comaleros, Cerro La Tetilla, Buena Vista, Cerro Tetillas, San Guillermo, El Picacho, Cerro Prieto, Cerro Chapín, Cerro Prieto-II, and Cerro La Cruz (Table S1). Group 2 is characterized by steeper slopes (9.1° to 15.4°) and high Hco/Wco ratios (0.070 to 0.105) (Figure 7B), suggesting volcanoes with greater heights in relation to their basal diameters. Shield volcanoes included in Group 2 are Cerro Culiacán, Cerro Tendido, Cerro Gordo, El Capulín, El Varal, Cerro Santiago, La Angostura, Cerro Blanco, and El Tule. Notably, El Tule deviates from Group 2 towards higher values in its average slope (Figure 7B). This discrepancy may be due to a cone occupying its summit and younger structures covering its slopes (Figure 2; Figure S3). Hasenaka (1994) classified MGVF shield volcanoes into two types: A and B based on slope angles and contour line spacing on topographic maps. Group 1 shield volcanoes likely correspond to type A of Hasenaka (1994), characterized by gentle slopes (around 5°) and widely spaced contour lines. Group 2 shields belong to type B, distinguished by steeper slopes (around 10°) and closely spaced contour lines.

In terms of their morphological characteristics, shield volcanoes in the VS area show symmetrical (e.g., Cerro Santiago), elongated (e.g., Cerro Comaleros, Cerro Grande, Buena Vista, Cerro Tendido), and truncated (e.g., El Varal, El Picacho, El Tule, Cerro La Cruz, Cerro Prieto-II) shapes (Table S1; Figure S3). The major axis orientation of elongated shields aligns with the regional tectonic regime, while truncated shield volcanoes have experienced obstruction by older structures (e.g., Cerro Tendido, Cerro Blanco), cutting by younger volcanoes and/or faults (e.g., Cerro Prieto, Cerro Chapín, Cerro La Cruz; Cerro Comaleros), or coverage by younger volcanoes or deposits (e.g., El Tule, El Picacho, Cerro Prieto, Cerro Prieto-II). Additionally, some shield volcanoes have small lava domes, spatter or scoria cones, small calderas (e.g., El Varal), or plateau-like flat summits (e.g., El Picacho, Cerro Prieto). A few shields have two summit cones (e.g., Cerro Tetillas), while others have parasitic scoria mounds and scoria cones aligned on their flanks (e.g., Cerro Grande, El Picacho, Cerro Prieto). The latter probably suggests a shift in vent position during the eruption or the existence of a fissure vent (Hasenaka, 1994). Moreover, some shield volcanoes are cut by ENE-WSW and NNW-SSE faults, while others are affected by drainage (Table S1; Figure S3).

Phreatomagmatic Volcanoes

The phreatomagmatic volcanoes within the VS area mainly consist of tuff rings and maars, although some tuff cones also exist (Table S1; Figure S3). These volcanoes define a main lineament with an NNW-SSE orientation and a secondary lineament-oriented E-W. The first lineament encompasses the phreatomagmatic volcanoes that lie from the southern region of Irapuato to the city of Yuriria. The second lineament is defined by Joya San

Nicolás, Joya Estrada, and Joya La Alberca volcanoes, situated in the central zone of the study area (Figure 2; Figure S3). Likewise, a few of these volcanoes formed on the El Bajío fluvio-lacustrine plain, while the majority formed on distal lava flows at the lower flanks of shield volcanoes, cutting them (Figure 2; Figure S3). Lavas from certain shield volcanoes and lava flows are exposed on the inner crater walls of the maars.

The phreatomagmatic volcanoes in the VS area have a variety of crater shapes, including elongated (e.g., Sanabria, San Roque East, La Mina Norte, La Mina Sur, and Joya Estrada tuff rings, Joya Blanca tuff cone, and Joya La Alberca, Joya Solís, Joya Cíntora, and Joya de Álvarez maars), breached (e.g., San Roque West and Isla de San Pedro tuff rings, as well as Providencia de Cuerunero and Joyuela de San Vicente tuff cones), irregular (e.g., Joya Rincón de Parangueo, Joya San Nicolás, and Joya de Yuriria maars and Joyuela tuff ring), circular (e.g., Isla de San Pedro tuff ring), and composite eight-like outlines (e.g., Magdalena de Araceo tuff ring). However, certain volcanoes in the area lack a defined shape due to a high degree of erosion and overexploitation of their materials by anthropic activity (e.g., La Ciénega, San Roque East, San Roque West, Sanabria, and Santa Rosa tuff rings) (Table S1; Figure S3). These craters have average depths (Dcr) ranging from 23 to 379 m, average diameters (Wcr) spanning from 0.36 to 3.51 km, areas (A) varying from 0.08 to 3.15 km^2, and elongation (EL) values ranging from 0.57 to 0.99 (Table S1). Among these volcanoes, La Ciénega tuff ring, and Providencia de Cuerunero tuff cone have the craters with the lowest values in Dcr, Wcr, and A, respectively. Conversely, Joya Rincón de Parangueo and Joya Cíntora maars, along with Santa Rosa tuff ring, are characterized by craters with the highest values of the abovementioned parameters. Isla de San Pedro tuff ring comes closest to having a circular crater and displays a value of EL = 0.99 (Table S1).

On the other hand, the tephra rings associated with the phreatomagmatic volcanoes in the

VS area exhibit average heights (Hco) varying from 7 to 150 m, average basal diameters (Wco) ranging between 0.57 and 5.12 km, Hco/Wco and Hco/Wcr ratios spanning from 0.005 to 0.082 and 0.006 to 0.131, volumes ranging from 0.0018 to 0.35 km^3, and average slope angles varying from 1.6 to 17.9°. Among the tephra rings, the ones associated with the Isla de San Pedro tuff ring, Providencia de Cuerunero tuff cone, and La Ciénega and Santa Rosa tuff rings have the lowest values for Hco, Wco, volume, and average slope, respectively. In contrast, the tephra rings linked to La Mina Sur and Santa Rosa tuff rings, Joya de Álvarez maar, and Providencia de Cuerunero tuff cone display the highest values for these parameters (Table S1).

Phreatomagmatic volcanoes in the VS area show remarkable additional features. These include the presence of lakes within some of the craters (e.g., Joya Rincón de Parangueo, Joya de Yuriria, and Joya Cíntora maars), as well as water springs (e.g., Joya Solís and Joya de Yuriria maars), stromatolites, and salt deposits (e.g., Joya Rincón de Parangueo and Joya La Alberca maars; Aranda-Gómez and Carrasco-Núñez et al., 2014). Likewise, the deposit sequences of certain phreatomagmatic volcanoes record changes in the eruptive style, which, in some cases, initiated or culminated with effusive or explosive magmatic activity (e.g., La Mina Sur, Joyuela, and Magdalena de Araceo tuff rings, Joya La Alberca, Joya Cíntora, and Joya de Álvarez maars, and Joya Blanca tuff cone) (Figure 2; Table S1 and Figure S3). This feature plays a crucial role in shaping the final morphology of the phreatomagmatic crater.

Lava Domes and Lava Flows

Lava domes in the VS area are distributed mainly to the north and south of the study area (Figure 2; Figure S3). These domes mainly developed on the El Bajío fluvio-lacustrine plain and on the flanks of shield volcanoes, except for one dome that formed within a phreatomagmatic crater (e.g., La Mina) (Figure 2; Figure S3). These structures present irregular (e.g., El Colloncle, Enguaro), coulee-type (e.g., El Cerrito, Cerro Blanco-II), and elongated-asymmetrical shapes (e.g., Palo Blanco, Cerro Perimal, Los Cuates, La Mina). Irregular shapes are represented by steep and smooth topographies in the same structure. A special case is the Enguaro dome, which is associated with a lava flow that dispersed in two directions, covering approximately 4.6 km to the west and 2 km to the northeast (Table S1; Figure S3). In terms of their morphometric parameters, the lava domes found in the VS area are characterized by 51-181 m in average height (Hco), 0.82-2.63 km in average basal diameter (Wco), 0.017-0.254 km^3 in volume, and slightly steeper slopes with average slope angles ranging from 6.4 to 18.8° (Table 3; Table S1). Among these domes, Enguaro is the one with the lowest values in Hco and average slope, while La Mina dome displays the lowest values in Wco and volume. Los Cuates, Palo Blanco, and La Mina domes display the highest values in Hco, Wco, volume, and average slope, respectively (Table S1).

Lava flows in the VS area are not very common. They do not seem to be directly linked to any volcanic structure, suggesting that their emplacement likely occurred through fissures (Figure 2; Figure S3). These flows were emplaced over low topographic regions, extending predominantly towards the northeast and north. The longest flow extended to a distance of ~3.7 km (La Compañía) (Table S1; Figure S3). Morphologically, these lava flows mainly show fan-like forms with lobe-shaped fronts (e.g., Guantes, Paredones, La Compañía) and, to a lesser extent, plateau-like forms (e.g., La Cumbita, Lava Plateau-2) on which some scoria cones were built (e.g., San Miguelito, Parangarico, Scoria cone-3, and Scoria cone-4). These lava flows have irregular surfaces and are not dissected by drainage (Figure 2; Figure S3). It is worth mentioning that there are two structures composed of lavas (e.g., Cerro Sanabria and Panales Jamaica) which are affected by normal faults oriented in an

NE-SW direction. The latter gives them an elongated appearance and a craggy morphology with very steep slopes, and as a result, these structures do not present a typical lava flow morphology (Figure 2; Figure S3). Likewise, a lava flow is only exposed on the inner crater walls of the Joya La Alberca maar. This lava flow appears not to be associated with any surrounding scoria cone or shield volcano, suggesting a fissural origin. Its limited exposure hindered the determination of its morphometric and morphological parameters; however, samples of the lava have been analyzed chemically, petrographically, and geochronologically (see below).

Regarding their morphometric parameters, the lava flows have areas ranging from 2.15 to 17 km^2, volumes varying from 0.013 to 0.52 km^3, and average thicknesses that range from 14 to 151 m. Among these lava flows, Paredones is the one with the smallest dimensions, displaying the lowest values in the aforementioned parameters. Conversely, the La Cumbita lava flow has the largest area, while the Cerro Sanabria lava flow shows the largest volume and average thickness values (Table 3; Table S1).

Stratigraphy and Geochemistry of the Volcanic Landforms of the Valle de Santiago Area

Based on new twenty-four $^{40}Ar/^{39}Ar$ and sixteen radiocarbon dates (Tables 1 and 2; Figures 2, 3, and 4; Figures S1 and S2), along with $^{40}Ar/^{39}Ar$ and $^{40}K/^{40}Ar$ ages from previous works (e.g., Murphy, 1986; Ban et al., 1992; Hasenaka and Carmichael, 1985b; Rincón-Herrera, 2005; Aranda-Gómez and Carrasco-Núñez, 2014), stratigraphic correlations, morphological features (e.g., depth of erosion channels, fault development, smooth surfaces, soil thickness), and morphometric parameters (Table S1), we established the chronological sequence for the volcanic landforms found in the VS area. It is important to mention that our Ar-Ar ages greater than 1 Ma, quoted as ka, are high-precision ages that are on the order of hundreds of years (e.g., 2415.8 ± 13.7 ka; see Table 1). Furthermore, for each epoch, we present the geochemical characteristics of the volcanic products associated with various structures. The geochemical results obtained in this study were complemented with data from previous works conducted by Murphy (1986), Ortega-Gutiérrez et al. (2014), Losantos (2017), and Losantos et al. (2017) (Table S2).

In terms of total alkalis versus silica content (TAS diagram; Figure 8A), rocks within the VS area exhibit a significant compositional diversity (46.65 to 75.03 wt.% SiO_2) and include basalts/trachybasalts (13.9 vol.%), basaltic andesites/basaltic trachyandesites (51.8 vol.%), andesites (32.9 vol.%), and a few trachyandesites (0.9 vol.%), and rhyolites (0.4 vol.%). Furthermore, these rocks belong to both the sub-alkaline and alkaline series with alkali contents varying from 4.25 to 10.09 wt.%. A map showing the spatial distribution of the different rock-types within the VS area is shown in Figure 9.

Miocene Volcanism

Miocene volcanism within the VS area is represented by the Cerro Sanabria and Panales Jamaica lava flows and the Cerro Comaleros shield volcano. These three volcanoes crop out north-northwest and east of the study area, near Irapuato, Salamanca, and Salvatierra, and they appear to form a lineament with an NW-SE orientation. These volcanoes are incomplete structures cut by NE-SW faults, resulting in linear and prominent cliffs (Figure 2). Cerro Sanabria was dated by $^{40}Ar/^{39}Ar$ at 8.09 ± 0.04 Ma (Plateau age: Table 1; Figures 2 and 4A), and even though Panales Jamaica and Cerro Comaleros were not dated, their morphological similarities with Cerro Sanabria suggest that they also originated during the Miocene. Furthermore, these volcanic structures collectively account for an estimated volume of erupted material of 1.58 km^3 (Table 3).

The rocks of these volcanoes have basaltic andesitic (67.15 vol.%) and basaltic (32.85 vol.%) compositions with silica contents ranging from 50.73 to 55.20 wt.%. Likewise, they belong to the sub-alkaline series (Table S2; Figures 8 and 9).

Pliocene Volcanism (5 to 2 Ma)

Pliocene volcanism within the VS area is predominantly concentrated in the northeastern-eastern region, with only a few structures found in the northern and central parts (Figure 2). This volcanism is characterized mainly by effusive activity, resulting in the construction of some shield volcanoes (such as Cerro Gordo, Cerro Tendido, Cerro Grande, and Cerro Culiacán), and to a lesser extent by explosive activity with the formation of a few scoria cones (such as Santa Teresa, Cerro Colorado-III, El Diezmo, El Potrerillo, Cerro Sotelo, El Vellanco, Los Lobos, and Cerrito Colorado-II). Some of these volcanoes are aligned with an NE-SW orientation, although in general, the distribution of the volcanoes in the area appears to follow an NW-SE orientation (Figure 2).

The oldest dated volcano is Cerro Gordo shield volcano (Plateau age: 4.87 ± 0.02 Ma; this study), followed by Cerro Tendido shield volcano (Plateau age: 4.00 ± 0.04 Ma; this study), Cerro Grande shield volcano (Inverse isochron age: 3.08 ± 0.05 Ma; this study – 2.27 ± 0.27 Ma; Ban et al., 1992), Santa Teresa scoria cone (2.78 ± 0.07 Ma; Hasenaka and Carmichael, 1985b), and Cerro Culiacán shield volcano (Mini-plateau age: 2415.8 ± 13.7 ka; this study – 2.10 ± 0.24 Ma; Ban et al., 1992) (Table 1; Figures 2, 3, 4A; Figure S1). Furthermore, likely, Cerro Colorado-III, El Diezmo, El Potrerillo, Cerro Sotelo, El Vellanco, Los Lobos, and Cerrito Colorado-II scoria cones erupted in the same timeframe as the Cerro Grande shield volcano. Although these scoria cones lack radiometric dating, their smoothed morphologies, gentle slopes (with average slope values ranging from 4.5° to 6.0°), and the significantly low values observed in their Hco/Wco ratios, ranging from

0.032 to 0.045 (Figure 7A; Table S1), suggest that these scoria cones have been subjected to advanced degrees of erosion, which could support the hypothesis of their Pliocene age.

The total volume of emitted material during the Pliocene was estimated at 68.30 km^3 (Table 3). Of this volume, 67.75 km^3 belongs to shield volcanoes, while only 0.543 km^3 corresponds to the scoria cones.

The chemical composition of the Pliocene rocks within the VS area comprises mainly andesites (69.03 vol.%), followed by basaltic andesites (30.53 vol.%), and only a few basaltic trachyandesites (0.44 vol.%), with silica contents ranging from 52.29 to 59.37 wt.%. Likewise, all the rocks belong to the sub-alkaline series (Figures 8 and 9; Table S2).

Outside the VS area, towards the south within the Sierra de Piñícuaro, lies a cluster of shield volcanoes that are strongly affected by NE-SW and ENE-WSW faults (Figure 2). One of these shield volcanoes (Blanco) was dated by ^{40}Ar/^{39}Ar at 2974.6 ± 27.6 ka (Plateau age: Table 1; Figure 2; Figure S1), hence it formed contemporaneously with the Cerro Grande volcano. Blanco shield volcano displays a volume of 1.93 km^3 (Table 3; Table S1). Furthermore, it exhibits a basaltic andesitic composition, with a silica content of 55.57 wt.%, and belongs to the sub-alkaline series (Figures 8 and 9; Table S2).

Early Pleistocene Volcanism (2 to 1 Ma)

In the Early Pleistocene, volcanic activity in the VS area resulted in the formation of various shield volcanoes and scoria cones, as well as a few lava plateaus and lava domes. These volcanic landforms are mainly distributed in the northern and southern regions of the study area, in the surroundings of Salamanca and Yuriria cities, while only a few structures are situated in the central part (Figure 2). In addition, the distribution of these landforms seems to be random without forming any significant linear pattern, although some volcanoes seem to be aligned with E-W and NE-SW orientations (Figure 2).

The chronological sequence of the volcanic landforms in the VS area during the Early Pleistocene has been established as follows: the oldest known volcano is Cerro La Tetilla shield, which has been dated by $^{40}Ar/^{39}Ar$ at 1.83 ± 0.02 Ma (Plateau age: Table 1; Figures 2 and 4B). Subsequently, in the southern region of the VS area, the La Cumbita lava plateau, the scoria cones that overlie it (Scoria cone-2, San Miguelito, Scoria cone-3, and Parangarico), the Lava Plateau-2, the Scoria cone-4, and the Buena Vista shield volcano, were probably erupted before the emplacement of the El Capulín shield volcano dated by $^{40}Ar/^{39}Ar$ at 1.44 ± 0.02 Ma (Plateau age: Table 1; Figures 2 and 4B). Then, in the central part of the study area, the El Varal shield volcano formed between 1412.8 ± 34.3 and 1046.9 ± 6.1 ka (both are inverse isochron ages; Table 1), followed by the Viejo de Torres scoria cone, which is located on the lower southeastern slope of the aforementioned shield volcano, and the Benito Juárez scoria cone dated by $^{40}K/^{40}Ar$ at 1.18 ± 0.17 Ma (Murphy, 1986). Later, towards the southern region of the VS area once again, Cerro Santiago shield volcano was emplaced, yielding $^{40}Ar/^{39}Ar$ ages ranging from 1017.6 ± 39.8 to 990.3 ± 3.4 ka (Inverse isochron and plateau ages: Table 1; Figures 2 and 4B; Figure S1).

It is worth mentioning that the oldest age of the El Varal shield volcano (1412.8 ± 34.3 ka; Table 1; Figure S1), the age of Benito Juárez scoria cone (1.18 ± 0.17 Ma; Murphy, 1986), and the youngest age of Cerro Santiago shield volcano (990.3 ± 3.4 ka; Table 1; Figure S1) were determined on samples collected from lava flows that are exposed on the inner crater walls of Joya de Álvarez, Joya San Nicolás, and Joya de Yuriria maars, respectively (Figure 2). The correlation between these samples with the lavas from the shield volcanoes was determined by comparing their trace and rare earth element concentrations in a multi-element diagram normalized with respect to the primitive mantle of Sun and McDonough (1989), where they present similar patterns (Figure 8B). Furthermore, the correlation between the Benito Juárez scoria cone and the sample from the inner crater wall of Joya San Nicolás maar was established through topographic profiles, revealing that the northward-flowing lavas associated with Benito Juárez were cut by this phreatomagmatic volcano.

Certain volcanic structures are identified as possible Early Pleistocene volcanoes despite lacking radiometric dating and clear stratigraphic relationships with other structures. These include Cerro Tetillas and La Angostura shield volcanoes, as well as the Los Cuates lava dome situated in the southeast and center of the VS area, along with San Guillermo shield volcano and Cerro La Cruz, Las Antenas, and Peña Colorada scoria cones that are distributed to the north of the study area (Figure 2; Figure S3). To figure out the relative age of these structures, various characteristics were taken into consideration. The scoria cones associated with the Early Pleistocene display relatively gentle slopes (5.8° to 10.6°) and relatively low Hco/Wco ratios (0.038 to 0.091) (Figure 7A; Table S1). These values are higher than those observed in Pliocene cones, implying a younger age for these scoria cones. Regarding Cerro La Cruz, Las Antenas, and Peña Colorada scoria cones, it is likely that they were formed contemporaneously with the cones found in the southern region of the study area (e.g., San Miguelito scoria cone) or possibly even more recently. However, due to the low degree of preservation of these cones, it is difficult to establish a more precise stratigraphic position for them. The morphologies of San Guillermo and Cerro Tetillas shield volcanoes closely resemble that of the Cerro La Tetilla shield volcano (dated at 1.83 Ma; Table 1). However, these volcanoes exhibit fewer and shallower erosion channels compared to Cerro La Tetilla (Figure 2), suggesting a younger age estimated to be ~1 Ma. Furthermore, with the aid of shaded terrain models, it is evident that the La Angostura shield volcano acted as a topographic barrier for the southward movement of the lava flows originating from the Cerro Blanco shield volcano, which has been assigned a Middle Pleistocene age (Figure 2), suggesting an older age for the La Angostura volcano (probably Early Pleistocene). In addition, the Los Cuates lava dome is observed cutting the Cerro Tendido shield volcano of Pliocene age, suggesting a relatively younger age for the Los Cuates dome (Figures 2 and 3).

Considering all the aforementioned volcanic landforms, the total volume of emitted material during the Early Pleistocene was estimated at 11.88 km^3 (Table 3). Of this volume, 11.33 km^3 corresponds to the shield volcanoes, 0.32 km^3 belongs to the lava plateaus, 0.17 km^3 accounts for the scoria cones, and only 0.06 km^3 was attributed to a lava dome.

The Early Pleistocene rocks present a range in silica content of 48.16 to 61.19 wt.% (Figure 8A; Table S2). These rocks are sub-alkaline andesites (81.96 vol.%) and basaltic andesites (16.63 vol.%), as well as alkaline trachybasalts (1.10 vol.%) and basaltic trachyandesites (0.30 vol.%) (Figures 8 and 9).

Outside the VS area, within the Sierra de Piñícuaro, another highly fault-affected shield volcano named El Comal has been dated by $^{40}Ar/^{39}Ar$ at 1760.9 ± 11.3 ka (Plateau age: Table 1; Figure 2; Figure S1). This age places its formation after the Cerro La Tetilla shield volcano but before the El Capulín shield volcano. El Comal shield volcano has a volume of 5.3 km^3 (Table S1) and exhibits a sub-alkaline andesitic composition with a silica content of 58.71 wt.% (Figures 8 and 9; Table S2).

Middle Pleistocene Volcanism (1 Ma to 100 ka)

During the Middle Pleistocene, volcanism within the VS area was characterized by both, effusive and explosive activity, resulting in the formation of a variety of volcanic landforms such as shield volcanoes, lava flows, lava domes, a pair of phreatomagmatic volcanos (La Ciénega and Santa Rosa tuff rings), and scoria cones, some of which produced lava fields.

These volcanic landforms are distributed throughout the western region of the VS area, with the central-western part showing the highest concentration of volcanic structures and also the most voluminous ones (Figure 2).

The volcanic activity in the Middle Pleistocene began with the nearly simultaneous formation of three shield volcanoes: El Picacho (987.1 ± 33.9 ka; Plateau age), Cerro Prieto (994.0 ± 15.0 to 862.8 ± 11.0 ka; Inverse isochron, mini-plateau, and plateau ages), and Cerro Chapín (899.7 ± 4.1 ka; Plateau age) (Table 1). Following this, the Guantes lava flow was emplaced before the formation of the Guantecillos scoria cone, dated at 844.2 ± 11.1 ka (Inverse isochron age; Table 1). Subsequently, the development of three additional shield volcanoes occurred: Cerro Blanco (806.4 ± 26.0 ka; Plateau age), El Tule (793.9 ± 3.1 ka; Inverse isochron age), and La Cruz (645.1 ± 3.3 ka; Mini-plateau age) (Table 1; Figures 2, 3, and 4C; Figure S1). Much later, a lava flow exposed within the inner crater wall of Joya La Alberca maar was emplaced between 250 ± 20 ka (Rincón-Herrera, 2005) and 146.4 ± 13.9 ka (Plateau age: Table 1; Figures 3 and 4C). Within this timeframe, the formation of the Ranchos Unidos scoria cone took place at 190 ± 44 ka (Murphy, 1986). Finally, the Santa Rosa tuff ring originated at 137 ± 90 ka (Aranda-Gómez and Carrasco-Núñez et al., 2014).

Several volcanic landforms lacking radiometric ages can be assigned to the Middle Pleistocene by evaluating their stratigraphic position and morphometrical characteristics. The location of several scoria cones, lava domes, and fissure-fed lava flows (El Cerrito, Cerro Blanco-II, Cerro Perimal, and El Colloncle lava domes, Paredones and La Compañía lava flows, and Cerro El Olivo, Cerro Quemado, El Sombrero, Cerritos-1, Cerritos-2, Cerritos-3, Scoria cone-1, Scoria cone-5, Scoria cone-6, Scoria cone-7, El Copalar, Cerro Colorado-IV, Scoria cone-9, Scoria cone-10, El Desmonte, El Bonete, San Jerónimo, Mandinga, San Roque, and La Chonchita scoria cones) over the slopes of some Pliocene (Cerro Grande), Early Pleistocene (San Guillermo and Buenavista), and Middle Pleistocene shield volcanoes (El Picacho, Cerro Prieto, Cerro Chapín, and Cerro Blanco), or below Late Pleistocene volcanic products, suggests an age range younger than ~800 ka but older than the Late Pleistocene for all these structures (Figures 2 and 3; Figure S3). Additionally, these scoria cones, exhibit steeper slopes (>7°) and higher Hco/Wco ratios (>0.06) than the Early Pleistocene cones, as well as gentler slopes (<18.4°) and lower Hco/Wco ratios (<0.13) in comparison with those formed during the Late Pleistocene (Figure 7A; Table S1). Furthermore, in the northwestern and southern regions of the VS area, several isolated volcanic landforms are located on the fluvio-lacustrine plain and do not exhibit any stratigraphic relationship with other nearby structures (such as El Tambor, Cerro Juan Diosdado, Cerrito Colorado, San Andrés, Cerro San Pedro, Las Jícamas, Cerro Colorado, Cerro Colorado-II, Cerro La Cruz-II, and Cerro Cupareo scoria cones, Palo Blanco and Enguaro lava domes, La Ciénega tuff ring, and Cerro Prieto-II shield volcano) (Figures 2 and 3; Figure S3). In all of these cases, the morphometric parameters of the scoria cones, which fall within the general ranges assigned to the Middle Pleistocene (average slope angles ranging from 6.7 to 21.6° and Hco/Wco ratios spanning from 0.058 to 0.184; Figure 7A; Table S1), and the tenuous expression of the surface morphologies of the lava flows (e.g., levees and flow channels associated with the Cerro Juan Diosdado scoria cone and the Cerro Prieto-II shield volcano; Figure 2; Figure S3) suggest that they probably also belong to the Middle Pleistocene.

It is important to highlight that the ages of certain shield volcanoes were determined by analyzing lava samples that are exposed at the inner crater walls of some of the younger maars that lie within the VS area (Table 1; Figure 3). Two ages attributed to Cerro Prieto shield volcano (993.8 ± 10.4 ka and 862.8 ± 11.0 ka; Table 1; Figure 3; Figure S1) were obtained from lava samples collected at the inner crater walls of Joya de Álvarez and Joya Cíntora maars. To test whether these crater samples indeed correspond to the Cerro Prieto shield, we compared their trace and rare earth element patterns, which display remarkable resemblances in a multi-element diagram (Figure 8C). The age assigned to Cerro Chapín shield volcano (899.7 ± 4.1 ka; Table 1; Figure 3; Figure S1) was obtained on a lava sample exposed at the inner crater wall of Joya Solís maar. In this case, there is no evident correlation between the trace and rare earth element patterns of a bomb sample collected from the scoria cone crowning the Cerro Chapín shield, and the lava sample taken from the lava exposed in the Joya Solís crater. The trace element geochemistry of this lava sample does not match that of the neighboring El Picacho and Cerro Prieto shields (Figure 8C). Nevertheless, from a topographic profile, it is clear that Joya Solís maar is emplaced on the northern slope of Cerro Chapín shield, where it cuts into its lavas. This observation strengthens our assumption that the lavas of Cerro Chapín are the ones exposed at the inner crater walls of Joya Solís maar. The age of El Tule shield volcano (793.9 ± 3.1 ka; Table 1; Figure 3; Figure S1) stems from a lava sample collected at the inner crater wall of Joya de Álvarez maar. In this case, we lack geochemical data to establish a correlation between El Tule and the inner crater sample. However, since this lava does not exhibit any geochemical resemblances to El Varal, El Picacho, Cerro Prieto, and Cerro Chapín shield volcanoes, we propose that it belongs to the El Tule shield volcano (Figure 8C). This would also be consistent with the older ages determined for the aforementioned shield volcanoes and with the stratigraphic position of El Tule, which indicates a younger age than that of its neighbors. The Cerro La Cruz shield volcano was partially destroyed by the emplacement of four phreatomagmatic volcanoes, namely La Mina Norte, La Mina Sur, Joya Rincón de

Parangueo, and Santa Rosa whose pyroclastic deposits cover most of its remnants. However, it is still possible to find a few exposures of its lava flows at various sites along the inner crater wall of Joya Rincón de Parangueo maar. A sample from one of these remnant lavas was dated by $^{40}Ar/^{39}Ar$ at 645.1 ± 3.3 ka (Table 1; Figure 3; Figure S1). Lava remnants from different sites were geochemically correlated, showing similar trace and rare earth element patterns in a multi-element diagram (Figure 8C).

The total volume emitted during the Middle Pleistocene was estimated at 24.02 km^3 (Table 3). Of these, 20.65 km^3 correspond to shield volcanoes, 2.31 km^3 to scoria cones and associated lava flows, 0.72 km^3 to domes, 0.24 km^3 to fissure-fed lava flows, and only 0.094 km^3 to the pair of phreatomagmatic volcanoes.

The Middle Pleistocene rocks have a silica content that ranges from 48.56 to 61.03 wt.% with chemical compositions dominated by basaltic andesites + basaltic trachyandesites (84.42 vol.%), followed by andesites (10.73 vol.%), and with lesser occurrences of trachyandesites (4.36 vol.%) and trachybasalts (0.49 vol.%) (Figures 8 and 9; Table S2). Furthermore, they classify within both, the alkaline and sub-alkaline series (Figure 8; Table S2).

Late Pleistocene Volcanism (100 to 11 ka)

In the Late Pleistocene, volcanic activity in the VS area was dominated by phreatomagmatism, resulting in the formation of numerous tuff rings (Sanabria, San Roque West, San Roque East, La Mina Norte, La Mina Sur, Joyuela, Joya Estrada, Magdalena de Araceo, Isla de San Pedro) and maars (Joya Rincón de Parangueo, Joya San Nicolas, Joya La Alberca, Joya Solís, Joya Címtora, Joya de Álvarez, Joya de Yuriria), as well as a few tuff cones (Joya Blanca, Providencia de Cuerunero, Joyuela de San Vicente). This phreatomagmatic activity was accompanied by both, explosive and effusive magmatic events leading to the formation of one lava dome (La Mina) and several scoria and spatter cones (El Tule-II, Cerro Prieto-III, Buenavista, La Batea, Blanca, Viejo, Cerro Poruyo, Cerro Las Silletas, La Alberca spatters-1 and 2, Los Molina), the majority of which produced lava fields. This volcanism is distributed along the western sector of the VS area, forming a clear lineament that extends ~52 km in an NW-SE orientation, between the cities of Irapuato and Yuriria (Figure 2). Many of these volcanic landforms formed on the lower slopes of shield volcanoes and lava flows, while others were emplaced on the fluvio-lacustrine plain.

To establish the chronological sequence for the Late Pleistocene, we combined radiocarbon ages (Table 2; Figure 3; Figure S2), stratigraphic and cross-cutting relationships, morphological observations (Table S1), as well as componentry analysis. Radiocarbon ages mentioned in the text are conventional ages denoted in years before present (yr BP). Morphologically, Late Pleistocene scoria cones exhibit the steepest slopes (ranging from 12 to 21°) and the higher Hco/Wco ratios (0.077 to 0.187; Figure 7A). Furthermore, lava flows associated with some scoria cones exhibit well-preserved surface morphologies, such as levees and flow channels (Cerro Prieto-II, Cerro Las Silletas, and Cerro Poruyo scoria cones) (Figure 2). Considering the above, the oldest Late Pleistocene landforms are likely El Tule-II scoria/spatter cone together with San Roque West, San Roque East, Sanabria, Isla de San Pedro, and La Mina Norte tuff rings. Subsequently, in the central-western region of the VS area, the La Mina Sur tuff ring and La Mina dome erupted, followed by Joya San Nicolás maar and La Batea (dated at >43,500 yr BP), Buenavista, and Viejo scoria cones. Then, Joya Cíntora erupted around 31,960 ± 220 yr BP (Table 2; Figure 3; Figure S2), probably around the same time as Joya de Yuriria maar and Cerro Poruyo scoria cone to the south of the study area. Next, Magdalena de Araceo tuff ring erupted between 28,290 ± 130 and 27,540 ± 120 yr BP (Table 2; Figure 3; Figure S2), while Joya Rincón de Parangueo maar, Blanca scoria cone, Joya Estrada, and Joyuela tuff rings were emplaced before Joya Solís maar, which was dated at 24,990 ± 100 yr BP (Table 2; Figure 3; Figure S2). In the case of Joya Estrada tuff ring, it was established that it is older than Joya Solís maar through a component analysis, where juvenile components (pumice fragments) from Joya Estrada were found within the pyroclastic deposits of Joya Solís. Subsequently, La Alberca spatters-1 and 2, together with their associated lava flows, and Joya Blanca tuff cone and Joya La Alberca maar were emplaced contemporaneously between 23,170 ± 90 and 20,960 ± 70 yr BP (Table 2; Figure 3; Figure S2). Finally, the Los Molina spatter cone and its associated lava flow, Cerro Prieto-III scoria/spatter cone, Cerro Las Silletas scoria cone, as well as Joyuela de San Vicente and Providencia de Cuerunero tuff cones were probably formed within the same timeframe as Joya de Álvarez maar, dated between 18,800 +225/-220 and 11,090 ± 40 yr BP (Table 2; Figure 3; Figure S2).

The total volume of material emitted during the Late Pleistocene was estimated at 5.05 km^3 (Table 3). Of these, 3.14 km^3 correspond to scoria and spatter cones and their associated lava flows, 1.90 km^3 to phreatomagmatic volcanoes (with an average of 0.11 km^3 and a median of 0.054 km^3), and only 0.017 km^3 to the lava dome.

The chemical composition of the Late Pleistocene rocks exhibits a wide variability ranging from basalts-trachybasalts to rhyolites (46.65 to 75.03 wt.% SiO_2) with a notable absence of dacites-trachydacites (Figure 8A). Among them, the predominant compositions are basaltic andesites + basaltic trachyandesites (59.60 vol.%), followed by basalts + trachybasalts (35.24 vol.%), andesites (3.0 vol.%), and rhyolites (2.15 vol.%). Furthermore, these rocks belong to both, the alkaline and sub-alkaline series.

Petrography

Petrographic analyses of the juvenile samples from representative magmatic and phreatomagmatic structures within the VS area were conducted following the rock-type classification of the TAS diagram (Figure 8A). The different minerals identified are mentioned in the text in order of decreasing abundance.

In general, mafic and intermediate rocks (basalts, trachybasalts, basaltic andesites, trachybasaltic andesites, andesites, and trachyandesites) exhibit porphyritic, glomeroporphyritic, interstitial (both intergranular and intersertal), seriate, and vesicular textures (Figure 10A-E), along with the occurrence of two distinct crystal populations. The first population comprises megacrysts (ranging in size from >1.5 mm to <2 cm) of plagioclase, clinopyroxene, olivine, feldspar, quartz, and opaque minerals (Figure 10A, B). They typically show disequilibrium textures such as embayments, corrosion gulfs, reaction coronas, and sieve textures, as well as exsolution lamellae (Figure 10C). They can be found either as isolated crystals or forming mineral clots (Figure 10B, C), and occasionally contain zircon and apatite inclusions. The second crystal population includes subhedral and euhedral phenocrysts (<1.5 mm) and micro-phenocrysts of plagioclase, olivine, clinopyroxene, oxides, amphibole, and orthopyroxene (Figure 10A, B, D, E), and its presence and abundance depend on the rock-type. In basalts and trachybasalts the typical mineral assemblage is plagioclase, olivine, clinopyroxene, and to a lesser extent, oxides (Figure 10A, B). In basaltic andesites and trachybasaltic andesites, the mineralogy includes plagioclase, clinopyroxene, olivine, oxides, amphibole, and to a lesser extent, orthopyroxene. Amphibole is present in samples from some scoria cones (La Chonchita, Cerrito Colorado, and Blanca) and phreatomagmatic volcanoes (Sanabria and Santa Rosa tuff rings), exhibiting anhedral shapes along with opacite rims of variable thicknesses (between 8 and 300 µm) (Figure 10D). Andesites and trachyandesites are composed of a mineral assemblage of plagioclase, orthopyroxene, clinopyroxene, olivine, and oxides (Figure 10E). Both crystal populations are embedded in a fine-to-medium grained interstitial-textured groundmass (Figure 10A) or a fine-grained groundmass made of glass, plagioclase and oxides microlites, tabular-acicular and dendritic crystallites, and vesicles (Figure 10B, D, E). The latter vary both in shape and size, depending on whether the sample was formed by magmatic or phreatomagmatic activity. In general, rocks formed by phreatomagmatic activity exhibit small and irregular vesicles, while those formed solely by magmatic activity show larger, round, oval, and coalescent vesicles. In a few samples, vesicles are partially filled by secondary minerals produced by precipitation from meteoric water percolating through the rock (Figure 10D). It is worth noting that megacrysts are more abundant in the juvenile products from certain Late Pleistocene phreatomagmatic volcanoes (Magdalena de Araceo tuff ring, and Joya Rincón de Parangueo, Joya Cíntora, and Joya de Álvarez maars) and scoria cones (La Batea and Buenavista). The rocks of these volcanoes also commonly contain subrounded and subangular lithics and xenolith fragments. The lithics consist of lava fragments with interstitial and porphyritic textures, while the xenoliths stem from holocrystalline rocks. Pliocene and Miocene rocks do not have megacrysts, lithics, or xenoliths.

The petrographic characterization of the rhyolitic rocks was carried out on a pumice sample from the pyroclastic surge deposits of the Joya Estrada tuff ring, which exhibits a vitrophyric and vesicular texture (Figure 10F). The pumice has a very low crystal content consisting of micro-phenocrysts and phenocrysts of sanidine, plagioclase, quartz, and clots of the same minerals. These crystals are immersed in a groundmass of vesicular glass (Figure 10F). Vesicles are irregular and elongate due to the conduit's flow dynamics during their formation.

Xenoliths

An important feature of certain phreatomagmatic volcanoes of the VS area (e.g., Magdalena de Araceo tuff ring and Joya Rincón de Parangueo, Joya Cíntora, and Joya de Álvarez maars) is the occurrence of holocrystalline xenoliths within their pyroclastic products. These xenoliths come in various shapes and sizes and have different mineral assemblages. In hand specimens, the xenoliths typically exhibit subangular and to a lesser extent subrounded shapes (Figure 10G). They are mesocratic to leucocratic in color, present a phaneritic texture, and their grain size ranges from medium to coarse (0.1 to 5.5 cm) (Figure 10G). Most are surrounded by a thin crust of juvenile magma which varies in thickness from <1 mm to up to 5 cm (Figure 10G). Moreover, some xenoliths exhibit a banded pattern given by changes in grain size and mineralogy. Common minerals in the xenoliths are plagioclase, olivine, pyroxene, opaque minerals with a metallic luster, quartz, and biotite. Irregular and rounded voids varying in size from <1 mm to 1 cm can also be observed within the xenoliths. Under the microscope, it was possible to identify at least five different types of xenoliths based on their mineralogy. The first type is usually medium-to-coarse grained and consists of xenomorphic crystals of clinopyroxene, olivine, plagioclase, and opaque minerals (Figure 10H). The second type is coarse-grained, hypidiomorphic, has a cumulate texture, and consists of plagioclase, olivine, and clinopyroxene crystals (Figure 10I). The third type is medium-to-coarse grained and composed of hypidiomorphic-xenomorphic crystals of plagioclase, orthopyroxene, clinopyroxene, feldspar, and to a lesser extent olivine, opaque minerals, and amphibole (Figure 10J). The fourth type is medium-to-coarse grained, hypidiomorphic, and has plagioclase, clinopyroxene, apatite, deformed (crenulated) biotite, opaque minerals, and olivine. Apatite occurs as phenocrysts or as inclusions in plagioclases and opaque minerals (Figure 10K). The fifth type of xenolith is fine-to-medium grained and consists of xenomorphic crystals of quartz, feldspar, and plagioclase displaying intergrowth textures (coarse-grained perthite) in some parts of the rock (Figure 10L), while in other parts the texture is granular.

In the first three types of xenoliths, it is common to find poikilitic and subophitic textures, which are characterized by centimetric crystals of pyroxene (ortho and clinopyroxene) and plagioclase that fully or partially enclose millimetric crystals of olivine, plagioclase, and pyroxene. Additionally, most xenoliths are observed with glass and vesicles (round and oval), and the minerals often show evidence of disequilibrium and metamorphism (polygonal texture), as well as oxidation.

DISCUSSION

Eruptive History

Between the Late Miocene and the Late Pleistocene, the VS area experienced intense volcanic activity characterized by a complex interplay of effusive and explosive (both magmatic and phreatomagmatic) eruptions. This activity led to the formation of a great variety of landforms including medium-sized shield volcanoes, scoria and spatter cones, fissure-fed lava flows, lava domes, tuff cones, tuff rings, and maars (Figure 11). Many of these volcanoes are aligned following two preferential orientations: ENE-WSW and NNW-SSE (Figures 2 and 11). These alignments run parallel to two principal fault systems prevailing in the region: first, the Morelia-Acambay fault system with an ENE-WSW orientation (Garduño-Monroy et al., 2009), and second, the Taxco-San Miguel de Allende fault system with an NNW-SSE orientation (Alaniz-Álvarez et al., 2002) (Figure 1). Between these two fault systems, the NNW-SSE had a greater influence, as it exerted significant control over the spatial arrangement of vent locations for many of the volcanic landforms within the VS area. This influence is particularly evident for the phreatomagmatic volcanoes, as they align along a distinctive stripe that extends for more than 50 km (Figures 2 and 11).

Our radiometric data reveals that the volcanic activity in the VS area follows an irregular temporal pattern (Figure 12). Activity began ~8 Ma ago during the Late Miocene in the northwest of the area (Figures 2 and 11; Table 1). During the Miocene, eruptions occurred sporadically and were exclusively effusive. This involved the repetitive ascent of small-volume magma batches (<0.7 km^3; Table 3) that emplaced lava flows, some of which accumulated to form shield volcanoes (e.g., Cerro Comaleros; Figure 2). It is important to note that part of the volcanism emitted during this period is likely buried either by fluvio-lacustrine sediments of the El Bajío basin or by younger volcanic activity, rendering the complete record of the Miocene volcanism inaccessible. In other regions of the MGVF, Miocene volcanic activity has been documented in the area northwest of Morelia (Figure 12), where a lava dome was $^{40}Ar/^{39}Ar$ dated at 6.7 Ma (Avellán et al., 2020). It has been proposed that this age marks the onset of volcanism in the MGVF; nevertheless, the ~8 Ma age reported in the present study indicates that the beginning of the volcanic history of the MGVF is older than reported in previous works (Guilbaud et al., 2011, 2012; Avellán et al., 2020). Our proposed onset of volcanic activity in the VS area (~8 Ma) also differs from previous studies (Murphy, 1986), which suggested that volcanism started 6.9 Ma ago with the formation of the Cerro Santiago shield volcano to the south of the VS area (Figure 2). In this study, a lava sample from this volcano was dated by the $^{40}Ar/^{39}Ar$ method, resulting in an Early Pleistocene age (1017.6 ± 39.8 ka; Table 1). We believe that this $^{40}Ar/^{39}Ar$ age is the correct one for the Cerro Santiago shield volcano since its morphology appears to be much younger in comparison to the Miocene and Pliocene shield volcanoes. These older volcanoes display deeper drainage channels (e.g., ~115 m for Cerro Culiacán versus ~35 m for Cerro Santiago) and/or are strongly dissected by faults (Figure 2).

After a long hiatus (~3 Ma), volcanism in the VS area resumed in the Pliocene at ~4.9 Ma (Figure 2; Table 1). Eruptions were less frequent at the beginning of the Pliocene but increased in frequency towards its end (Figure 12). Furthermore, volcanic activity was mainly focused on the east of the study area, where an effusive eruptive style dominated (Figures 2 and 11). This effusive volcanism involved large-volume magma batches resulting in the formation of voluminous shield volcanoes such as Cerro Grande and Cerro Culiacán (Table 3). In fact, the Cerro Grande shield volcano stands as the most voluminous among all the shield volcanoes within the entire MGVF (Hasenaka, 1994), with a volume of ~47 km^3 (Table 3). Also, during the Pliocene, small-volume magma batches ascended (~0.05 km^3) and produced a few scoria cones (e.g., Santa Teresa) (Figures 2 and 11; Table 3). In other regions of the MGVF such as the northwest of Morelia (Avellán et al., 2020), Pátzcuaro (Osorio-Ocampo et al., 2018), Tacámbaro-Puruarán (Guilbaud et al., 2012), and the Jorullo areas (Guilbaud et al., 2011), evidence for Pliocene volcanism is also present and follows a similar pattern of activity to that observed in the VS area, although the Jorullo area records the highest activity (Figure 12).

Volcanic activity continued in the Early Pleistocene, beginning ~1.8 Ma ago (Figure 2; Table 1). After this time, volcanic events increased in frequency, intensifying during the Middle Pleistocene, where eruptions occurred within close time intervals or even simultaneously (Figure 12; Table 1). During the Early to Middle Pleistocene, volcanic activity was concentrated primarily along the western sector of the VS area (Figures 2 and 11). Furthermore, the predominant eruptive style was effusive, giving rise to several shield volcanoes of considerable volume (e.g., El Picacho-Cerro Prieto; Table 3), as well as some lava flows and domes (Figure 11). Notably, Middle Pleistocene shield volcanoes are more voluminous compared to those formed in the Early Pleistocene (Table 3). In addition, during the Early-Middle Pleistocene, an increase in explosive volcanic activity led to the formation of various scoria cones (Figures 2 and 11). This activity was more intense in the Middle Pleistocene. However, it should be noted that this activity was not exclusively explosive since many of the scoria cones produced lava flows (Figures 2 and 11; Table S1). Unlike the Pliocene, which is characterized by predominantly effusive volcanic activity, the increase in explosive eruptions during the Early-Middle Pleistocene can be attributed to shifts in the local tectonic regime. These changes facilitated a more rapid and direct ascent of magmas from their mantle source to the surface, preventing them from stagnating in the upper crust and becoming degassed prior to eruption (Kereszturi and Nemeth, 2012a; Chevrel et al., 2016b; Reyes-Guzmán et al., 2018). In other regions of the MGVF such as the area NW of Morelia (Avellán et al., 2020), Pátzcuaro (Osorio-Ocampo et al., 2018), Zacapu (Reyes-Guzmán et al., 2018), and Tacámbaro-Puruarán (Guilbaud et al., 2012) the peak of volcanic activity occurred during the Middle Pleistocene (Figure 12). Conversely, during the Early Pleistocene, the Jorullo area exhibited the most intense activity (Figure 12).

In the Late Pleistocene, volcanism continued in the western sector of the VS area, but mainly along an NNW-SSE oriented stripe where a phreatomagmatic explosive eruptive style predominated (Figures 2 and 11). This eruptive style occurred in conjunction with both effusive and explosive magmatic activity (Figures 2 and 11) and differs from that observed in other regions of the MGVF, where phreatomagmatic activity is scarce (e.g., Zacapu, Pátzcuaro, and Tacámbaro-Puruarán areas; Reyes-Guzmán et al., 2018; Osorio-

Ocampo et al., 2018; Guilbaud et al., 2012) or nil (e.g., NW Morelia and Jorullo areas; Avellán et al., 2020; Guilbaud et al., 2011).

Previous studies (Murphy, 1986; Peñaloza-Turrubiates, 2005; Cano-Cruz and Carrasco-Núñez, 2008; Aranda-Gómez and Carrasco-Nuñez, 2014) have suggested with the aid of $^{40}K/^{40}Ar$ and $^{40}Ar/^{39}Ar$ dating that phreatomagmatic activity in the VS area occurred between approximately 1.2 Ma with the Joya San Nicolás maar eruption and 0.07 Ma with the Joya La Alberca maar eruption. However, our radiocarbon dating performed on paleosol samples directly underlying pyroclastic deposits from several of the phreatomagmatic volcanoes places their activity in the Late Pleistocene, between 32,000 and 11,000 yr BP (Figure 3; Table 2; Figure S2). Older, more eroded phreatomagmatic volcanoes exist in the north and south of the VS area (e.g., Sanabria, San Roque West, San Roque East, La Mina Norte, La Mina Sur, and Isla de San Pedro tuff rings, and Joya San Nicolás maar; Figure 2). Their morphologies indicate an older age for the onset of phreatomagmatism, yet not extending before the Late Pleistocene, except for La Ciénega and Santa Rosa tuff rings, whose degree of erosion, together with the age determination for Santa Rosa (137 ± 90 ka; Aranda-Gómez and Carrasco-Núñez, 2014) place these volcanoes to the end of the Middle Pleistocene (Figures 2 and 11). The discrepancy between the radiocarbon ages presented in this study and the $^{40}K/^{40}Ar$ and $^{40}Ar/^{39}Ar$ ages from previous works arises from the fact that the latter ages do not correspond to the age of the eruptive event. In certain instances (e.g., Joya La Alberca maar; Murphy, 1986), the reported ages stem from pre-existing lava flows that were cut by the phreatomagmatic volcanoes and are exposed in their inner crater walls, rather than from the juveniles in the pyroclastic deposits produced by the maars. In other cases (e.g., Joya San Nicolás and Joya Estrada maars; Murphy, 1986 and Cano-Cruz and Carrasco-Núñez, 2008, respectively), the $^{40}K/^{40}Ar$ and

^{40}Ar/^{39}Ar ages were derived from crystal concentrates separated from juvenile fragments that probably recorded a non-radiogenic Ar-excess, which is commonly found in young rocks (e.g., Gillespie et al., 1983; Ellis et al., 2017; Schaen et al., 2020). In addition, the relatively well-preserved morphologies of most of the phreatomagmatic volcanoes in the VS area resemble those of the nearby Zacapu basin (El Caracol tuff cone and Alberca de Guadalupe maar, dated at 28,300 and 21,000 yr BP, respectively; Kshirsagar et al., 2015; 2016). Since they were subjected to similar climate and erosional conditions, this would suggest that the phreatomagmatic volcanoes of the VS area may be contemporaneous with those of the Zacapu basin, further supporting our radiocarbon ages.

One distinctive feature within the VS area is the high concentration of phreatomagmatic volcanoes when compared to the rest of the MGVF. This means that the tectonic, hydrogeological, and climatic conditions necessary for the generation of phreatomagmatism were met in this region during the Late Pleistocene. The formation of phreatomagmatic volcanoes requires two basic ingredients: water (surficial or ground) and small-volume magma batches, as well as an optimal ratio of these two variables (water/magma ratio), which ranges between 0.1 and 0.3 (Sheridan and Wohletz, 1983). Evidently, in the VS area, the basic ingredients were available, and the optimal water/magma ratio was reached. However, a question arises: How were these ideal conditions achieved? Most phreatomagmatic volcanoes in the VS area are situated on the lower slopes of shield volcanoes (Figure 3). This fact suggests that the highly fractured lavas of these shields acted as aquifers. These aquifers must have had a high hydraulic gradient to supply groundwater relatively continuously to the eruption site (e.g., Kshirsagar et al., 2015, 2016; Siebe et al., 2016; Join et al., 2005). This phenomenon likely gave rise to purely phreatomagmatic eruptions (Kshirsagar et al., 2015; Siebe et al., 2016) forming structures such as Joya San Nicolás, Joya Rincón de Parangueo, Joya Solís, and Joya de Yuriria maars. In other cases, the water supply underwent significant changes during the eruption. As a result, phreatomagmatic activity was either immediately preceded or followed by magmatic activity. Cases where phreatomagmatic activity was preceded by magmatic activity, include Magdalena de Araceo tuff ring, Joya Cíntora, and Joya La Alberca maars, while cases where phreatomagmatic activity was followed by magmatic activity are Joya de Álvarez maar, Joya Blanca tuff cone, and La Mina Sur tuff ring. Furthermore, climate conditions prevailing at the end of the Late Pleistocene in the VS area could have also played an important role in the formation of phreatomagmatic volcanoes. Multi-proxy studies (involving radiocarbon dating and pollen, sediment geochemistry, ostracods, diatoms, stable isotopes, mineral magnetic properties, and total organic carbon analyses) carried out on sediment records of the lakes in the Zacapu basin (Ortega et al., 2002; Correa-Metrio et al., 2012) and the Joya de Yuriria and Joya Rincón de Parangueo maars (Holmes et al., 2016; Domínguez-Vázquez et al., 2019), revealed that climatic conditions during the Late Pleistocene (from 52,000 to 11,000 cal BP) were highly variable, characterized by rapid shifts between wet and dry periods because of the Late Quaternary glaciation. Despite this variability, key insights can be summarized as follows: between 52,000 and 27,500 cal BP, the climate in the study area was colder and wetter compared to present conditions (Ortega et al., 2002; Correa-Metrio et al., 2012; Holmes et al., 2016). From 27,500 to 11,000 cal BP, the climatic conditions were cold and dry with some fluctuations towards wetter conditions, especially during the Last Glacial Maximum (LGM) around 22,000 to 18,000 cal BP (Correa-Metrio et al., 2012; Holmes et al., 2016; Domínguez-Vázquez et al., 2019). Based on our radiocarbon ages (Table 2) and the stratigraphic position of the phreatomagmatic volcanoes, many of these structures erupted between 28,000 and 37,000 cal BP (e.g., Joya Cíntora, Magdalena de Araceo, Joya Solís) during a cold and wet climate. Fewer eruptions occurred between 27,000 and 25,000 cal BP (e.g., La Alberca-Joya Blanca) during a trend toward drier conditions, or during or shortly after the LGM (e.g., Joya de Álvarez) when a cold and wet climate dominated due to winter precipitation (Correa-Metrio et al., 2012; Dominguez-Vázquez et al., 2019). During the wetter conditions, it is likely that the climate was characterized by high annual precipitation (~ >1500 mm; Kshirsagar et al., 2016), favoring the saturation of fractured aquifers, providing enough water for the formation of phreatomagmatic volcanoes (Kshirsagar et al., 2015; 2016; Siebe et al., 2016).

Another important feature that characterizes the Late Pleistocene volcanism in the VS area is the presence of a wide variety of xenoliths (gabbros, felsic xenoliths) within the pyroclastic deposits associated with some of the phreatomagmatic volcanoes (e.g., Magdalena de Araceo tuff ring, and Joya Rincón de Parangueo, Joya Cíntora, Joya de Álvarez maars). These xenoliths are similar to those reported by Urrutia-Fucugauchi and Uribe-Cifuentes (1999) and Ortega-Gutiérrez et al. (2014) in the Joya Rincón de Parangueo and Joya Cíntora maars, who interpret them to either stem from basaltic cumulates that stagnated in the local lower crust, where they underwent metamorphism into granulite facies, or from a granitic crust formed during the Late Cretaceous (Ortega-Gutierrez et al., 2014). This crystalline basement is different from the one that seems to underlie the southern sector of the MGVF, which consists of Eocene-Oligocene granites and granodiorites (McBirney et al., 1987; Corona-Chávez et al., 2006; Guilbaud et al., 2011; Reyes-Guzmán et al., 2018).

It is important to point out that in contrast to other regions of the MGVF (e.g., Zacapu, Pátzcuaro, Jorullo, and Parícutin areas) where Holocene volcanic activity has been frequent, it is notably absent in the VS area. The youngest (historical) volcanic activity within the MGVF has occurred in its southern sector (Jorullo and Paricutin volcanoes), close to the current volcanic front of the TMVB (Ferrari et al., 2012), while the oldest ages are recorded in the north-central part of the MGVF (NW of Morelia; Avellán et al., 2020 and the Valle de Santiago areas), in regions further away from the volcanic front. Such a pattern does not necessarily suggest a southward migration of activity as postulated by Hasenaka and Carmichael (1985b), but rather an increase of intensity toward the south that could be explained by the peculiar dynamics (dip variations of the subducting Cocos Plate through time) of the subduction process (Manea et al., 2013). On the other hand, given the frequency of eruptions in the Late Pleistocene along the active NNW-SSE fault system (Alaniz-Álvarez et al., 2002; Suter and Morelos-Rodríguez, 2023), it seems premature to rule out future activity in the VS area. The observed Holocene hiatus might only be temporary, especially because the stress configuration seems not to have changed since the Late Pleistocene.

Compositional Variability

The rock-types found in the VS area are basalts, trachybasalts, basaltic andesites, basaltic trachyandesites, andesites, trachyandesites, and rhyolites (Figure 8A). Their relative proportions do not vary systematically with time (Figure 13), although basaltic andesites and andesites are the predominant compositions. Basaltic andesitic magmas erupted in all periods throughout the Late Miocene to the Late Pleistocene, with a peak in the Miocene, whereas the andesitic magmas were more abundant during the Pliocene and the Early Pleistocene. A greater diversity of magma types erupted in the Middle and Late Pleistocene when the sum of basaltic andesite and basaltic trachyandesite compositions predominated. During the Late Pleistocene, the sum of basaltic and trachybasaltic magmas was the second most abundant. The coalescence (or sum) of compositions (e.g., basaltic andesite + basaltic trachyandesite) is related to both, variations in composition within the same volcano (e.g., Cerro Chapín shield volcano and La Chonchita scoria cone; Table 3; Table S2) and to overlapping volcanic structures whose total volumes were calculated as belonging to a single structure (e.g., El Picacho and Cerro Prieto shield volcanoes; Table 3; Figure 9). Rocks with basaltic compositions were produced during the Miocene and Late Pleistocene but are absent in the Pliocene and Early and Middle Pleistocene. Basaltic trachyandesitic eruptions were scarce in the Pliocene and Early Pleistocene but became more frequent in the Middle and Late Pleistocene. Trachyandesites, trachybasalts, and rhyolites are the least common compositions within the VS area, with only subordinate eruptions during the Early and Middle Pleistocene for the two mafic compositions and during the Late Pleistocene for the rhyolites. An important feature in the VS area is the absence of dacitic compositions (Figure 8A) in comparison to other regions in the MGVF where they abound such as Zacapu (Reyes-Guzmán et al., 2018), Pátzcuaro (Osorio-Ocampo et al., 2018), and Tacámbaro-Puruarán (Guilbaud et al., 2012) or even to other monogenetic volcanic fields in the TMVB (e.g., Sierra de Chichinautzin; Wallace and Carmichael, 1999; Meriggi et al., 2008), where this type of magma is quite common.

Regarding the magmatic affinity of the rocks, the sub-alkaline series dominates through time (Figure 13). Nevertheless, alkaline compositions first appeared in the Early Pleistocene with subordinate eruptions and then increased their frequency in the Late Pleistocene, constituting nearly half of the total erupted volume during this period (Figure 13). Notably, the VS area stands out as the region with the highest occurrence of alkaline volcanism within the entire MGVF (Losantos et al., 2017; Torres-Sánchez et al., 2022). This concentrated alkaline volcanism in the northern sector of the MGVF, situated far behind the present-day volcanic front, and its increase during the Late Pleistocene, can be attributed to crustal extension in the backarc region. This extension can be related to a rollback process of the Cocos plate, which started in the Early Pleistocene (Johnson et al., 2009). Such a geodynamic process generates magmas via decompression melting of an OIB-like source poor in volatiles (Johnson et al., 2009). An alternate hypothesis to explain the coexistence of alkaline and sub-alkaline magmas in the VS area suggests that by the Late Pleistocene, a slab window or disruption in the Cocos plate had developed, which facilitated the ascent of OIB melts (Losantos et al., 2017).

Eruption Rate

From the Late Miocene, ~8 Ma ago, to the Late Pleistocene, ~11 ka ago, volcanism in the VS area produced a minimum volume of 111 km^3, which erupted at different rates through time (Table 3). Taking into account the volume of erupted material for each period, we calculated a minimum eruption rate (km^3/ka) of 0.0005 for the Late Miocene (8-5 Ma), 0.023 for the Pliocene (5-2 Ma), 0.012 for the Early Pleistocene (2-1 Ma), 0.027 for the Middle Pleistocene (1 Ma-100 ka), and of 0.057 for the Late Pleistocene (100-11 ka) (Table 3; Figure 13). The total eruption rate for the VS area (excluding the Miocene) is 0.016 km^3/ka. This value is lower in comparison to the eruption rate of 0.36 km^3/ka reported by Hasenaka (1994) for the entire MGVF but is higher when compared to the Pátzcuaro area (0.005 km^3/ka; Osorio-Ocampo et al., 2018). Both, the MGVF and Pátzcuaro regions span from the Pliocene to the Holocene. On the other hand, for the last one million years, Osorio-Ocampo et al. (2018), Guilbaud et al. (2012), and Reyes-Guzman et al. (2018) reported eruption rates of 0.013, 0.017, and 0.042 km^3/ka for the Pátzcuaro, Tacámbaro-Puruarán, and Zacapu regions, respectively. Within this context, the eruption rate in the VS area for the last one million years (0.029 km^3/ka) is higher than in Pátzcuaro and

Tacámbaro-Puruarán, but lower than in Zacapu. For comparative reference, Hasenaka (1994) reported an eruption rate of 0.7 km^3/ka over the last one million years for the entire MGVF.

CONCLUSIONS

Geological mapping of the VS quadrangle (2800 km^2) in the northeastern sector of the MGVF, allowed the identification of 118 monogenetic volcanoes. These include 61 scoria and spatter cones with or without associated lava flows (5.6 vol.%), 21 phreatomagmatic volcanoes (1.8 vol.%), 20 shield volcanoes (90.6 vol.%), 8 lava domes (0.7 vol.%), and 8 fissure-fed lava flows (1.3 vol.%).

New $^{40}Ar/^{39}Ar$ and ^{14}C radiometric dating revealed that volcanism in the VS area started ~8 Ma ago in the Late Miocene and intensified during the Middle and Late Pleistocene.

The most common eruptive style in the VS area was effusive, followed by Strombolian and phreatomagmatic explosive volcanic activity. Effusive activity dominated during the Pliocene to the Middle Pleistocene, resulting in the formation of voluminous medium-sized shield volcanoes, as well as some lava flows and domes. Notably, this region hosts the Cerro Grande, the most voluminous shield volcano in the entire MGVF, with a minimum volume of ~47 km^3. Furthermore, the products of this effusive volcanism are mostly andesites, basaltic andesites, and basaltic trachyandesites, with sub-alkaline affinities. Explosive volcanic activity is associated with the development of various scoria cones and phreatomagmatic volcanoes. The latter formed during the Late Pleistocene, mainly on the lower slopes of the Early and Middle Pleistocene shield volcanoes. They preferentially erupted along a pre-existing NNW-SSE fault zone, which could have served as the most favorable path through which small magma batches ascended. The presence of these phreatomagmatic volcanoes indicates that the VS area reached an optimal combination of climatic, tectonic, and hydrogeological conditions for such activity. Interestingly, these volcanoes formed before, during, and after the period of the LGM, which occurred in the study area between 22,000 and 18,000 cal BP (Holmes et al., 2016). It seems that the highly permeable rocks of the older shield volcanoes which acted as aquifers, along with the high annual precipitation that occurred due to the cold and humid climate conditions that prevailed in the region during the Late Pleistocene, promoted aquifer saturation and ensured a sufficient water supply for the formation of phreatomagmatic volcanoes. On the other hand, the volcanic products associated with the explosive activity are predominantly basalts, trachybasalts, and basaltic trachyandesites with mainly an alkaline affinity. It should be noted that rhyolitic compositions are rare in the VS area, while dacitic compositions are absent.

The estimated total eruption rate for the VS area during the Late Pliocene-Pleistocene (from 5 Ma to 11 ka) is 0.016 km^3/ka. Minimum eruption rates for each period are 0.023 km^3/ka for the Pliocene, 0.012 km^3/ka for the Early Pleistocene, 0.027 km^3/ka for the Middle Pleistocene, and 0.057 km^3/ka for the Late Pleistocene. The total eruption rate in the VS area is one order of magnitude lower than the rate reported for the entire MGVF for a period between 3 Ma and the Holocene. Finally, the absence of Holocene volcanism in the VS area is worth highlighting, especially when compared to other regions of the MGVF such as the Zacapu, Pátzcuaro, Jorullo, and Parícutin areas, where Holocene volcanism is important.

APPENDIX 1. METHODOLOGY FOR AREA AND VOLUME CALCULATIONS

The procedure employed for calculating the area and volume of the VS volcanic landforms with the ESRI ArcMap computer program is as follows: Firstly, a TIN model is created of a rectangular area that encloses the structure to be measured (ArcToolbox > 3D Analyst

Tools > Data Management > TIN > Create TIN). Then, the surface polygon of the structure is interpolated with the created TIN by assigning height values (Z) to the vertices of that polygon (ArcToolbox > 3D Analyst Tools > Functional Surface > Interpolate Shape). Subsequently, the volcanic structure is removed (ArcToolbox > Analysis Tools > Overlay > Erase). Next, a second TIN model is generated without the structure (ArcToolbox > 3D Analyst Tools > Data Management > TIN > Create TIN). Finally, the difference between the two TIN models is calculated to determine the area and volume of the volcanic structure (ArcToolbox > 3D Analysts Tools > Triangulated Surface > Surface difference).

ACKNOWLEDGMENTS

Field and laboratory costs were defrayed by project DGAPA-UNAM IN104221 (Dirección General de Asuntos del Personal Académico, UNAM) granted to C. Siebe. Elizabeth Rangel-Granados benefited from a CONAHCYT (Consejo Nacional de Humanidades, Ciencias y Tecnologías) postdoctoral fellowship awarded from 2021 to 2023. The authors extend their appreciation to Dra. Marcela Areli Araiza-Ortiz, the environmental director of the municipality of Valle de Santiago, Guanajuato, and ranger José Luis Cornejo-González for their invaluable support during our fieldwork campaigns. We also thank M.Sci. Jaime Díaz-Ortega at the “Taller de Laminación de Suelos y Sedimentos” at the Instituto de Geología, UNAM, and Silvia Martínez-Cruz for their assistance in the preparation of thin sections. The first author kindly acknowledges M.Sci. Guillermo Cisneros-Máximo for his guidance in the methodology used for volume calculations, Geoffrey A. Lerner for dedicating his time to review an initial version of the manuscript and for his valuable comments, and Dr. Alberto Vásquez-Serrano for his unconditional support throughout this study. C. Siebe benefited from a sabbatical stay at the Senckenberg Naturhistorische Sammlungen, Dresden, and the kind hospitality of Jan-Michael Lange and Peter Suhr.

REFERENCES CITED

Abrams, M.J., and Siebe, C., 1994, Cerro Xalapaxco: an unusual tuff cone with multiple explosion craters, in central Mexico (Puebla): Journal of Volcanology and Geothermal Research, v. 63, p. 183-199, https://doi.org/10.1016/0377-0273(94)90073-6.

Aguirre-Diaz, G.J., 2001, Calderas of the Central Sector of the Mexican Volcanic Belt: Abstract V32D-1020 presented at 2001 Fall Meeting, AGU, San Francisco, California 10-14 December.

Aguirre-Díaz, G.J., Jaimes-Viera, M.C., Nieto-Obregón, J., 2006, The Valle de Bravo Volcanic Field: Geology and geomorphometric parameters of a Quaternary monogenetic field at the front of the Mexican Volcanic Belt, *in* Siebe, C., Macías, J.L., Aguirre-Díaz, G.J., eds., Neogene-Quaternary Continental Margin Volcanism: A perspective from México: Geological Society of America, Special Papers 402, p. 39-154, https://doi.org/10.1130/2006.2402(06).

Alaniz-Álvarez, S.A., Nieto-Samaniego, A.F., Orozco-Esquivel, M.T., Vassallo, L.F., Xu, S., 2002, El sistema de fallas Taxco-San Miguel de Allende: Implicaciones en la deformación post-eocénica del centro de México: Boletín de la Sociedad Geológica Mexicana, v. 55, p. 12-29, https://doi.org/10.18268/bsgm2005v57n1a4.

Alcocer, J., Escobar, E., Lugo, A., 2000, Water use (and abuse) and its effects on the crater-lakes of Valle de Santiago, Mexico: Lakes & Reservoirs: Science, Policy and Management for Sustainable Use, v. 5, p. 145-149, https://doi.org/10.1046/j.1440-1770.2000.00113.x.

Aranda-Gómez, J.J., Mcdowell, F.W., 1998, Paleogene extension in the southern Basin and Range province of Mexico: Syndepositional tilting of Eocene red beds and Oligocene volcanic rocks in the Guanajuato Mining District: International Geology Review, v. 40, p. 116-134, https://doi.org/10.1080/00206819809465201.

Aranda-Gómez, J.J., Levresse, G., Pacheco-Martínez, J., et al., 2013, Active sinking at the bottom of the Rincón de Parangueo Maar (Guanajuato, México) and its probable relation with subsidence faults at Salamanca and Celaya: Boletín de la Sociedad Geológica Mexicana, v. 65, p. 169-188.

Aranda-Gómez, J.J., Carrasco-Núñez, G., 2014, The Valle de Santiago maars, México: the record of magma-water fluctuations during the formation of a basaltic maar (La Alberca) and active post-desiccation subsidence at the bottom of a maar lake (Rincón de Parangueo), *in* International Maar Conference, 5th, Field Trip Guidebook: Querétaro, México, 30 p., https://theghub.org/resources/3706.

Arce, J.L., Macías, J.L., Rangel, E., Layer, P., Garduño-Monroy, V.H., Saucedo, R., García, F., Castro, R., Pérez-Esquivias, H., 2012, Late Pleistocene rhyolitic explosive volcanism at Los Azufres volcanic field, central Mexico, *in* Aranda-Gómez, J.J., Tolson, G., Molina-Garza, R.S., eds., The Southern Cordillera and Beyond: Geological Society of America, Field Trip Guidebook 25, p. 45-82, https://doi.org/10.1130/2012.0025(04).

Arce, J.L., Layer, P.W., Macías, J.L., Morales-Casique, E., García-Palomo, A., Jiménez-Domínguez, F.J., Benowitz, J., Vásquez-Serrano, A., 2019, Geology and stratigraphy of the Mexico Basin (Mexico City), central Trans-Mexican Volcanic Belt: Journal of Maps, v. 15, p. 320-332, https://doi.org/10.1080/17445647.2019.1593251.

Arce, J.L., Rangel, E., Valdez-Moreno, G., Saucedo, R., Castro-Govea, R., Macías, J.L., 2021, Caracterización geoquímica, petrográfica y evolución magmática del Campo Volcánico de Los Azufres, Michoacán, durante el Pleistoceno: Revista Mexicana de

Ciencias Geológicas, v. 38, p. 122-140, https://doi.org/10.22201/cgeo.20072902e.2021.2.1646.

Armienta, M.A., Vilaclara, G., De la Cruz-Reyna, S., Ramos, S., Ceniceros, N., Cruz, O., Aguayo, A., Arcega-Cabrera, F., 2008, Water chemistry of lakes related to active and inactive Mexican volcanoes: Journal of Volcanology and Geothermal Research, v. 78, p. 249-258, https://doi.org/10.1016/j.jvolgeores.2008.06.019.

Avellán, D.R., Cisneros-Máximo, G., Macías, J.L., Gómez-Vasconcelos, M.G., Layer, P., Sosa-Ceballos, G., Robles-Camacho, J., 2020, Eruptive chronology of monogenetic volcanoes northwestern of Morelia - Insights into volcano-tectonic interactions in the central-eastern Michoacán-Guanajuato Volcanic Field, México: Journal of South American Earth Science, v. 100, p. 102554, https://doi.org/10.1016/j.jsames.2020.102554.

Ban, M., Hasenaka, T., Delgado-Granados, H., Takaoka, N., 1992, K-Ar ages of lavas from shield volcanoes in the Michoacán-Guanajuato volcanic field, Mexico: Geofísica Internacional, v. 31, p. 467-473, https://doi.org/10.22201/igeof.00167169p.1992.31.4.1367.

Becerra-Ramírez, R., Dóniz-Páez, J., González, E., 2022, Morphometric analysis of scoria cones to define the 'volcano-type' of the Campo de Calatrava Volcanic Region (Central Spain): Land, v. 11, p. 917, https://doi.org/10.3390/land11060917.

Bolós, X., Delgado-Torres, A., Cifuentes, G., Macías, J.L., Boijseauneau-López, M., Tinoco, C., Salguero, D., 2020, Internal structure and hydrothermal fluid circulation of Parícutin volcano, Mexico: Insights gained from near-surface geophysics: Geophysical Research Letters, v. 47, https://doi.org/10.1029/2020GL089270.

Botero-Santa, P.A., Alaniz-Álvarez, S.A., Nieto-Samaniego, A.F., López-Martínez, M., Levresse, G., Xu, S., Ortega-Obregón, C., 2015, Origen y desarrollo de la cuenca El Bajío en el sector central de la Faja Volcánica Transmexicana: Revista Mexicana de Ciencias Geológicas, v. 32, p. 84-98.

Bronk-Ramsey, C., 2009, Bayesian analysis of radiocarbon dates: Radiocarbon, v. 51, p. 337-360, https://doi.org/10.1017/S0033822200033865.

Brown, R.B., 1984, The paleoecology of the northern frontier of Mesoamerica [Ph.D. thesis]: The University of Arizona, 188 p.

Cano-Cruz, M., Carrasco-Núñez, G., 2008, Evolución de un cráter de explosión (maar) riolítico: Hoya de Estrada, campo volcánico Valle de Santiago, Guanajuato, México: Revista Mexicana de Ciencias Geológicas, v. 25, p. 549-564.

Cañón-Tapia, E., 2016, Reappraisal of the significance of volcanic fields: Journal of Volcanology and Geothermal Research, v. 310, p. 26-38, https://doi.org/10.1016/j.jvolgeores.2015.11.010.

Carmichael, I.S.E., Lange, R.A., Luhr, J.F., 1996, Quaternary minettes and associated volcanic rocks of Mascota, western Mexico: a consequence of plate extension above a subduction modified mantle wedge: Contributions to Mineralogy and Petrology, v. 124, p. 302-333, https://doi.org/10.1007/s004100050193.

Carrasco-Núñez, G., Hernández, J., Cavazos-Álvarez, J., Norini, G., Orozco-Esquivel, T., López-Quiroz, P., Jáquez, A., De León-Barragán, L., 2021, Volcanic geology of the easternmost sector of the Trans-Mexican Volcanic Belt, Mexico: Journal of Maps, v. 17, p. 486-496, https://doi.org/10.1080/17445647.2021.1970037.

Cerca-Martínez, L.M., Aguirre-Díaz, G.J., López-Martínez, M., 2000, The geologic evolution of the southern Sierra de Guanajuato, Mexico: A documented example of the transition from the Sierra Madre Occidental to the Mexican Volcanic Belt: International Geology Review, v. 42, p. 131-151, https://doi.org/10.1080/00206810009465073.

Chako-Tchamabé, B., Ohba, T., Kereszturi, G., Németh, K., Tongwa-Aka, F., Youmen, D., Issa., Miyabuchi, Y., Ooki, S., Tanyileke, G., Victor-Hell, J., 2015, Towards the reconstruction of the shallow plumbing system of the Barombi Mbo Maar (Cameroon) Implications for diatreme growth processes of a polygenetic maar volcano: Journal of Volcanology and Geothermal Research, v. 201, p. 293-313, https://doi.org/10.1016/j.jvolgeores.2015.06.004.

Chako-Tchamabé, B., Kereszturi, G., Németh, K., Carrasco-Núñez, G., 2016, How Polygenetic are Monogenetic Volcanoes: Case Studies of Some Complex Maar-Diatreme Volcanoes, *in* Németh, K., ed., Updates in Volcanology - From Volcano Modelling to Volcano Geology: InTech, p. 355-389, http://dx.doi.org/10.5772/63486.

Chako-Tchamabé, B., Carrasco-Núñez, G., Miggins, D.P., Németh, K., 2020, Late Pleistocene to Holocene activity of Alchichica maar volcano, eastern Trans-Mexican Volcanic Belt: Journal of South American Earth Sciences, v. 97, p. 102404, https://doi.org/10.1016/j.jsames.2019.102404.

Chédeville, C., Guilbaud, M-N., Siebe, C., 2020, Stratigraphy and radiocarbon ages of late-Holocene Las Derrumbadas rhyolitic domes and surrounding vents in the Serdán-Oriental basin (Mexico): implications for archeology, biology, and hazard assessment: The Holocene, v. 30, p. 402-419, https://doi.org/10.1177/0959683619887417.

Chevrel, M.O., Siebe, C., Guilbaud, M-N., Salinas, S., 2016a, The AD 1250 El Metate shield volcano (Michoacán): Mexico’s most voluminous Holocene eruption and its significance for archeology and hazards: The Holocene, v. 26, p. 471–488, https://doi.org/10.1177/0959683615609757.

Chevrel, M.O., Guilbaud, M-N., Siebe, C., 2016b, The ~ AD 1250 effusive eruption of El Metate shield volcano (Michoacán, Mexico): magma source, crustal storage, eruptive dynamics, and lava rheology: Bulletin of Volcanology, v. 78, p. 28, https://doi.org/10.1007/s00445-016-1020-9.

Clark, P.U., Dyke, A.S., Shakun, J.D., Carlson, A.E., Clark, J., Wohlfarth, B., Mitrovica, J.X., Hostetler, S.W., McCabe, A.M., 2009, The Last Glacial Maximum: Science, v. 325, p. 710–714, https://doi.org/10.1126/science.1172873.

Connor, C.B., Conway, F.M., 2000, Basaltic volcanic fields, *in* Sigurdsson, H., Houghton, B., Rymer, H., Stix, J., McNutt, S., eds., Encyclopedia of Volcanoes (1ST Edition): San Diego, California, Academic Press, p. 331-343.

Corona-Chávez, P., Reyes-Salas, M., Garduño-Monroy, V.H., Israde-Alcántara, I., Lozano-Santa Cruz, R., Morton-Bermea, O., Hernández-Álvarez, E., 2006, Asimilación de xenolitos graníticos en el Campo Volcánico Michoacán-Guanajuato: el caso de Arócutin Michoacán, México: Revista Mexicana de Ciencias Geológicas, v. 23, p. 233–245.

Correa-Metrio, A., Lozano-García, S., Xelhuantzi-López, S., Sosa-Nájera, S., Metcalfe, S.E., 2012, Vegetation in western Central Mexico during the last 50 000 years: modern analogs and climate in the Zacapu Basin: Journal of Quaternary Sciences, v. 27, p. 509-518, https://doi.org/10.1002/jqs.2540.

Del Pilar-Martínez, A., Nieto-Samaniego, A.F., Angeles-Moreno, E., Suárez-Arias, A.M., Olmos-Moya, M.J.P., Alaniz-Álvarez, S.A., Levresse, G., 2021, Digital geological map and geochronological database of the Cenozoic cover of the southern Mesa Central province, Mexico: Terra Digitalis, v. 5, p. 1-10, https://doi.org/10.22201/igg.25940694e.2021.2.89.

Domínguez-Vázquez, G., Osuna-Vallejo, V., Castro-López, V., Israde-Alcántara, I., Bischoff, J.A., 2019, Changes in vegetation structure during the Pleistocene-Holocene transition in Guanajuato, central Mexico: Vegetation History and Archaeobotany, v. 28, p. 81-91, https://doi.org/10.1007/s00334-018-0685-8.

Echegoyén-Sánchez, J., Romero-Martínez, S., Velázquez-Silvia, S., 1970, Geología y yacimientos minerales de la parte central del distrito minero de Guanajuato: Consejo de Recursos Naturales no Renovables, Boletín, v. 75, p. 36.

Ellis, B.S., Mark, D.F., Troch, J., Bachmann, O., Guillong, M., Kent, A.J.R., von Quadt, A., 2017, Split-grain ^{40}Ar/^{39}Ar dating: Integrating temporal and geochemical data from crystal cargoes: Chemical Geology, v. 457, p. 15-23, https://doi.org/10.1016/j.chemgeo.2017.03.005.

Escolero, O.A., Alcocer, J., 2004, Desecación de los lagos cráter del Valle de Santiago, Guanajuato, *in* Jiménez, B., Marín, L., eds., El Agua en México vista desde la academia: Academia Mexicana de Ciencias, México, p. 99-115.

Ferrari, L., Orozco-Esquivel, T., Manea, V., Manea, M., 2012, The dynamic history of the Trans-Mexican Volcanic Belt and the Mexico subduction zone: Tectonophysics, v. 522-523, p. 122-149, https://doi.org/10.1016/j.tecto.2011.09.018.

García-Palomo, A., Macías, J.L., Tolson, G., Valdez, G., Mora, J.C., 2002, Volcanic stratigraphy and geological evolution of the Apan region, east-central sector of the Trans-Mexican Volcanic Belt: Geofísica Internacional, v. 41, p. 133-150, https://doi.org/10.22201/igeof.00167169p.2002.41.2.282.

Garduño-Monroy, V.H., Pérez-Lopez, R., Israde-Alcantara, et al., 2009, Paleoseismology of the southwestern Morelia-Acambay fault system, central Mexico: Geofísica Internacional, v. 48, p. 319-335.

Gillespie, A.R., Huneke, J.C., Wasserburg, G.J., 1983, Eruption age of a Pleistocene basalt from ^{40}Ar-^{39}Ar analysis of partially degassed xenoliths: Journal Geophysical Research, v. 88, p. 4997-5008, https://doi.org/10.1029/JB088iB06p04997.

Gómez-Tuena, A., Orozco-Esquivel, M.T., Ferrari, L., 2007, Igneous petrogenesis of the Trans-Mexican Volcanic Belt, *in* Alaniz-Álvarez, S.A., Nieto-Samaniego, A.F., eds., Geology of México: Celebrating the Centenary of the Geological Society of México: Geological Society of America, p. 129-181, https://doi.org/10.1130/2007.2422(05).

Gómez-Vasconcelos, M.G., Macías, J.L., Avellán, D.R., Sosa-Ceballos, G., Garduño-Monroy, V.H., Cisneros-Máximo, G., Layer, P.W., Benowitz, J., López-Loera, H., Mendiola-López, F., Perton, M., 2020, The control of preexisting faults on the distribution, morphology, and volume of monogenetic volcanism in the Michoacán-Guanajuato Volcanic Field: Geological Society of America Bulletin, v. 132, p. 2455-2474, https://doi.org/10.1130/B35397.1.

Gómez-Vasconcelos, M.G., Avellán, D.R., Macías, J.L., Cisneros-Máximo, G., Sánchez-Núñez, J.M., Miggins, D., 2023, New Insights into Feeder Dike Swarms in Scoria Cones and Their Structural Control: A Case Study in the Michoacán-Guanajuato Volcanic Field: GSA Today, v. 33, p. 4-10, https://doi.org/10.1130/GSATG539A.1.

González-Becerra, P.C., 2005, Evolución geológica del maar Hoya de Solís, Valle de Santiago, Guanajuato, México [Undergraduate thesis]: Universidad Autónoma de Nuevo León, México.

Graettinger, A.H., 2018, Trends in maar crater size and shape using the global Maar Volcano Location and Shape (MaarVLS) database: Journal of Volcanology and Geothermal Research, v. 357, p. 1-13, https://doi.org/10.1016/j.jvolgeores.2018.04.002.

Green, J., 1986, Associations of zooplankton in six crater lakes in Arizona, Mexico and New Mexico: Journal of Zoology, v. 208, p. 135-159, https://doi.org/10.1111/j.1469-7998.1986.tb04715.x.

Guilbaud, M-N., Siebe, C., Layer, P., Salinas, S., Castro-Govea, R., Garduño-Monroy, V.H., Le Corvec, N., 2011, Geology, geochronology, and tectonic setting of the Jorullo Volcano region, Michoacán, México: Journal of Volcanology and Geothermal Research, v. 201, p. 97-112, https://doi.org/10.1016/j.jvolgeores.2010.09.005.

Guilbaud, M-N., Siebe, C., Layer, P., Salinas, S., 2012, Reconstruction of the volcanic history of the Tacámbaro-Puruarán area (Michoacán, México) reveals high frequency of Holocene monogenetic eruptions: Bulletin of Volcanology, v. 74, p. 1187-1211, https://doi.org/10.1007/s00445-012-0594-0.

Hasenaka, T., Carmichael, I.S.E., 1985a, A compilation of location, size, and geomorphological parameters of volcanoes of the Michoacán-Guanajuato Volcanic Field, Central Mexico: Geofísica Internacional, v. 24, p. 577-607, https://doi.org/10.22201/igeof.00167169p.1985.24.4.2179.

Hasenaka, T., Carmichael, I.S.E., 1985b, The cinder cones of Michoacán-Guanajuato, central Mexico: their age, volume and distribution, and magma discharge rate: Journal of Volcanology and Geothermal Research, v. 25, p. 105-124, https://doi.org/10.1016/0377-0273(85)90007-1.

Hasenaka, T., 1994, Size, distribution and magma output rates for shield volcanoes of the Michoacán-Guanajuato volcanic field, Central Mexico: Journal of Volcanology and Geothermal Research, v. 63, p. 13-31, https://doi.org/10.1016/0377-0273(94)90016-7.

Holmes, J.A., Metcalfe, S.E., Jones, H.L., Marshall, J.D., 2016, Climatic variability over the last 30 000 years recorded in La Piscina de Yuriria, a Central Mexican crater lake: Journal of Quaternary Sciences, v. 31, p. 310-324, https://doi.org/10.1002/jqs.2846.

Irvine, T.N., Baragar, W.R.A., 1971, A guide to the chemical classification of the common volcanic rocks: Canadian Journal of Earth Sciences, v. 8, p. 523-548, https://doi.org/10.1139/e71-055.

Jácome-Paz, M.P., Torres-Orozco, R., Espinasa-Pereña, R., de la Fuente-Rivera, J.R., Ruiz-Sánchez, J.O., Delgado-Granados, H., 2022, Review of geology and geomorphology of the Xalapa Monogenetic Volcanic Field, eastern Trans-Mexican Volcanic Belt: Journal of Volcanology and Geothermal Research, v. 432, p. 107689, https://doi.org/10.1016/j.jvolgeores.2022.107689.

Jaimes-Viera, M.C., Martin Del Pozzo, A.L., Layer, P.W., Benowitz, J.A., Nieto-Torres, A., 2018, Timing the evolution of a monogenetic volcanic field: Sierra Chichinautzin, Central Mexico: Journal of Volcanology and Geothermal Research, v. 356, p. 225-242, https://doi.org/10.1016/j.jvolgeores.2018.03.013.

Johnson, E.R., Wallace, P.J., Delgado-Granados, H., Manea, V.C., Kent, A.J.R., Bindeman, I.N., Donegan, C.S., 2009, Subduction-related volatile recycling and magma generation beneath Central Mexico: Insights from melt inclusions, oxygen isotopes and geodynamic models: Journal of Petrology, v. 50, p. 1729-1764, https://doi.org/10.1093/petrology/egp051.

Johnson, C.A., Harrison, C.G.A., 1990, Neotectonics in central Mexico: Physics of the Earth and Planetary Interiors, v. 64, p. 187-210, https://doi.org/10.1016/0031-9201(90)90037-X.

Join, J-L., Folio, J.L., Robineau, B., 2005, Aquifers and groundwater within active shield volcanoes. Evolution of conceptual models in the Piton de la Fournaise volcano: Journal of Volcanology and Geothermal Research, v. 147, p. 187-201, https://doi.org/10.1016/j.jvolgeores.2005.03.013.

Kereszturi, G., Németh, K., 2012a, Monogenetic basaltic volcanoes: genetic classification, growth, geomorphology and degradation, *in* Németh, K., ed., Updates in volcanology - new advances in understanding volcanic systems: InTech, https://doi.org/10.5772/51387.

Kereszturi, G., Németh, K., 2012b, Structural and morphometrical irregularities of eroded scoria cones at the Bakony-Balaton Highland Volcanic Field, Hungary: Geomorphology, v. 136, p. 45-58, https://doi.org/10.1016/j.geomorph.2011.08.005.

Kereszturi, G., Németh, K., Cronin, S.J., Agustín-Flores, J., Smith, I.E.M., Lindsay, J., 2013, A model for calculating eruptive volumes for monogenetic volcanoes - Implication for the Quaternary Auckland Volcanic Field, New Zealand: Journal of Volcanological Geothermal Research, v. 266, p. 16-33, https://doi.org/10.1016/j.jvolgeores.2013.09.003.

Kienel, U., Bowen, S.W., Byrne, R., Park, J., Böhnel, H., Dulski, P., Luhr, J.F., Siebert, L., Haug, G.H., Negendank, J.F., 2009, First lacustrine varve chronologies from Mexico: impact of droughts, ENSO and human activity since AD 1840 as recorded in maar sediments from Valle de Santiago: Journal of Paleolimnology, v. 42, p. 587-609, https://doi.org/10.1007/s10933-009-9307-x.

Koppers, A.A.P., Staudigel, H., Wijbrans, J.R., 2000, Dating crystalline groundmass separates of altered Cretaceous seamount basalts by the $^{40}Ar/^{39}Ar$ incremental heating technique: Chemical Geology, v. 166, p. 139-158, https://doi.org/10.1016/S0009-2541(99)00188-6.

Koppers, A.A.P., 2002, ArArCALC-software for ^{40}Ar/^{39}Ar age calculations: Computers & Geosciences, v. 28, p. 605-619, https://doi.org/10.1016/S0098-3004(01)00095-4.

Koppers, A.A.P., Staudigel, H., Pringle, M.S., Wijbrans, J.R., 2003, Short-lived and discontinuous intraplate volcanism in the South Pacific: Hot spots or extensional volcanism?: Geochemistry, Geophysics, Geosystems, v. 4, https://doi.org/10.1029/2003GC000533.

Kshirsagar, P., Siebe, C., Guilbaud, M-N., Salinas, S., Layer, P.W., 2015, Late Pleistocene Alberca de Guadalupe maar volcano (Zacapu basin, Michoacán): Stratigraphy, tectonic setting, and paleo-hydrogeological environment: Journal of Volcanology of Geothermal Research, v. 304, p. 214-236, https://doi.org/10.1016/j.jvolgeores.2015.09.003.

Kshirsagar, P., Siebe, C., Guilbaud, M-N., Salinas, S., 2016, Geological and environmental controls on the change of eruptive style (phreatomagmatic to Strombolian-effusive) of Late Pleistocene El Caracol tuff cone and its comparison with adjacent volcanoes around the Zacapu basin (Michoacán, México): Journal of Volcanology and Geothermal Research, v. 318, p. 114-133, https://doi.org/10.1016/j.jvolgeores.2016.03.015.

Kuiper, K.F., Deino, A., Hilgen, F.J., Krijgsman, W., Renne, P.R., Wijbrans, J.R., 2008, Synchronizing rock clocks of Earth history: Science, v. 320, p. 500-504, https://doi.org/10.1126/science.1154339.

Le Bas, M.J., Le Maitre, R.W., Streckeisen, A., Zanettin, B., 1986, A chemical classification of volcanic rocks based on the Total Alkali-Silica diagram: Journal of Petrology, v. 27, p. 745-750, https://doi.org/10.1093/petrology/27.3.745.

Le Corvec, N., Bebbington, M.S., Lindsay, J.M., McGee, L.E., 2013, Age, distance, and geochemical evolution within a monogenetic volcanic field: Analyzing patterns in the

Auckland Volcanic Field eruption sequence: Geochemistry, Geophysics, Geosystems, v. 14, p. 3648-3665, https://doi.org/10.1002/ggge.20223.

Lee, J.Y., Marti, K., Severinghaus, J.P., Kawamura, K., Yoo, H.S., Lee, J.B., Kim, J.S., 2006, A redetermination of the isotopic abundances of atmospheric Ar: Geochimica et Cosmochimica Acta, v. 70, p. 4507-4512, https://doi.org/10.1016/j.gca.2006.06.1563.

Legrand, D., Perton, M., Macías, J.L., Siebe, C., Pacheco, J., Chacón, F., Lermo, J., Quintanar, L., Cisneros, G., 2023, Repeated seismic swarms near Paricutin volcano: precursors to the birth of a new monogenetic volcano in the Michoacán-Guanajuato volcanic field, México?: Bulletin of Volcanology, v. 85, p. 30, https://doi.org/10.1007/s00445-023-01645-0.

Losantos, E., 2017, El vulcanismo monogenético del campo volcánico de Michoacán-Guanajauto (México) petrogénesis e implicaciones geodinámicas [Ph.D. thesis]: Universidad Complutense de Madrid, 341 p.

Losantos, E., Cebriá, J.M., Morán-Zenteno, D.J., Martiny, B.M., López-Ruiz, J., Solís-Pichardo, G., 2017, Petrogenesis of the alkaline and calcalkaline monogenetic volcanism in the northern sector of the Michoacán-Guanajuato Volcanic Field (Central Mexico): Lithos, v. 288289, p. 295-310, https://doi.org/10.1016/j.lithos.2017.07.013.

Luhr, J.F., Carmichael, I.S.E., 1981, The Colima volcanic complex, Mexico: Part II. Late-quaternary cinder cones: Contributions to Mineralogy and Petrology, v. 76, p. 127-147, https://doi.org/10.1007/BF00371954.

Luhr, J.F., Carmichael, I.S.E., 1985, Jorullo Volcano, Michoacán, Mexico (1759-1774): The earliest stages of fractionation in calc-alkaline magmas: Contributions to Mineralogy and Petrology, v. 90, p. 142-161, https://doi.org/10.1007/BF00378256.

Luhr, J.F., Simkin, T., 1993, Paricutin: the volcano born in a cornfield: Phoenix, Geoscience Press, 427 p., https://doi.org/10.1007/BF00371954.

Luhr, J.F., Kimberly, P., Siebert, L., Aranda-Gómez, J.J., Housh, T.B., Mattietti, G.K., 2006, México's Quaternary volcanic rocks: Insights from the MEXPET petrological and geochemical database, *in* Siebe, C., Macías, J.L., Aguirre-Díaz, G.J., eds., Neogene-Quaternary Continental Margin Volcanism: A perspective from México: Geological Society of America, Special Papers 402, p. 1-44, https://doi.org/10.1130/2006.2402(01).

Manea, V.C., Manea, M., Ferrari, L., 2013, A geodynamical perspective on the subduction of Cocos and Rivera plates beneath Mexico and Central America: Tectonophysics, v. 609, p. 56-81, https://doi.org/10.1016/j.tecto.2012.12.039.

Martí, J., López, C., Bartolini, S., Becerril, L., Geyer, A., 2016, Stress controls of monogenetic volcanism: A review: Frontiers in Earth Science, v. 4, p. 106, https://doi.org/10.3389/feart.2016.00106.

Martin Del Pozzo, A.L., 1982, Monogenetic vulcanism in Sierra Chichinautzin, Mexico: Bulletin of Volcanology, v. 45, p. 9-24, https://doi.org/10.1007/BF02600386.

McBirney, A.R., Taylor, H.P., Armstrong, R.L., 1987, Paricutin re-examined: a classic example of crustal assimilation in calc-alkaline magma: Contribution to Mineralogy and Petrology, v. 95, p. 4-20, https://doi.org/10.1007/BF00518026.

Meriggi, L., Macías, J.L., Tommasini, S., Capra, L., Conticelli, S., 2008, Heterogeneous magmas of the Quaternary Sierra Chichinautzin volcanic field (central Mexico): the role of an amphibole-bearing mantle and magmatic evolution processes: Revista Mexicana de Ciencias Geológicas, v. 25, p. 197-216.

Metcalfe, S.E., Street-Perrott, F.A., Brown, R.B., Hales, P.E., Perrott, R.A., Steininger, F.M., 1989, Late Holocene human impact on lake basins in Central Mexico:

Geoarchaeology An International Journal, v. 4, p. 119-141, https://doi.org/10.1002/gea.3340040203.

Metcalfe, S.E., O'Hara, S.L., Caballero, M., Davies, S.J., 2000, Records of Late Pleistocene–Holocene climatic change in Mexico - a review: Quaternary Science Reviews, v. 19, p. 699-721, https://doi.org/10.1016/S0277-3791(99)00022-0.

Min, K., Mundil, R., Renne, P.R., Ludwig, K.R., 2000, A test for systematic errors in $^{40}Ar/^{39}Ar$ geochronology through comparison with U/Pb analysis of a 1.1-Ga rhyolite: Geochimica et Cosmochimica Acta, v. 64, p. 73-98, https://doi.org/10.1016/S0016-7037(99)00204-5.

Murphy, G.P., 1986, The chronology, pyroclastic stratigraphy, and petrology of the Valle de Santiago maar field, central Mexico [Master thesis]: Berkeley, University of California, 61 p.

Németh, K., 2010, Monogenetic volcanic fields: Origin, sedimentary record, and relationship with polygenetic volcanism, *in* Cañón-Tapia, E., Szakács, A., eds., What Is a Volcano?: Geological Society of America, Special Papers 470, p. 43-66, https://doi.org/10.1130/2010.2470(04).

Németh, K., Kereszturi, G., 2015, Monogenetic volcanism: personal views and discussion: International Journal of Earth Sciences (Geologische Rundschau), v. 104, p. 2131-2146, https://doi.org/10.1007/s00531-015-1243-6.

Nieto-Samaniego, A.F., 1990, Fallamiento y estratigrafía cenozoicos en la parte sudoriental de la Sierra de Guanajuato: Revista del Instituto de Geología, Universidad Nacional Autónoma de México, v. 9, p. 146-155.

Nieto-Samaniego, A.F., Alaniz-Álvarez, S.A., Camprubí í Cano, A., 2005, La Mesa Central de México: estratigrafía, estructura y evolución tectónica cenozoica: Boletín de la

Sociedad Geológica Mexicana, v. 57, p. 285-318, https://doi.org/10.18268/bsgm2005v57n3a3.

Nixon, G.T., 1982, The relationship between Quaternary volcanism in central Mexico and the seismicity and structure of subducted ocean lithosphere: Geological Society of America Bulletin, v. 93, p. 514-523, https://doi.org/10.1130/0016-7606(1982)93<514:TRBQVI>2.0.CO;2.

Ordóñez, E., 1900, Les volcanoes du Valle de Santiago: Memorias de la Sociedad Científica (México), v. 14, p. 229-326.

Ordóñez, E., 1906, Les cratères d'explosion de Valle de Santiago, *in* X Congreso Geológico Internacional: México City, Guía de excursión de campo 14, p. 1-8.

Ortega, B., Caballero, C., Lozano, S., Israde, I., Vilaclara, G., 2002, 52000 years of environmental history in Zacapu basin, Michoacan, Mexico: the magnetic record: Earth and Planetary Science Letters, v. 202, p. 663-675, https://doi.org/10.1016/S0012-821X(02)00802-6.

Ortega-Gutiérrez, F., Gómez-Tuena, A., Elías-Herrera, M., Solari, L.A., Reyes-Salas, M., Macías-Romo, C., 2014, Petrology and geochemistry of the Valle de Santiago lower-crust xenoliths: Young tectonothermal processes beneath the central Trans-Mexican volcanic belt: Lithosphere, v. 6, p. 335-360, https://doi.org/10.1130/L317.1.

Osorio-Ocampo, S., Macías, J.L., Pola, A., Cardona-Melchor, S., Sosa-Ceballos, G., Garduño-Monroy, V.H., Layer, P., García-Sánchez, L., Perton, M., Benowitz, J., 2018, The eruptive history of the Pátzcuaro Lake area in the Michoacán Guanajuato Volcanic Field, central México: Field mapping, C-14 and ^{40}Ar/^{39}Ar geochronology: Journal of Volcanology and Geothermal Research, v. 358, p. 307-328, https://doi.org/10.1016/j.jvolgeores.2018.06.003.

Oviedo-Padrón, E.G., 2005, Análisis geológico-estructural del complejo de maares de Valle de Santiago, Campo Volcánico Michoacán-Guanajuato, México [Undergraduate thesis]: Universidad Autónoma de Nuevo León, México, 119 p.

Ownby, S.E., Granados, H.D., Lange, R.A., Hall, C.M., 2007, Volcán Tancítaro, Michoacán, Mexico, $^{40}Ar/^{39}Ar$ constraints on its history of sector collapse: Journal of Volcanology and Geothermal Research, v. 161, p. 1-14, https://doi.org/10.1016/j.jvolgeores.2006.10.009.

Ownby, S.E., Lange, R.A., Hall, C.M., 2008, The eruptive history of the Mascota volcanic field, western Mexico: Age and volume constraints on the origin of andesite among a diverse suite of lamprophyric and calc-alkaline lavas: Journal of Volcanology and Geothermal Research, v. 177, p. 1077-1091, https://doi.org/10.1016/j.jvolgeores.2008.08.002.

Pardo, M., Suárez, G., 1995, Shape of the subducted Rivera and Cocos plates in southern Mexico: Seismic and tectonic implications: Journal of Geophysical Research, v. 100, p. 12357-12373, https://doi.org/10.1029/95JB00919.

Park, J., 2005, Holocene environmental change and human impact in Hoya Rincón de Parangueo, Guanajuato, Mexico: The Korean Journal of Ecology, v. 28, p. 245-254, https://doi.org/10.5141/JEFB.2005.28.5.245.

Park, J., Byrne, R., Böhnel, H., Molina-Garza, R., Conserva, M., 2010, Holocene climate change and human impact, central Mexico: a record based on maar lake pollen and sediment chemistry: Quaternary Science Reviews, v. 29, p. 618-632, https://doi.org/10.1016/j.quascirev.2009.10.017.

Pasquarè, G., Ferrari, L., Garduño-Monroy, V.H., Tibaldi, A., Vezzoli, L., 1991, Geologic map of the central sector of the Mexican Volcanic Belt, states of Guanajuato and Michoacan, Mexico: Geological Society of America, Map and Chart Series MCH072.

Peñaloza-Turrubiates, N.E., 2005, Las paragénesis minerales en tefras asociadas a actividad freatomagmática como criterio de correlación estratigráfica: complejo de maares de Valle de Santiago, Guanajuato, México. [Undergraduate thesis]: Universidad Autónoma de Nuevo León.

Porter, S.C., 1972, Distribution, morphology, and size frequency of cinder cones on Mauna Kea volcano, Hawaii: Geological Society of America Bulletin, v. 83, p. 3607-3612, https://doi.org/10.1130/0016-7606(1972)83[3607:DMASFO]2.0.CO;2.

Puente-Solis, I.R., 2004, Estratigrafía e historia eruptiva del cráter de explosión Hoya La Cíntora, Gto. [Undergraduate thesis]: Universidad Autónoma de San Luis Potosí, 125 p.

Reimer, P.J., Austin, W.E.N., Bard, E., et al., 2020, The IntCal20 Northern Hemisphere Radiocarbon Age Calibration Curve (0–55 cal kBP): Radiocarbon, v. 62, p. 725-757, https://doi.org/10.1017/RDC.2020.41.

Reyes-Guzmán, N., Siebe, C., Chevrel, M.O., Guilbaud, M-N., Salinas, S., Layer, P., 2018, Geology and radiometric dating of Quaternary monogenetic volcanism in the western Zacapu lacustrine basin (Michoacán, México): implications for archeology and future hazard evaluations: Bulletin of Volcanology, v. 80, p. 18, https://doi.org/10.1007/s00445-018-1193-5.

Rincón-Herrera, N., 2005, Estratigrafía del cráter de explosión Hoya La Alberca [Undergraduate thesis]: Instituto Tecnológico de Ciudad Madero, 75 p.

Rodríguez-Elizarrarás, S.R., Morales-Barrera, W., Layer, P., González-Mercado, E., 2010, A quaternary monogenetic volcanic field in the Xalapa region, eastern Trans-Mexican volcanic belt: Geology, distribution and morphology of the volcanic vents: Journal of Volcanology and Geothermal Research, v. 197, p. 149-166, https://doi.org/10.1016/j.jvolgeores.2009.08.003.

Rodríguez-Elizarrarás, S.R., Morales-Barrera, W.V., Pompa-Mera, V., Siebe, C., Benowitz, J., Layer, P.W., Lozano-Santacruz, R., Girón, P., 2023, Geochemistry and ^{40}Ar/^{39}Ar dating of the Sierra de Santa Marta in the tectonically controversial Los Tuxtlas Volcanic Field (Veracruz, Mexico): Journal of South American Earth Sciences, v. 124, p. 104250, https://doi.org/10.1016/j.jsames.2023.104250.

Schaen, A.J., Jicha, B.R., Hodges, K.V., et al., 2020, Interpreting and reporting ^{40}Ar/^{39}Ar geochronologic data: Geological Society of America Bulletin, v. 133, p. 461-487, https://doi.org/10.1130/B35560.1.

Sheridan, M.F., Wohletz, K.H., 1983, Hydrovolcanism: Basic considerations and review: Journal of Volcanology and Geothermal Research, v. 17, p. 1-29, https://doi.org/10.1016/0377-0273(83)90060-4.

Siebe, C., Rodríguez-Lara, V., Schaaf, P., Abrams, M., 2004, Radiocarbon ages of Holocene Pelado, Guespalapa, and Chichinautzin scoria cones, south of Mexico City: implications for archaeology and future hazards: Bulletin of Volcanology, v. 66, p. 203-225, https://doi.org/10.1007/s00445-003-0304-z.

Siebe, C., Kshirsagar, P., Guilbaud, M-N., Salinas, S., 2016, Paleo-environmental and geological controls on Late Pleistocene Phreatomagmatism in the Lacustrine Zacapu Basin (Michoacán, Mexico), *in* Jiaqi, L., ed.: International Maar Conference, 6th, Changchung, China, Abstracts, p. 85-86, http://dx.doi.org/10.5772/64766.

Sieron, K., Siebe, C., 2008, Revised stratigraphy and eruption rates of Ceboruco stratovolcano and surrounding monogenetic vents (Nayarit, Mexico) from historical documents and new radiocarbon dates: Journal of Volcanology and Geothermal Research, v. 176, p. 241-264, https://doi.org/10.1016/j.jvolgeores.2008.04.006.

Sieron, K., Juárez-Cerrillo, S.F., González-Zuccolotto, K., Córdoba-Montiel, F., Connor, C.B., Connor, L., Tapia-McClung, H., 2021, Morphology and distribution of monogenetic volcanoes in Los Tuxtlas Volcanic Field, Veracruz, Mexico: implications for hazard assessment: Bulletin of Volcanology, v. 83, p. 47, https://doi.org/10.1007/s00445-021-01467-y.

Smith, I.E.M., Németh, K., 2017, Source to surface model of monogenetic volcanism: A critical review, *in* Németh, K., Carrasco-Núñez, G., Aranda-Gómez, J.J., Smith, I.E.M., eds., Monogenetic Volcanism: Geological Society, London, Special Publications 446, p. 1-28, https://doi.org/10.1144/SP446.14.

Sosa-Ceballos, G., Boijseauneau-López, M.E., Pérez-Orozco, J.D., Cifuentes-Nava, G., Bolós, X., Perton, M., Simón-Velázquez, D., 2021, Silicic magmas in the Michoacán-Guanajuato volcanic field: An overview of plumbing systems, crustal storage, and genetic processes: Revista Mexicana de Ciencias Geológicas, v. 38, p. 210-225, https://doi.org/10.22201/cgeo.20072902e.2021.3.1668.

Steiger, R.H., Jäger, E., 1977, Subcommission on geochronology: Convention on the use of decay constants in geo- and cosmochronology: Earth and Planetary Science Letters, v. 36, p. 359-362, https://doi.org/10.1016/0012-821X(77)90060-7.

Stuiver, M., Reimer, P.J., 1993, CALIB rev. 8: Radiocarbon, v. 35, p. 215-230.

Suárez-Jiménez, J.E., 2022, Entorno hidrológico del cráter de explosión Joya La Alberca (Valle de Santiago, Guanajuato, México) y origen de la concentración de cráteres freato-magmáticos en el Campo Volcánico de Valle de Santiago [Master thesis]: Ciudad de México, Universidad Nacional Autónoma de México, 331 p.

Sun, S-s., McDonough, W.F., 1989, Chemical and isotopic systematics of oceanic basalts: Implications for mantle composition and processes: Geological Society, London, Special Publications, v. 42, p. 313-345, http://doi:10.1144/GSL.SP.1989.042.01.19.

Suter, M., Morelos-Rodríguez, L., 2023, Seismotectonics of the Querétaro Region (Central Mexico) and the 1934 M, 4.8 Earthquake North of Celaya: Seismological Research Letters, p. 1-14, https://doi.org/10.1785/0220230256.

Taylor, J.R., 1997, An Introduction to Error Analysis: The Study of Uncertainties in Physical Measurements (2ND Edition): Sausalito, California, University Science Books, 327 p.

Torres-Sánchez, D., Sosa-Ceballos, G., Bolós, X., Macías, J.L., 2022, Petrogenesis of mafic-intermediate magmatism of the Michoacán–Guanajuato volcanic field in Western Mexico. A geochemical review: Frontiers in Earth Science, v. 10, p. 932588, https://doi.org/10.3389/feart.2022.932588.

Uribe-Cifuentes, R.M., 2006, Xenolitos y volcanismo en la región de Valle de Santiago, Guanajuato - Estudios paleomagnéticos y de magnetismo de rocas [Ph.D. thesis]: Ciudad de México, Universidad Nacional Autónoma de México, 210 p.

Urrutia-Fucugauchi, J., Uribe-Cifuentes, R.M., 1999, Lower-crustal xenoliths from the Valle de Santiago maar field, Michoacan-Guanajuato volcanic field, Central Mexico: International Geology Review, v. 41, p. 1067-1081, https://doi.org/10.1080/00206819909465192.

Valentine, G.A., Gregg, T.K.P., 2008, Continental basaltic volcanoes - Processes and problems: Journal of Volcanology and Geothermal Research, v. 177, p. 857-873, https://doi.org/10.1016/j.jvolgeores.2008.01.050.

Valentine, G.A., Connor, C.B., 2015, Basaltic volcanic fields, *in* Sigurdsson, H., ed., The Encyclopedia of Volcanoes (2ND Edition): San Diego, California, Academic Press, p. 423-439, https://doi.org/10.1016/B978-0-12-385938-9.00023-7.

Wallace, P.J., Carmichael, I.S.E., 1999, Quaternary volcanism near the Valley of Mexico: implications for subduction zone magmatism and the effects of crustal thickness variations on primitive magma compositions: Contributions to Mineralogy and Petrology, v. 135, p. 291-314, https://doi.org/10.1007/s004100050513.

Wood, C.A., 1980, Morphometric analysis of cinder cone degradation: Journal of Volcanology and Geothermal Research, v. 8, p. 137-160, https://doi.org/10.1016/0377-0273(80)90101-8.

York, D., 1968, Least squares fitting of a straight line with correlated errors: Earth and Planetary Science Letters, v. 5, p. 320-324, https://doi.org/10.1016/S0012-821X(68)80059-7.

Yutsis, V., Aranda-Gómez, J.J., Arzate-Flores, J.A., Böhnel, H., Pacheco-Martínez, J., López-Loera, H., 2014, Maar geophysics: Valle de Santiago study, *in* Carrasco-Núñez, G., Aranda-Gómez, J.J., Ort, M.H., Silva-Corona, J.J., eds.: International Maar Conference, 5th, Querétaro, México, Abstracts, p. 32-33.

FIGURE CAPTIONS

Figure 1. Shaded relief map of the Michoacán-Guanajuato volcanic field (MGVF) showing the location of the Valle de Santiago area (enclosed in the yellow rectangle). This map also includes the distribution of scoria cones, medium-sized shield volcanoes, phreatomagmatic volcanoes (AT: Alberca de Tacámbaro, C: Costo or Cojti, T: Tangancícuaro, AE: Alberca de Los Espinos, EC: El Caracol, AG: Alberca de Guadalupe, YJ: Yuriria Joyas, VSJ: Valle

de Santiago Joyas, and IJ: Irapuato Joyas), and the two stratovolcanoes Tancítaro (Ta) and Patambán (Pa). The scoria cone and medium-sized shield volcano database is modified from Chevrel et al. (2016a). The location of the Paricutin (P) and Jorullo (Jo) scoria cones and main lineaments associated with the Chapala-Oaxaca (COFS), Taxco-San Miguel de Allende (TSMAFS), Tzitzio-Valle de Santiago (TVSFS), and Morelia-Acambay (MAFS) fault systems are also indicated. Additionally, the map shows the Sierra Codornices (SC), Caldera de Apaseo (CAp), Caldera de los Agustinos (CAg), Sierra de Piñícuaro (SP), and Tzitzio anticline (TA). The inset map at the lower right corner shows the location of the MGVF within the Trans-Mexican Volcanic Belt (TMVB) and main tectonic features of southern Mexico (RFZ: Rivera Fracture Zone and EPR: East Pacific Rise), and the three sectors into which the TMVB is commonly divided (western, central, and eastern).

Figure 2. Geologic map of the Valle de Santiago area. Sample locations of some radiometric dates (^{40}Ar/^{39}Ar and ^{40}K/^{40}Ar dating) are also shown. The black rectangle encloses the core of the study area which is presented in more detail in Figure 3. The phreatomagmatic volcanoes are 1: Sanabria tuff ring; 2: San Roque West; 3: San Roque East; 4: La Ciénega tuff ring; 5: La Mina Norte tuff ring; 6: La Mina Sur tuff ring; 7: Joya Rincón de Parangueo maar; 8: Santa Rosa tuff ring; 9: Joyuela tuff ring; 10: Joya Estrada tuff ring; 11: Joya San Nicolás maar; 12: Joya La Alberca maar; 13: Joya Blanca tuff cone; 14: Joya Solís maar; 15: Joya Cíntora maar; 16: Joya de Álvarez maar; 17: Magdalena de Araceo tuff ring; 18: Providencia de Cuerunero tuff cone; 19: Joyuela de San Vicente tuff cone; 20: Isla de San Pedro tuff ring; 21: Joya de Yuriria maar. The letter C in the structure names denotes the abbreviation of the Spanish word “Cerro” which means hill. The names of all volcanic structures in the VS area can be consulted in Figure S3. pc: parasitic cone.

Figure 3. Detailed geologic map of the central region of the Valle de Santiago area showing radiocarbon (C^{14}), $^{40}Ar/^{39}Ar$, and $^{40}K/^{40}Ar$ dates. Radiocarbon dates are denoted in years (yr) before present. The yellow circles show sample locations for radiocarbon dating (see Table 2). The phreatomagmatic volcanoes are 1: La Mina Norte tuff ring; 2: La Mina Sur tuff ring; 3: Joya Rincón de Parangueo maar; 4: Santa Rosa tuff ring; 5: Joyuela tuff ring; 6: Joya Estrada tuff ring; 7: Joya San Nicolás maar; 8: Joya La Alberca maar; 9: Joya Blanca tuff cone; 10: Joya Solís maar; 11: Joya Cíntora maar; 12: Joya de Álvarez maar; 13: Magdalena de Araceo tuff ring. spa: spatter.

Figure 4. $^{40}Ar/^{39}Ar$ age spectra and inverse isochron plots for some representative Miocene-Pliocene (**A**), Early Pleistocene (**B**), and Middle Pleistocene (**C**) volcanic rock samples from the Valle de Santiago area. Age spectra plots show the incremental heating steps and the weighted plateau ages (WPA). MSWD: mean square of weighted deviates; P: probability; IIA: inverse isochron age; $(^{40}Ar/^{36}Ar)_i$: initial $^{40}Ar/^{36}Ar$. Ages greater than 1 Ma, quoted as ka, denote high-precision ages.

Figure 5. Topographic profiles illustrating the methodology for measuring morphometric parameters at shield volcanoes (**A**), lava domes (**B**), scoria cones (**C**), and phreatomagmatic volcanoes (**D**) in the Valle de Santiago area. *Hco max*: maximum structure height; *Hco min*: minimum structure height; *Wco*: structure basal diameter; *Dcr*: crater depth; *Wcr:* crater diameter; S_{ave}: average slope; *Max CrD*: major axis of the crater; *Min CrD*: minor axis of the crater.

Figure 6. Diversity of volcanic landforms in the Valle de Santiago area. **A**) Aerial view towards the E showing the fluvio-lacustrine plain of the Lerma River. In the foreground are La Mina dome (LMd), La Mina Sur (LMS), Joya Rincón de Parangueo (JRP), and Santa Rosa (SR) phreatomagmatic volcanoes. Cerro Culiacán (CC) and Cerro Grande (CG) shield volcanoes can be distinguished at the horizon. **B**) View of Cerro Culiacán (CC) shield volcano from the south. **C**) View of La Batea (LB) scoria cone from the SE. In the middle ground are Joya Cíntora (JC) maar, Joya La Alberca (JLA) maar, Joya Blanca (JB) tuff cone, Viejo (V), El Copalar (Co), and Blanca (B) scoria cones, and in the background is Joya Rincón de Parangueo (JRP) maar. **D**) Aerial view towards the W showing Los Cuates (CLC) lava dome in the foreground. Joya de Álvarez (JA) and Joya Cíntora (JC) maars, as well as Ranchos Unidos (RU) and La Batea (LB) scoria cones are in the middle ground. At the horizon are El Tule (ET-II) and Buenavista (Bv) scoria cones, and El Tule (ET), El Picacho (EP), and Cerro Chapín (CCh) shield volcanoes. **E**) View of Joya Solís (JS) maar from the NE. In the middle ground are Cerro Chapín (CCh) shield volcano, Buenavista (Bv), and Viejo (V) scoria cones. In the background are El Tule (ET-II) scoria cone, El Tule (ET), Cerro Prieto (CP), and El Picacho (EP) shield volcanoes. **F**) View from the NW towards the Yuriria lake intermontane basin. In the front is the Magdalena de Araceo (MA) compound tuff ring. In the middle ground is the El Varal (EV) shield volcano; Cerro Santiago (CS) and El Capulín (EC) shield volcanoes are in the background. **G**) Panoramic view toward the E showing Joya de Álvarez (JA) and Magdalena de Araceo (MA) phreatomagmatic volcanoes in the foreground. In the middle ground are the La Batea (LB) scoria cone, Los Cuates (CLC) lava dome, Cerro Tendido (CT), Cerro Blanco (CB), and La Angostura (LA) shield volcanoes. At the horizon are Cerro La Tetilla (CLT), Cerro Culiacán (CC), and Cerro Santiago (CS) shield volcanoes. Photos were taken by Claus

Siebe on Nov. 30, 2011, Sergio Salinas on Jan. 26, 2022, and Elizabeth Rangel on Nov. 16, 2022.

Figure 7. Hco/Wco versus average slope angle plots for scoria/spatter cones (**A**) and shield volcanoes (**B**). All morphometric parameters are listed in Table S1.

Figure 8. **A**) Total alkalis (Na_2O + K_2O) vs. silica diagram after Le Bas et al. (1986) showing the whole-rock composition variability of the volcanic products of the Valle de Santiago and Sierra de Piñícuaro areas. Samples are colored according to the age units shown in Figure 2. Data are normalized to 100% on an anhydrous basis. The division between the alkaline and sub-alkaline rocks is from Irvine and Baragar (1971). Some of the data are from Murphy (1986), Ortega-Gutiérrez et al. (2014), Losantos (2017), and Losantos et al. (2017). **B, C**) Primitive mantle-normalized multielement diagrams for some lava samples from certain shield volcanoes of the Valle de Santiago area. The primitive mantle normalization values are from Sun and McDonough (1989).

Figure 9. Shaded relief map showing the distribution of volcanic rock-types in the Valle de Santiago area. The coordinates of the sampling sites for geochemical analysis are presented in Table S2. The phreatomagmatic volcanoes names are shown in Figure 2.

Figure 10. **A-F)** Photomicrographs showing the main petrographic features of the different volcanic rock-types that occur in the Valle de Santiago area. All photomicrographs were taken under crossed nicols, except for photomicrographs (**D**) and (**F**) which were taken with parallel nicols. **A)** Basalt from Magdalena de Araceo tuff ring (sample VS-1219A) showing

subhedral clinopyroxene crystals and glass occupying the spaces between plagioclase laths (interstitial texture). **B)** Basalt from Cerro Sanabria lava flow (sample VS-1774) showing clinopyroxene (Cpx) and plagioclase (Plg) megacrysts coexisting with smaller plagioclase, clinopyroxene, and olivine (Ol) phenocrysts and micro-phenocrysts. **C)** Basaltic trachyandesite from La Alberca spatter-1 showing feldspar (Fld) megacrysts with exsolution textures (white arrows). **D**) Basaltic andesite from La Chonchita scoria cone (sample VS-1525B) showing an anhedral amphibole (Amph) phenocryst surrounded by a thin opacite rim. This crystal is set in a vesicular and glassy groundmass. The vesicles (V) are partially filled by a precipitation secondary mineral (red arrow). **E**) Andesite from Cerro Santiago shield volcano (sample VS-1743) displaying porphyritic textures with orthopyroxene (Opx) and plagioclase micro-phenocrysts. **F**) Rhyolite from Joya Estrada tuff ring (sample VS-1503D) showing vitrophyric and vesicular textures. Clots composed of sanidine (Sn), quartz, and plagioclase micro-phenocrysts are commonly present. **G)** Hand sample of a subrounded and mesocratic xenolith found within the pyroclastic surge deposits from Joya de Álvarez maar. The yellow arrow points to the thin crust of juvenile magma enveloping the xenolith, while the red arrow points to a remnant of a wet pyroclastic surge deposit. **H-L**) Photomicrographs under crossed nicols of the different types of xenoliths of crystalline rocks that can be found in the pyroclastic deposits of certain phreatomagmatic volcanoes. **H**) Type-1 xenoliths are characterized by medium-to-coarse grained xenomorphic crystals of clinopyroxene, olivine, plagioclase, and opaque minerals (op min). **I**) Type-2 xenoliths commonly consist of coarse-grained plagioclase and olivine crystals. **J**) Type-3 xenoliths are typically composed of medium-to-coarse grained plagioclase, orthopyroxene, clinopyroxene, and feldspar crystals. K) Type-4 xenoliths are characterized by medium-to-coarse grained plagioclase, clinopyroxene, and apatite (Ap;

yellow arrows) crystals. **L**) Type-5 xenoliths are of felsic composition and typically show intergrowth textures (red arrows) between two feldspars.

Figure 11. Schematic diagram illustrating the evolution of volcanic activity in the Valle de Santiago area during the Late Miocene to the Late Pleistocene. The names of some volcanoes are shown for reference: CSan: Cerro Sanabria; ST: Santa Teresa; CGo: Cerro Gordo; CG: Cerro Grande; CC: Cerro Culiacán; CT: Cerro Tendido; B: Blanco; SG: San Guillermo; BJ: Benito Juárez; CLT: Cerro La Tetilla; EV: El Varal; LA: La Angostura; CS: Cerro Santiago; EC: El Capulín; CTs: Cerro Tetillas; ECo: El Comal; LCi: La Ciénega; Gu: Guantecillos; LC: La Cruz; SR: Santa Rosa; EP-CP: El Picacho-Cerro Prieto; CB: Cerro Blanco; CCup: Cerro Cupareo; CP-II: Cerro Prieto-II; M: Mandinga; SRE: San Roque East; JRP: Joya Rincón de Parangueo; LB: La Batea; JA: Joya de Álvarez; CLS: Cerro Las Silletas; ET: El Tule-II; JSV: Joyuela de San Vicente; CP-III: Cerro Prieto-III; JY: Joya de Yuriria; CPo: Cerro Poruyo.

Figure 12. Probability distribution plots of $^{40}Ar/^{39}Ar$ ages from the areas of Valle de Santiago (this study; Table 1); NW Morelia (Avellán et al., 2020), Western Zacapu (Reyes-Guzmán et al., 2018), Pátzcuaro (Osorio-Ocampo et al., 2018); Tacámbaro-Puruarán (Guilbaud et al., 2012), and Jorullo (Guilbaud et al., 2011).

Figure 13. Bar-graph showing the variation of the proportions of volcanic rock-types found in the Valle de Santiago area over time, during the Late Miocene (~8 Ma ago) and the Late Pleistocene. T: eruption rate. The colors used for the rock-types are the same as those in the map of Figure 9. The coalescence of compositions (e.g., basaltic + basaltic trachyandesite)

denotes that a single volcano varies in composition or that the volume of two or three structures that are overlapping but have different compositions, was calculated as if they were a single structure.

FIGURE CAPTIONS OF SUPPLEMENTAL MATERIAL

Figure S1. $^{40}Ar/^{39}Ar$ age spectra and inverse isochron plots for the remaining dated samples from the Valle de Santiago area. Age spectra plots show the incremental heating steps and the weighted plateau age (WPA). MSWD: mean square of weighted deviates; P: probability; IIA: inverse isochron age; $(^{40}Ar/^{39}Ar)_i$: initial $^{40}Ar/^{36}Ar$. Ages greater than 1 Ma, quoted as ka, denote high-precision ages.

Figure S2. Stratigraphic columns and photographs showing the stratigraphic context of the paleosol samples that were obtained for radiocarbon dating. The location of the stratigraphic columns is shown in Figure 3, while the $^{40}Ar/^{39}Ar$ and the radiocarbon ages are listed in Tables 1 and 2, respectively. FA: Fine ash; CA: Coarse ash; FL: Fine lapilli; CL: Coarse lapilli; B: Blocks.

Figure S3. Shaded relief map of the Valle de Santiago area showing the distribution and names of the different types of volcanic landforms found in the region.

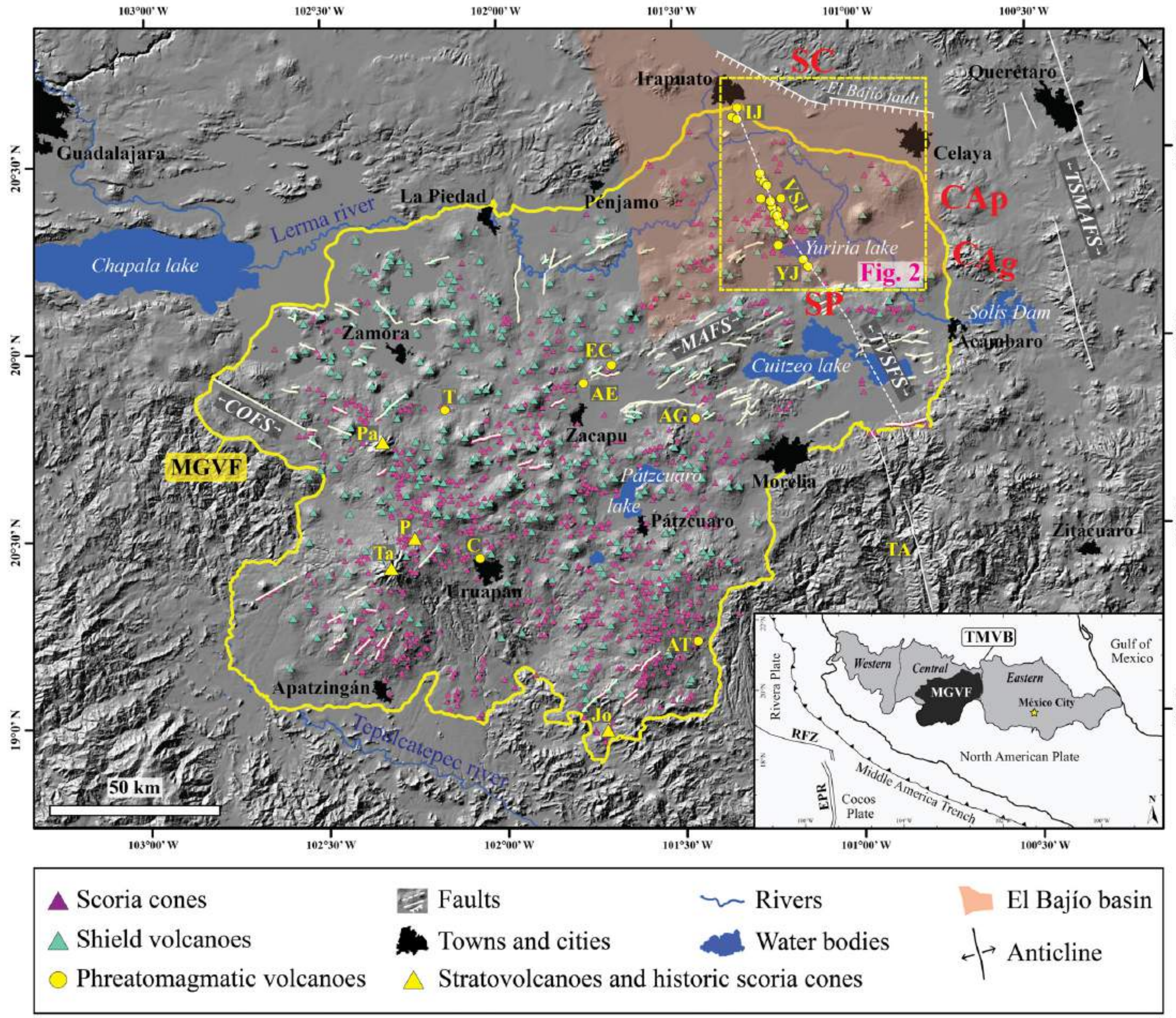

Figure 1. Rangel-Granados et al.

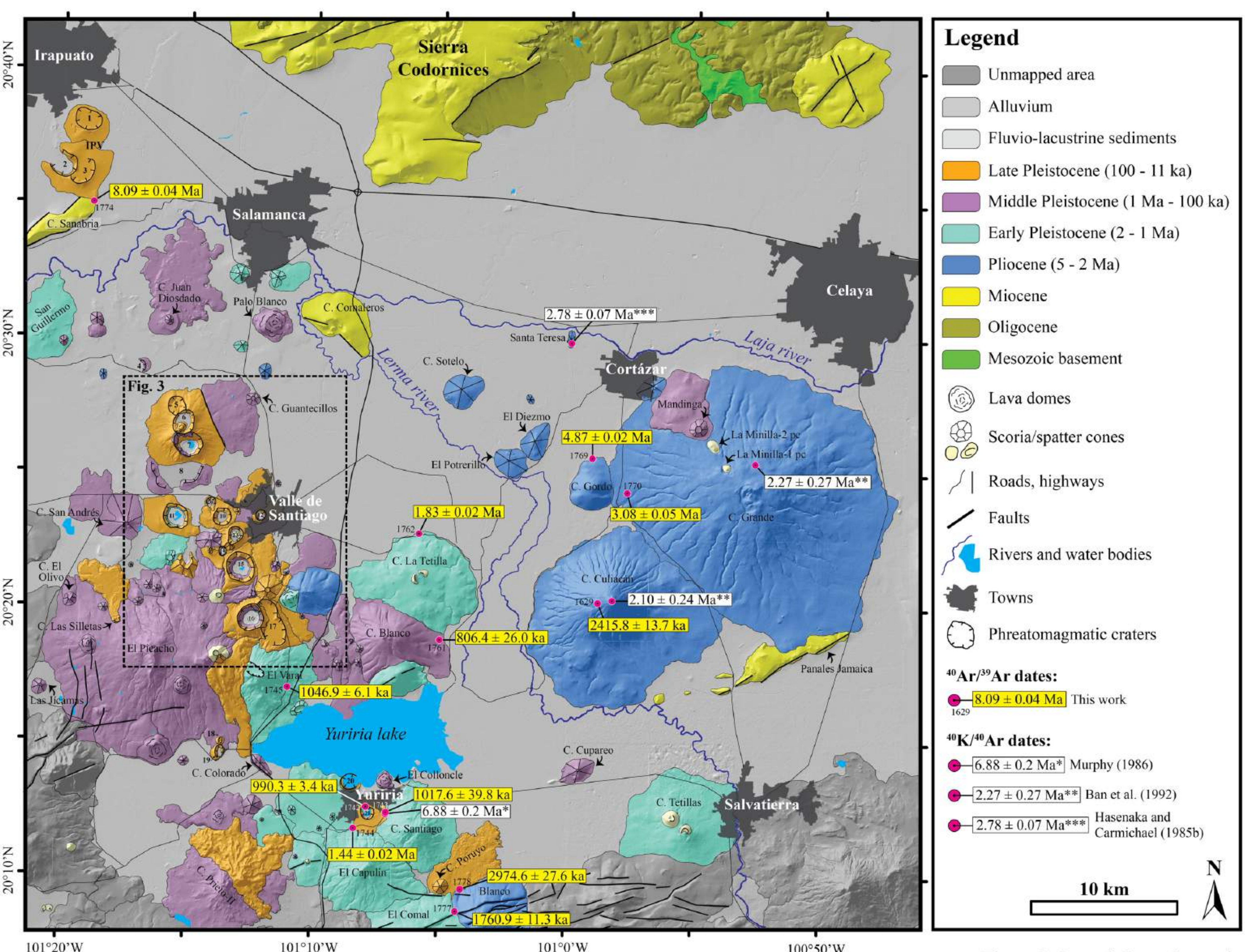

Figure 2. Rangel-Granados et al.

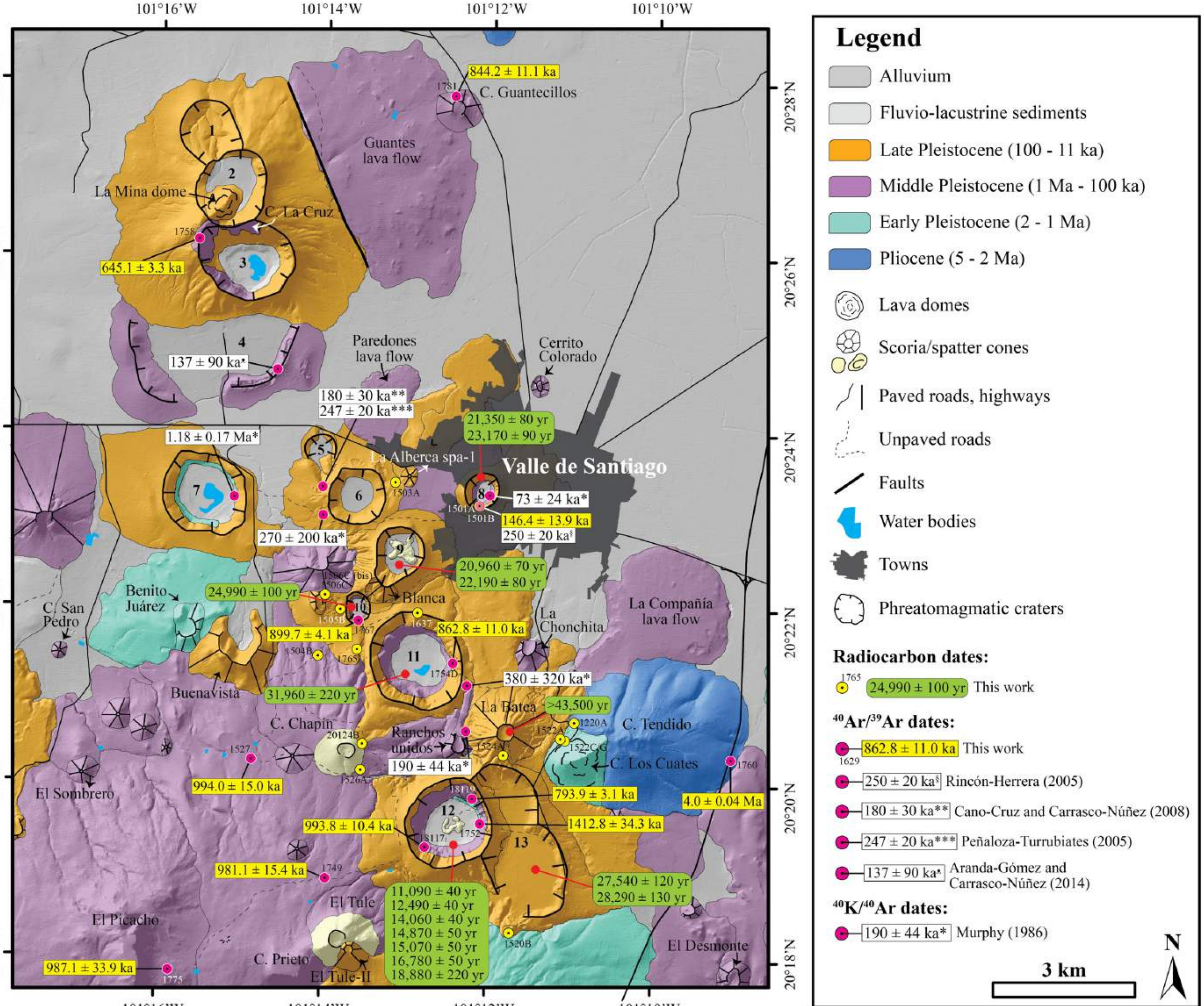

Figure 3. Rangel-Granados et al.

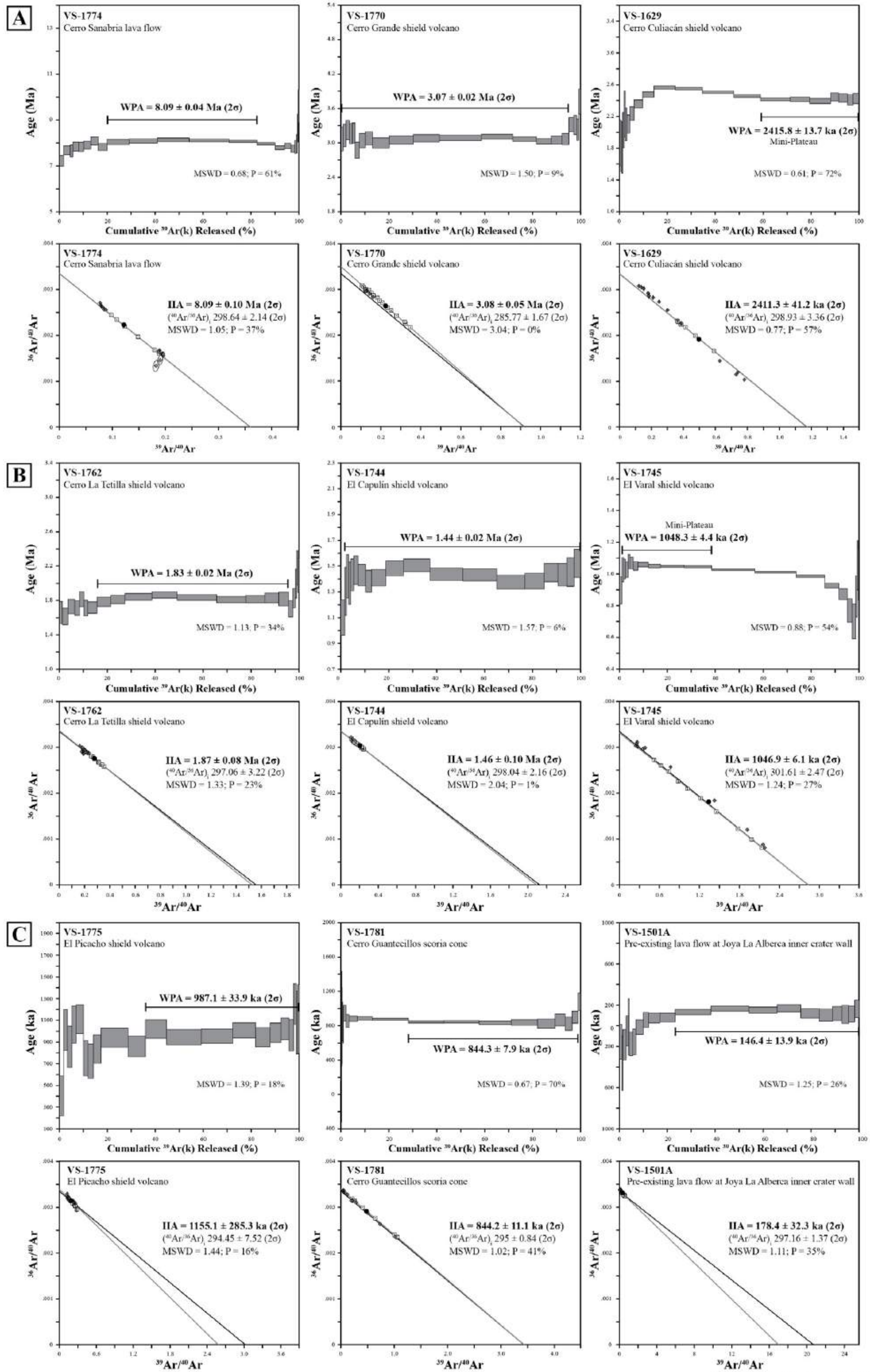

Figure 4. Rangel-Granados et al.

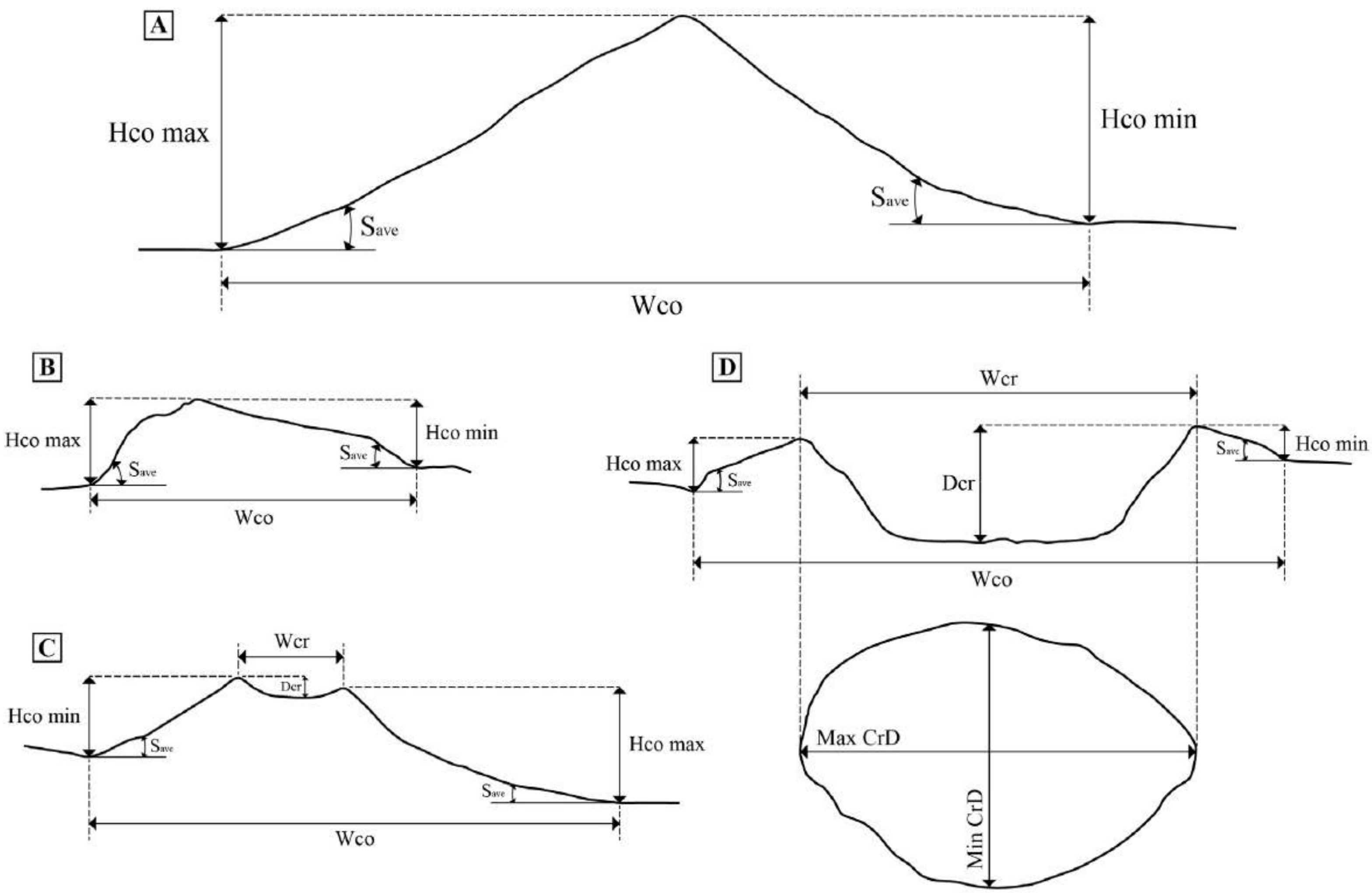

Figure 5. Rangel-Granados et al.

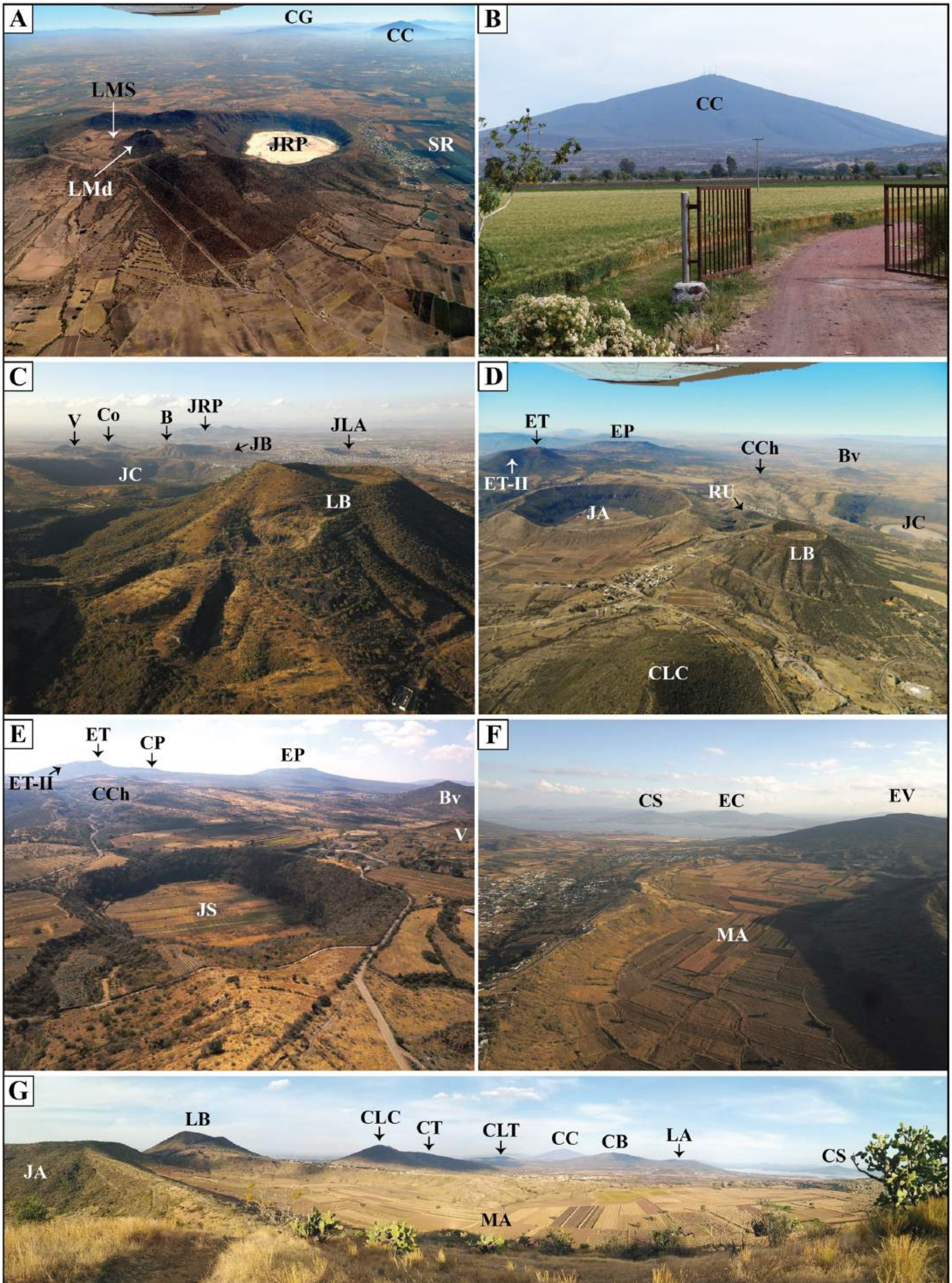

Figure 6. Rangel-Granados et al.

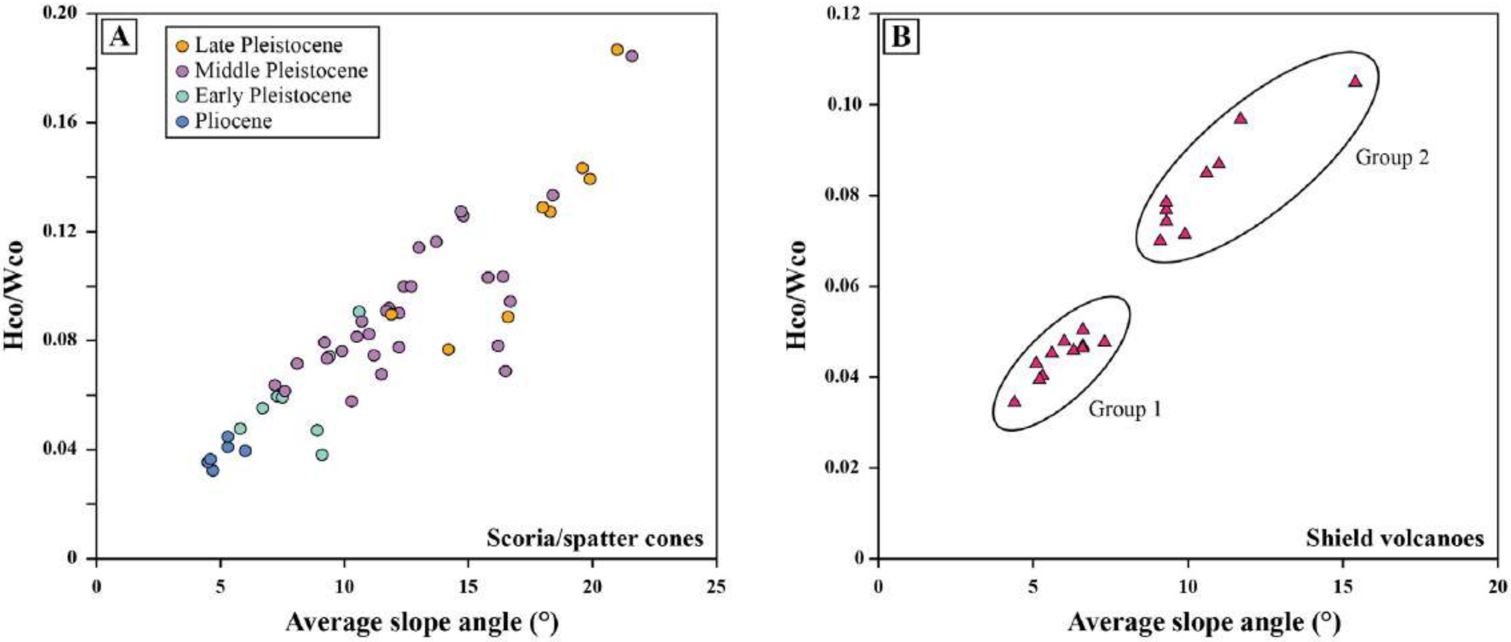

Figure 7. Rangel-Granados et al.

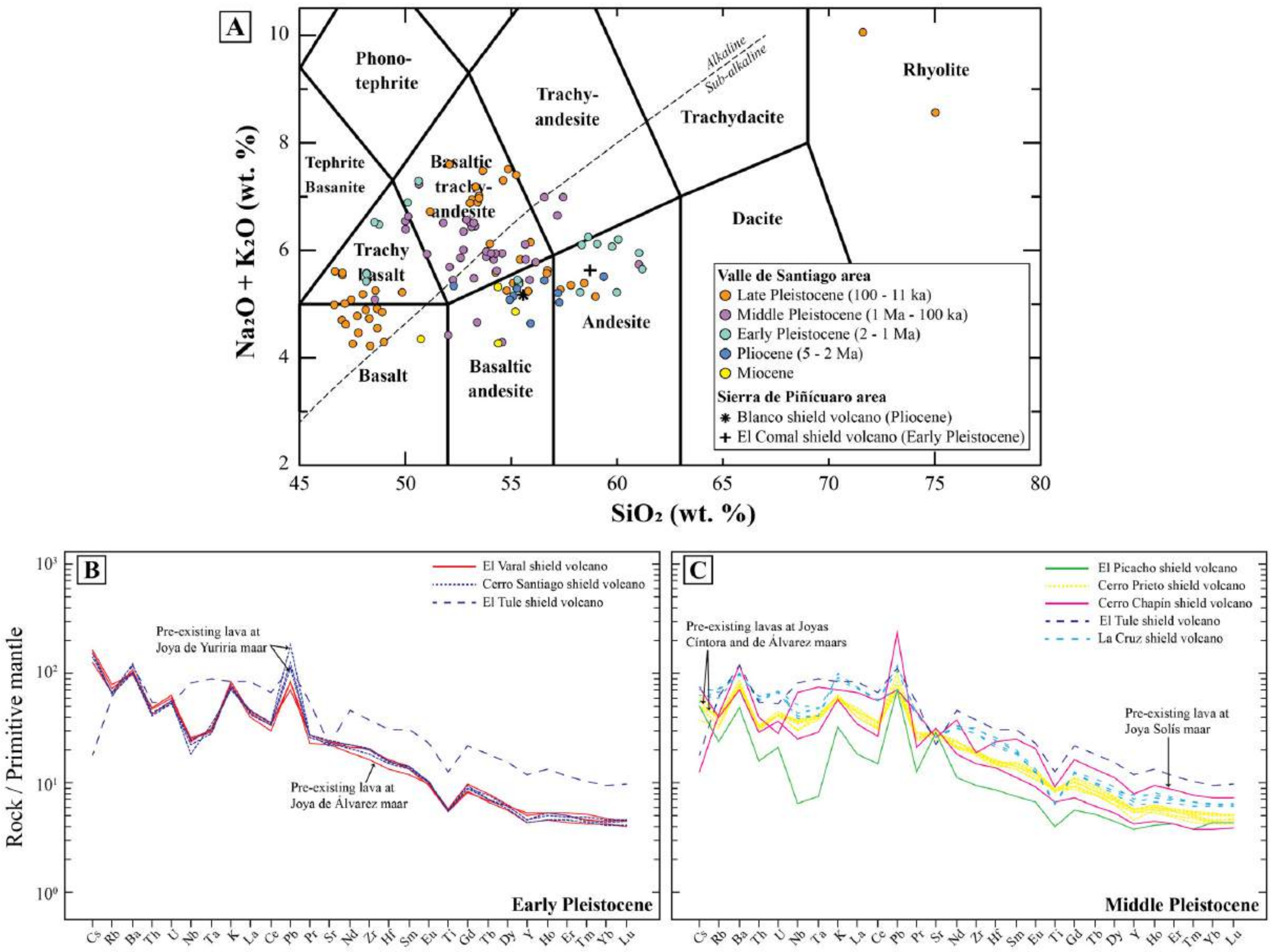

Figure 8. Rangel-Granados et al.

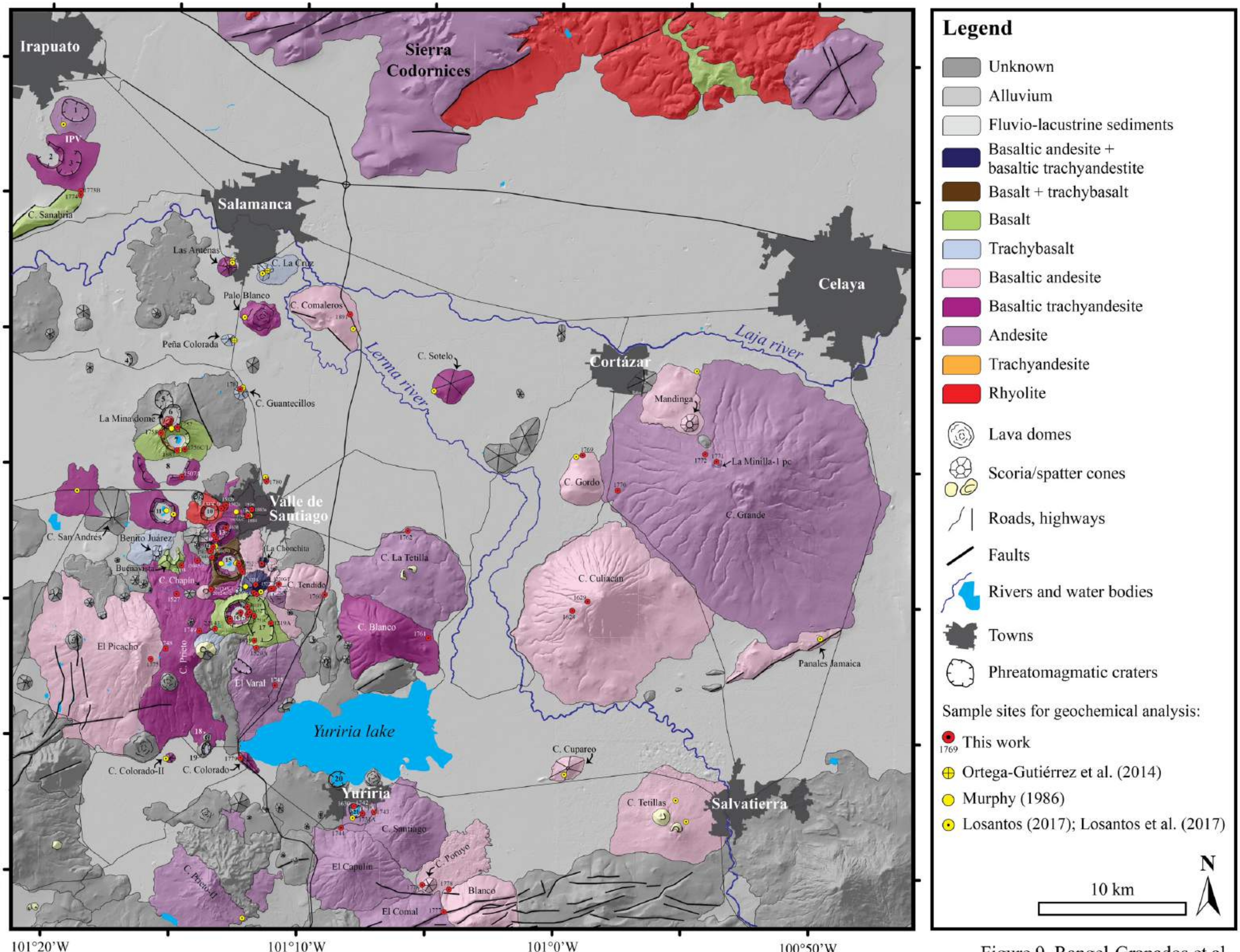

Figure 9. Rangel-Granados et al.

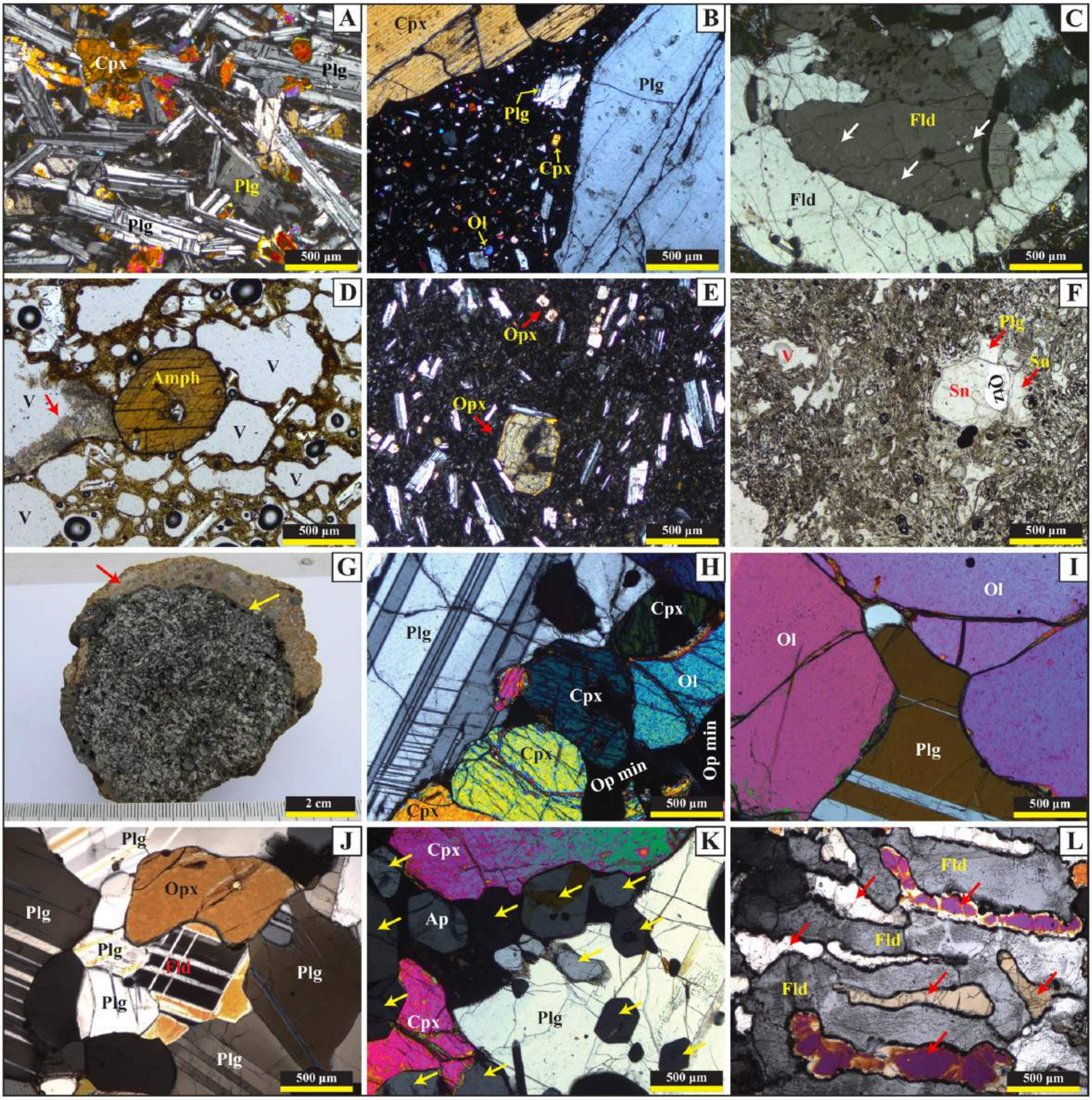

Figure 10. Rangel-Granados et al.

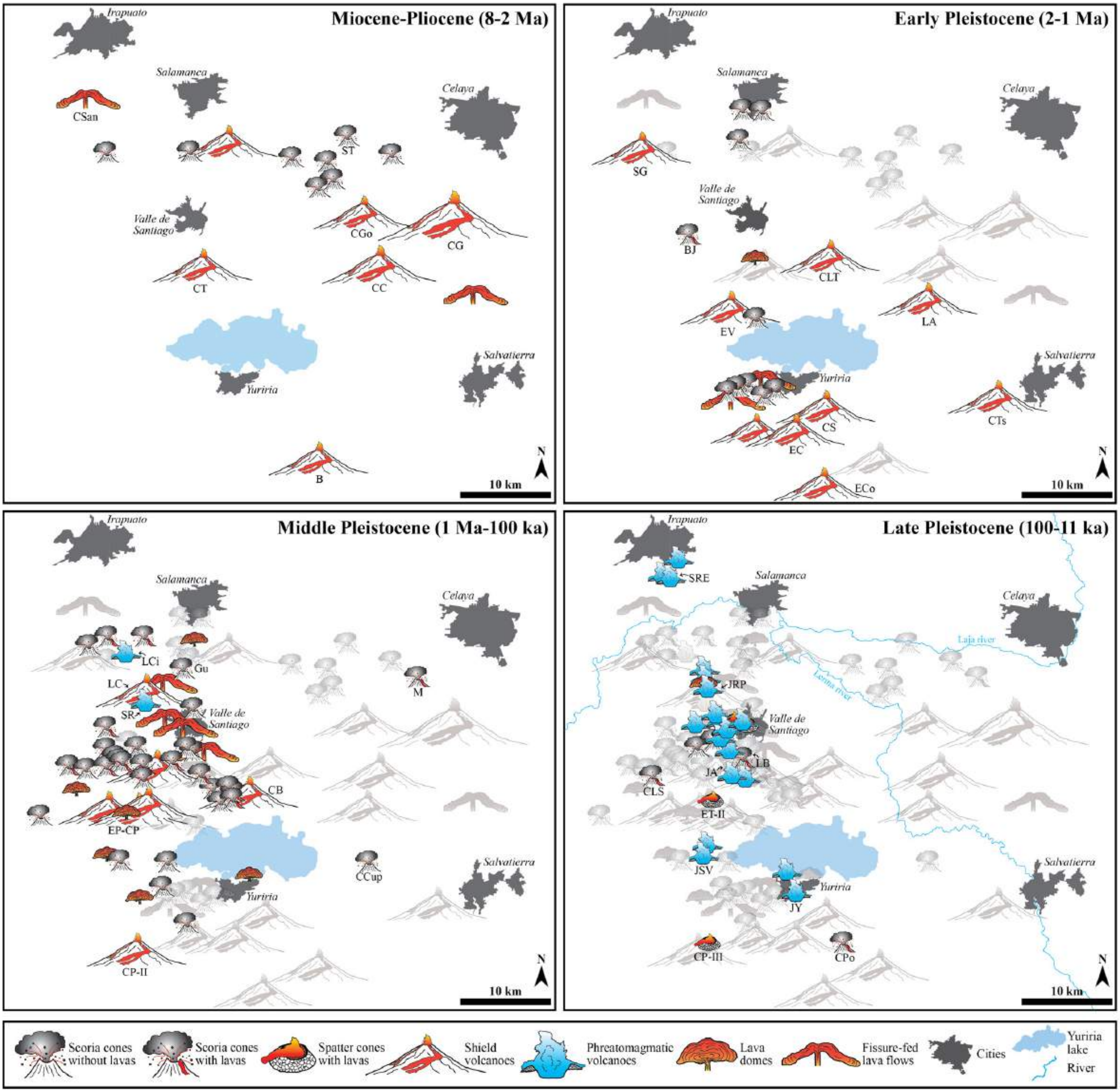

Figure 11. Rangel-Granados et al.

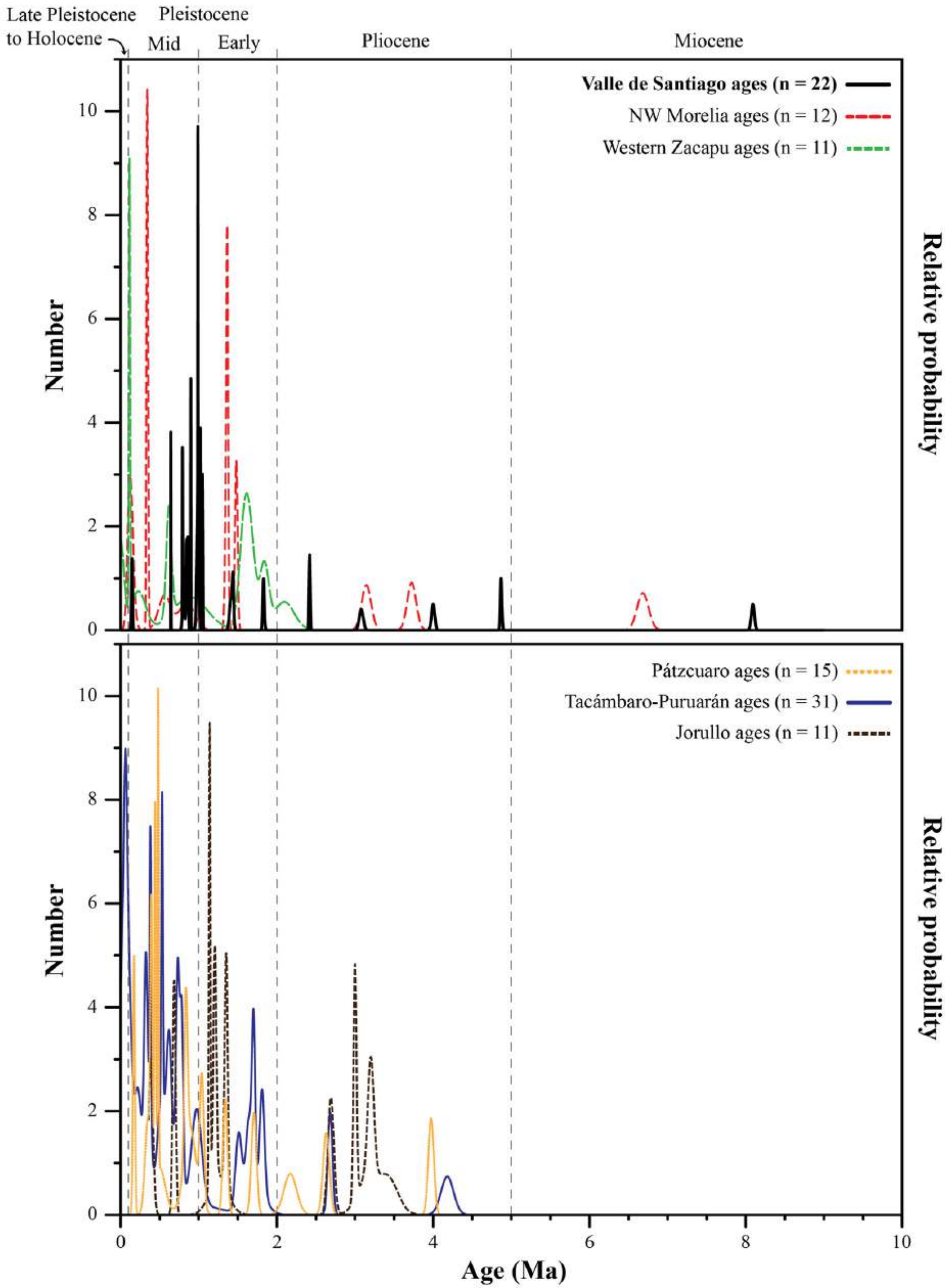

Figure 12. Rangel-Granados et al.

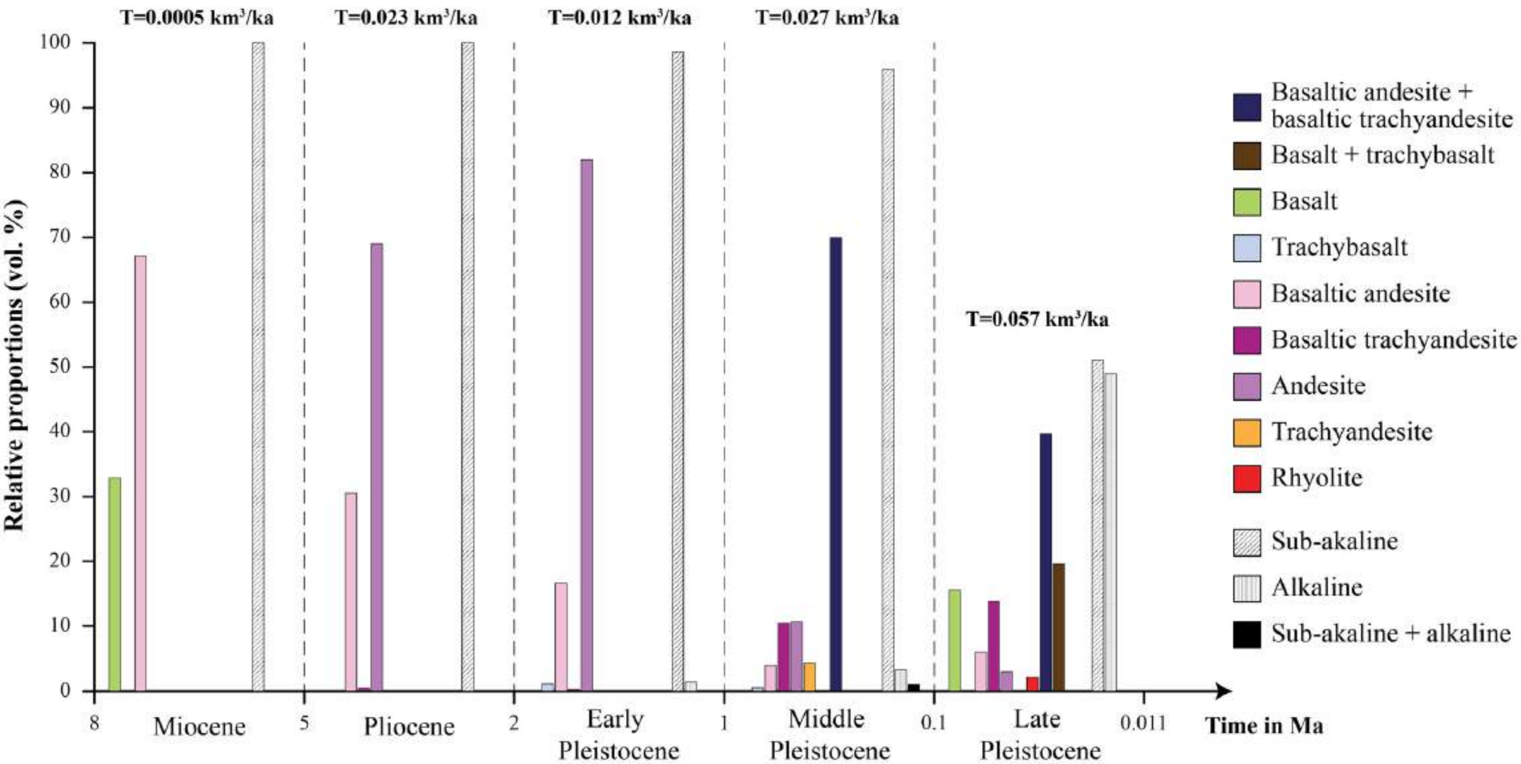

Figure 13. Rangel-Granados et al.

TABLE 1.- $^{40}Ar/^{39}Ar$ RADIOMETRIC DATES FOR VOLCANIC ROCKS IN THE VALLE DE SANTIAGO AREA.

Sample number	Volcano	Location			Sample type	Preferred age type	Plateau							Inverse Isochron				
		Lat	Long	Alt (m asl)			Age ± 2σ	^{39}Ar (%)	K/Ca ± 2σ	MSWD	P (%)	n	N	Age ± 2σ	$^{40}Ar/^{36}Ar$ intercept ± 2σ	SF (%)	MSWD	P (%)
Valle de Santiago area																		
Mid Pleistocene (1 Ma - 100 ka)																		
VS-1501A	Pre-existing lava at Joya La Alberca inner crater wall	20.3862°	-101.2022°	1734	Lava	Plateau	**146.4 ± 13.9 ka**	77	0.323 ± 0.057	1.25	26	10	21	178.4 ± 32.3 ka	297.16 ± 1.37	2	1.11	35
VS-1758	Pre-existing lava from Cerro La Cruz shield volcano at Joya Rincón de Parangueo inner crater wall	20.4365°	-101.2592°	1978	Lava	Mini-Plateau	**645.1 ± 3.3 ka**	44	0.767 ± 0.253	0.98	42	5	19	624.7 ± 26.6 ka	307.84 ± 12.08	8	0.51	67
VS-18119	Pre-existing lava from El Tule shield volcano? at Joya de Álvarez inner crater wall	20.3305°	-101.2028°	1882	Lava	Inverse Isochron	793.7 ± 2.6 ka	78	0.715 ± 0.127	0.79	67	14	21	**793.9 ± 3.1 ka**	307.24 ± 2.49	80	1.16	31
VS-1761	Cerro Blanco shield volcano	20.3125°	-101.0829°	1751	Lava	Plateau	**806.4 ± 26.0 ka**	61	0.221 ± 0.117	0.94	49	11	21	833.0 ± 120.2 ka	297.91 ± 2.95	4	1.17	31
VS-1781	Cerro Guantecillos scoria cone	20.4641°	-101.2079°	1711	Dike	Inverse Isochron	844.3 ± 7.9 ka	71	0.579 ± 0.212	0.67	70	8	21	**844.2 ± 11.1 ka**	295.00 ± 0.84	25	1.02	41
VS-1754	Pre-existing lava from Cerro Prieto shield volcano at Joya Cíntora inner crater wall	20.3562°	-101.2070°	1788	Lava	Plateau	**862.8 ± 11.0 ka**	70	0.251 ± 0.097	1.78	5	12	21	869.9 ± 32.0 ka	297.86 ± 3.08	16	2.06	2
VS-1767	Pre-existing lava from Cerro Chapín shield volcano at Joya Solís inner crater wall	20.3642°	-101.2262°	1771	Lava	Plateau	**899.7 ± 4.1 ka**	72	0.618 ± 0.079	0.89	56	13	21	890.5 ± 11.0 ka	307.91 ± 10.40	68	0.67	77
VS-1749	Cerro Prieto shield volcano	20.3151°	-101.2323°	2150	Lava	Plateau	**981.1 ± 15.4 ka**	65	0.372 ± 0.022	1.85	10	6	22	1034.9 ± 66.3 ka	294.65 ± 4.74	9	1.55	19
VS-1775	El Picacho shield volcano	20.2974°	-101.2637°	2255	Lava	Plateau	**987.1 ± 33.9 ka**	64	0.101 ± 0.039	1.39	18	11	21	1155.1 ± 285.3 ka	294.45 ± 7.52	4	1.44	16
VS-1742	Pre-existing lava from Cerro Santiago shield volcano at Joya de Yuriria inner crater wall	20.2084°	-101.1300°	1740	Lava	Plateau	**990.3 ± 3.4 ka**	80	2.102 ± 0.489	0.80	65	13	19	990.9 ± 5.1 ka	298.13 ± 2.85	59	0.88	56
VS-18117	Pre-existing lava from Cerro Prieto shield volcano at Joya de Álvarez inner crater wall	20.3212°	-101.2123°	1934	Lava	Mini-Plateau	**993.8 ± 10.4 ka**	37	0.411 ± 0.017	0.53	59	3	21	1044.0 ± 99.4 ka	293.59 ± 9.78	4	0.22	64
VS-1527	Cerro Prieto shield volcano	20.3376°	-101.2475°	1983	Lava	Inverse Isochron	994.6 ± 7.7 ka	81	1.982 ± 0.612	0.84	60	12	21	**994.0 ± 15.0 ka**	292.73 ± 1.82	31	1.38	18
Early Pleistocene (2 - 1 Ma)																		
VS-1743	Cerro Santiago shield volcano	20.2051°	-101.1169°	1831	Lava	Inverse Isochron	1066.8 ± 8.3 ka	45	1.387 ± 0.424	3.39	2	4	21	**1017.6 ± 39.8 ka**	365.8 ± 54.13	6	0.65	52
VS-1745	El Varal shield volcano	20.2822°	-101.1826°	1903	Lava	Inverse Isochron	1048.3 ± 4.4 ka	37	2.480 ± 0.442	0.88	54	10	21	**1046.9 ± 6.1 ka**	301.61 ± 2.47	57	1.24	27
VS-1752	Pre-existing lava from El Varal shield volcano at Joya de Álvarez inner crater wall	20.3258°	-101.2012°	1844	Lava	Inverse Isochron	1412.8 ± 13.7 ka	97	2.176 ± 0.765	0.86	61	16	21	**1412.8 ± 34.3 ka**	285.22 ± 1.16	15	1.52	10
VS-1744	El Capulín shield volcano	20.1951°	-101.1383°	1780	Lava	Plateau	**1.44 ± 0.02 Ma**	98	0.983 ± 0.370	1.57	6	18	19	1.46 ± 0.10 Ma	298.04 ± 2.16	6	2.04	1
VS-1762	Cerro La Tetilla shield volcano	20.3782°	-101.0971°	1748	Lava	Plateau	**1.83 ± 0.02 Ma**	80	0.704 ± 0.355	1.13	34	9	21	1.87 ± 0.08 Ma	297.06 ± 3.22	11	1.33	23
Pliocene (5 - 2 Ma)																		
VS-1629	Cerro Culiacán shield volcano	20.3362°	-100.9792°	2585	Lava	Mini-Plateau	**2415.8 ± 13.7 ka**	41	0.294 ± 0.022	0.61	72	7	21	2411.3 ± 41.2 ka	298.93 ± 3.36	19	0.77	57
VS-1770	Cerro Grande shield volcano	20.4046°	-100.9605°	1825	Lava	Inverse Isochron	3.07 ± 0.02 Ma	95	1.200 ± 0.470	1.50	9	17	21	**3.08 ± 0.05 Ma**	285.77 ± 1.67	26	3.04	0
VS-1760	Cerro Tendido shield volcano	20.3383°	-101.1508°	1787	Lava	Plateau	**4.00 ± 0.04 Ma**	100	0.888 ± 0.364	1.04	41	21	21	4.00 ± 0.12 Ma	293.08 ± 1.83	11	2.26	0
VS-1769	Cerro Gordo shield volcano	20.4259°	-100.9837°	1745	Lava	Plateau	**4.87 ± 0.02 Ma**	51	1.379 ± 0.435	1.56	14	8	21	4.88 ± 0.08 Ma	297.89 ± 4.45	17	1.97	7
Miocene																		
VS-1774	Cerro Sanabria lava flow	20.5821°	-101.3137°	1705	Lava	Plateau	**8.09 ± 0.04 Ma**	63	0.293 ± 0.103	0.68	61	5	21	8.09 ± 0.10 Ma	298.64 ± 2.14	23	1.05	37
Sierra de Piñícuaro area																		
Early Pleistocene (2 - 1 Ma)																		
VS-1777	El Comal shield volcano	20.1440°	-101.0707°	2001	Lava	Plateau	**1760.9 ± 11.3 ka**	64	0.424 ± 0.049	0.59	79	9	21	1758.4 ± 27.7 ka	247.04 ± 13.52	14	4.99	0
Pliocene (5 - 2 Ma)																		
VS-1778	Blanco shield volcano	20.1579°	-101.0675°	1849	Lava	Plateau	**2974.6 ± 27.6 ka**	51	0.303 ± 0.048	1.32	26	5	21	2981.2 ± 83.0 ka	298.33 ± 2.78	20	1.99	11

Note: Ages were obtained by incremental heating experiments using the bulk laser heating method on groundmass. All the samples were monitored against the Fish Canyon Tuff sanidine (FCT-2-NM sanidine) standard with a calibrated age of 28.201 ± 0.023 Ma (Kuiper et al., 2008). The ages highlighted in bold are preferred. Those ages greater than 1 Ma, quoted as ka, denote high-precision ages. Sample location is given in the WGS84 geographic coordinate system.

MSWD: mean square of weighted deviates.

P: probability.

n: number of steps included in the plateau age.

N: total number of incremental heating steps.

SF: spreading factor.

TABLE 2. RADIOCARBON DATES FOR SOME PHREATOMAGMATIC VOLCANOES AND SCORIA CONES FROM THE VALLE DE SANTIAGO AREA

Sample number	Volcano/eruptive event	Location			Lab. Code	Conventional age (yr BP)	Calibrated age (2 sigma)	$\partial^{13}C$ (o/oo)	Deposit dated	Locality
		Lat	Long	Alt (m asl)						
Late Pleistocene (100 - 11 ka)										
VS-1504B	Joya de Álvarez maar	20.3574°	-101.2343°	1873	B-407859	11,090 ± 40	Cal BC 11,115 to 10,875 (Cal BP 13,065 to 12,825)	-18.8	Paleosol under 85 cm of distal pyroclastic surge deposits from Joya de Álvarez maar.	Road cut outcrop on an unpaved road that connects Buenavista de Parangueo and La Hoya de Arriba towns, at 2.20 km W from Joya Cíntora maar crater.
VS-1524A	Joya de Álvarez maar	20.3388°	-101.1966°	2016	B-438561	12,490 ± 40	Cal BC 13,015 to 12,495 (Cal BP 14,965 to 14,445)	-20.9	Paleosol under 550 cm of proximal-medial pyroclastic surge deposits from Joya de Álvarez maar.	Quarry at the southern flank of La Batea scoria cone, at 0.5 km from the crater.
VS-1526A	Joya de Álvarez maar	20.3358°	-101.2254°	2011	B-464876	14,060 ± 40	Cal BC 15,381 to 14,933 (Cal BP 17,330 to 16,882)	-16.8	Paleosol under 100 cm of medial-distal pyroclastic surge deposits from Joya de Álvarez maar.	Road cut outcrop on the southeastern slope of Cerro Chapín shield volcano, at 2.3 km NW from Joya de Álvarez maar crater.
VS-1522G	Joya de Álvarez maar	20.3417°	-101.1843°	1911	B-426282	14,870 ± 50	Cal BC 16,250 to 16,010 (Cal BP 18,200 to 17,960)	-17.0	Paleosol under 200 cm of distal pyroclastic surge deposits from Joya de Álvarez maar.	Quarry near Valle de Santiago-Uriangato highway, at 1.14 km E from La Batea scoria cone.
VS-1637	Joya de Álvarez maar	20.3658°	-101.2143°	1845	B-438561	15,070 ± 50	Cal BC 16,490 to 16,250 (Cal BP 18,440 to 18,200)	-17.2	Paleosol under 30 cm of distal pyroclastic surge deposits from Joya de Álvarez maar.	Outcrop on an unpaved road that connects to the town of Hoya de Arriba, at the northern crater rim of Joya Cíntora maar (1.10 km from the center of the crater)
VS-1765	Joya de Álvarez maar	20.3587°	-101.2264°	1896	B-471554	16,780 ± 50	Cal BC 18,491 to 18,095 (Cal BP 20,440 to 20,044)	-20.2	Paleosol under distal surge deposits from Joya de Álvarez maar.	Quarry at the northwestern outer slope of Joya Cíntora maar tephra ring, at 1.4 km from Joya de Álvarez maar crater.
PAZ-1220A	Joya de Álvarez maar	20.3451°	-101.1824°	1903	A-15896	18,880 +225/-220	Cal BC 21,419 to 20,389 (Cal BP 22,338 to 23,368)	-15.4	Paleosol under 210 cm of distal pyroclastic surge deposits from Joya de Álvarez maar.	Outcrop near Valle de Santiago-Uriangato highway, at 1.6 km E of La Batea scoria cone.
VS-1505B	Joya Blanca tuff cone	20.3663°	-101.2298°	1848	B-407860	20,960 ± 70	Cal BC 23,525 to 23,215 (Cal BP 25,475 to 25,165)	-13.4	Paleosol under 350 cm of proximal-medial pyroclastic surge deposits from Joya Blanca tuff-cone.	Western quarry at Joya Solís maar, 0.42 km from the crater.
VS-1501B	La Alberca spatter-2	20.3862°	-101.2022°	1734	B-407857	21,350 ± 80	Cal BC 23,875 to 23,610 (Cal BP 25,825 to 25,560)	-14.1	Paleosol under 30 cm of proximal scoria fallout deposit associated with the La Alberca spatter-2.	Outcrop on the southern inner crater wall of Joya La Alberca maar.
VS-1506C	Joya Blanca tuff cone	20.3691°	-101.2329°	1893	B-407862	22,190 ± 80	Cal BC 24,625 to 24,230 (Cal BP 26,575 to 26,180)	-13.6	Paleosol under 180 cm of proximal-medial pyroclastic surge deposits from Joya Blanca tuff cone.	Northwestern quarry at Joya Solís maar, 0.80 km from the crater.
VS-1503A	La Alberca spatter-1	20.3905°	-101.2191°	1757	B-407858	23,170 ± 90	Cal BC 25,625 to 25,395 (Cal BP 27,575 to 27,345)	-12.9	Paleosol under 50 cm of proximal scoria fallout deposit associated with the La Alberca spatter-1.	Northeastern quarry at Joya Estrada tuff ring, 0.85 km from the crater.
VS-1506C (bis)	Joya Solís maar	20.3691°	-101.2330°	1893	Beta-627758	24,990 ± 100	Cal BC 27,660 to 26,995 (Cal BP 29,609 to 28,944)	-18.7	Paleosol under 500 cm of proximal pyroclastic surge deposits from Joya Solís maar.	Northwestern quarry at Joya Solís maar, 0.80 km from the crater.
VS-1520B	Magdalena de Araceo compound tuff ring	20.3051°	-101.1951°	1975	B-426280	27,540 ± 120	Cal BC 29,510 to 29,245 (Cal BP 31,460 to 31,195)	-16.1	Paleosol under proximal pyroclastic deposits (scoria fallout and surge deposits) from Magdalena de Araceo compound tuff ring.	Southern quarry of Magdalena de Araceo compound tuff ring, at 2.1 km from Magdalena de Araceo crater center.
VS-1522C	Magdalena de Araceo compound tuff ring	20.3417°	-101.1843°	1911	B-426281	28,290 ± 130	Cal BC 30,705 to 29,710 (Cal BP 32,655 to 31,660)	-15.9	Paleosol under medial pyroclastic deposits (scoria fallout and surge deposits) from Magdalena de Araceo compund tuff ring.	Quarry near Valle de Santiago-Uriangato highway, at 1.14 km E from La Batea scoria cone.
VS-20124B	Joya Cíntora maar	20.3408°	-101.2251°	2046	Beta-627759	31,960 ± 220	Cal BC 34,911 to 33,873 (Cal BP 36,860 to 35,822)	-21.0	Paleosol under 790 cm of medial-distal pyroclastic deposits (scoria fallout and surge deposits) from Joya Cíntora maar.	Quarry on a topographic high at the NE upper slope of Cerro Chapín shield volcano, 2.2 km SW from Joya Cíntora maar crater.
VS-1522A	La Batea scoria cone	20.3421°	-101.1852°	1896	Beta-627760	>43,500		-18.7	Paleosol under 320 cm of proximal scoria fallout deposit from La Batea scoria cone.	Quarry near Valle de Santiago-Uriangato highway, at 1.14 km E from La Batea scoria cone.

Note: The conventional radiocarbon ages were calculated using the Libby half-life of 5,568 years and are reported as years before present (yr BP), where "present" = AD 1950. The conventional ages were also calibrated with the BetaCal 4.20 and CALIB 7.1 computer programs, using the IntCal13 and IntCal14 databases for the northern hemisphere radiocarbon age curves (Stuiver and Reimer, 1993; Reimer et al., 2020). The reported $\delta^{13}C$ values were measured separately in an isotope ratio mass spectrometer (IRMS) and are on the material itself. Sample location is given in the WGS84 geographic coordinate system.

TABLE 3. SUMMARY OF THE MORPHOMETRIC PARAMETERS MEASURED FOR THE VOLCANIC LANDFORMS OF THE VALLE DE SANTIAGO AREA.

Volcano	Volcano type	Compostion	Magmatic series	Area (km^2)*	Total volume (km^3)†	Eruption rate (km^3/ka)
Miocene						
Cerro Sanabria	Lava flow?	Basalt	Sub-alkaline	9.20	0.52	
Panales Jamaica	Lava flow?	Basaltic andesite	Sub-alkaline	10.46	0.37	
Cerro Comaleros	Shield volcano	Basaltic andesite	Sub-alkaline	13.06	0.70	
				Subtotal	**1.58**	**0.0005§**
Pliocene (2 - 5 Ma)						
Cerro Gordo	Shield volcano	Basaltic andesite	Sub-alkaline	8.78	0.731	
Cerro Tendido	Shield volcano	Basaltic andesite	Sub-alkaline	9.23	0.208	
Cerro Grande	Shield volcano	Andesite	Sub-alkaline	270.15	46.98	
Santa Teresa	Scoria cone			0.50	0.030	
Cerro Culiacán	Shield volcano	Basaltic andesite	Sub-alkaline	101.57	19.84	
Cerro Colorado-III	Scoria cone			0.11	0.001	
El Diezmo	Scoria cone			3.21	0.070	
El Potrerillo	Scoria cone			3.46	0.090	
Cerro Sotelo	Scoria cone	Basaltic trachyandesite	Sub-alkaline	4.92	0.302	
El Vellanco	Scoria cone			0.32	0.005	
Los Lobos	Scoria cone			0.76	0.011	
Cerrito Colorado-II	Scoria cone			2.60	0.034	
				Subtotal	**68.30**	**0.023**
Early Pleistocene (2 - 1 Ma)						
Cerro La Tetilla	Shield volcano	Andesite	Sub-alkaline	39.71	2.456	
La Cumbita	Lava plateau			17.00	0.260	
Scoria cone-2	Scoria cone			0.12	0.001	
San Miguelito	Scoria cone			0.28	0.003	
Scoria cone-3	Scoria cone			0.12	0.001	
Parangarico	Scoria cone			0.11	0.002	
Lava Plateau-2	Lava plateau			4.29	0.061	
Scoria cone-4	Scoria cone			0.51	0.004	
Buena Vista	Shield volcano			8.04	0.174	
El Capulín	Shield volcano	Andesite	Sub-alkaline	30.98	2.849	
El Varal	Shield volcano	Andesite	Sub-alkaline	25.15	1.402	
Viejo de Torres	Scoria cone			0.66	0.011	
Benito Juárez	Scoria cone Associated lava flow	 Trachybasalt	 Alkaline	0.86 4.19	0.073	
Cerro Santiago	Shield volcano	Andesite	Sub-alkaline	26.71	1.944	
Cerro Tetillas	Shield volcano	Basaltic andesite	Sub-alkaline	43.70	1.767	
San Guillermo	Shield volcano			15.04	0.261	
La Angostura	Shield volcano			8.36	0.475	
Los Cuates	Lava dome	Andesite	Sub-alkaline	1.74	0.056	
Peña Colorada	Scoria cone	Trachybasalt	Alkaline	0.75	0.007	
Cerro La Cruz	Scoria cone	Trachybasalt	Alkaline	2.48	0.037	
Las Antenas	Scoria cone	Basaltic trachyandesite	Alkaline	1.58	0.032	
				Subtotal	**11.88**	**0.012**
Middle Pleistocene (1 Ma - 100 ka)						
El Picacho Cerro Prieto	Shield volcano Shield volcano	Basaltic andesite Basaltic trachyandesite	Sub-alkaline Sub-alkaline	156.87	15.37	
Cerro Chapín	Shield volcano	Basaltic andesite to basaltic trachyandesite	Sub-alkaline to alkaline	8.88	0.201	
Guantes	Lava flow			15.51	0.148	
Cerro Guantecillos	Scoria cone	Trachybasalt	Alkaline	0.53	0.007	
Cerro Blanco	Shield volcano	Basaltic trachyandesite	Sub-alkaline	23.15	1.633	
El Tule	Shield volcano	Trachybasalt	Alkaline	5.51	0.094	
La Cruz	Shield volcano	Trachyandesite	Sub-alkaline	25.15	0.970	
Ranchos Unidos	Scoria cone Associated lava flow	 Trachybasalt	 Alkaline	0.39 0.71	0.007	
El Cerrito	Lava dome			3.89	0.138	
Cerro Blanco-II	Lava dome			1.94	0.075	
Cerro Perimal	Lava dome			1.85	0.045	
Cerro El Olivo	Scoria cone Associated lava flow			0.61 2.81	0.030	
Cerro Quemado	Scoria cone			0.95	0.017	
El Sombrero	Scoria cone Associated lava flow			0.31 1.43	0.021	
Cerritos-1	Scoria cone Associated lava flow			0.14 1.59	0.004	
Cerritos-2	Scoria cone Associated lava flow			0.34 0.96	0.009	
Cerritos-3	Scoria cone			0.37	0.007	
Scoria cone-5	Scoria cone			0.51	0.007	
Scoria cone-6	Scoria cone			0.27	0.003	
El Copalar	Scoria cone			1.84	0.026	
Cerro Colorado-IV	Scoria cone Associated lava flow			0.43 2.27	0.020	
Scoria cone-9	Scoria cone Associated lava flow			0.42 4.57	0.078	
Scoria cone-10	Scoria cone			0.24	0.004	
El Desmonte	Scoria cone			0.65	0.013	
El Bonete	Scoria cone			0.37	0.041	

El Bonete	Associated lava flow			5.70	0.041	
San Jerónimo	Scoria cone Associated lava flow			0.17 5.84	0.014	
Mandinga	Scoria cone Associated lava flow	Basaltic andesite	Sub-alkaline	1.87 14.65	0.748	
San Roque	Scoria cone			0.51	0.010	
Scoria cone-1	Scoria cone			0.12	0.002	
Paredones	Lava flow			2.15	0.013	
La Compañía	Lava flow			6.03	0.078	
La Chonchita	Scoria cone	Basaltic andesite to basaltic trachyandesite	Sub-alkaline	0.43	0.006	
Scoria cone-7	Scoria cone			0.12	0.002	
El Colloncle	Lava dome			1.34	0.040	
Cerro Prieto-II	Shield volcano	Andesite	Sub-alkaline	59.39	2.387	
El Tambor	Scoria cone Associated lava dome			0.53 1.08	0.032	
Cerro Juan Diosdado	Scoria cone Associated lava flows			0.33 28.80	0.651	
Cerrito Colorado	Scoria cone	Basaltic trachyandesite	Alkaline	0.10	0.001	
San Andrés	Scoria cone Associated lava flow	Basaltic trachyandesite	Alkaline	5.42 21.63	0.316	
Cerro San Pedro	Scoria cone			0.08	0.003	
Las Jícamas	Scoria cone			0.77	0.021	
Cerro Colorado	Scoria cone	Basaltic trachyandesite	Alkaline	1.06	0.032	
Cerro Colorado-II	Scoria cone	Basaltic trachyandesite	Alkaline	0.17	0.003	
Cerro La Cruz-II	Scoria cone			1.05	0.044	
Cerro Cupareo	Scoria cone	Basaltic andesite	Sub-alkaline	2.94	0.128	
Palo Blanco	Lava dome	Basaltic trachyandesite	Alkaline	6.11	0.254	
Enguaro	Lava dome Associated lava flow			9.22	0.171	
La Cienega	Tuff ring			0.35	0.002	
Santa Rosa	Tuff ring	Basaltic trachyandesite	Sub-alkaline	7.71	0.093	
				Subtotal	**24.02**	**0.027**
Late Pleistocene (100 - 11 ka)						
El Tule-II	Scoria or spatter cone Associated lava flow			14.15	0.310	
San Roque West San Roque East	Tuff ring Tuff ring	Basaltic trachyandesite	Alkaline	12.31	0.189	
Sanabria	Tuff ring	Andesite	Sub-alkaline	8.36	0.068	
Isla de San Pedro	Tuff ring			3.61	0.031	
La Mina Norte La Mina Sur	Tuff ring Tuff ring			12.22	0.178	
La Mina	Lava dome	Rhyolite	Sub-alkaline	0.56	0.017	
Joya San Nicolás	Maar	Basaltic trachyandesite	Alkaline	7.29	0.147	
La Batea	Scoria cone Associated lava flows	Basaltic andesite, basaltic trachyandesite to andesite	Sub-alkaline	2.27 9.04	1.317	
Buenavista	Scoria cone	Basalt	Alkaline	2.60	0.101	
Viejo	Scoria cone			0.41	0.005	
Joya Cíntora	Maar	Basalt to trachybasalt	Alkaline	5.81	0.303	
Joya de Yuriria	Maar	Basaltic andesite to andesite	Sub-alkaline	5.24	0.032	
Cerro Poruyo	Scoria cone Associated lava flows	Basaltic andesite	Sub-alkaline	1.30 15.66	0.203	
Magdalena de Araceo	Tuff ring	Basalt	Alkaline	5.90	0.084	
Joya Rincón de Parangueo	Maar	Basalt	Alkaline	8.83	0.332	
Blanca	Scoria cone	Basaltic trachyandesite	Sub-alkaline	0.33	0.005	
Joya Estrada	Tuff ring	Rhyolite and Basaltic trachyandesite	Sub-alkaline	4.35	0.055	
Joyuela	Tuff ring			0.52	0.003	
Joya Solís	Maar			0.83	0.014	
La Alberca spatter-1	Spatter cones Associated lava flow	Basaltic trachyandesite	Alkaline	0.56 1.56	0.012	
La Alberca spatter-2	Associated lava flow	Basaltic trachyandesite	Alkaline	1.28	0.007	
Joya Blanca	Tuff cone	Basaltic trachyandesite	Alkaline	2.91	0.074	
Joya La Alberca	Maar	Basaltic trachyandesite	Alkaline	1.46	0.026	
Joya de Álvarez	Maar	Basalt to trachybasalt	Alkaline	5.72	0.351	
Los Molina	Spatter cone Associated lava flow			0.22 3.42	0.033	
Cerro Prieto-III	Scoria or spatter cone Associated lava flow			20.44	0.931	
Cerro Las Silletas	Scoria cone Associated lava flows			0.62 8.26	0.210	
Joyuela de San Vicente	Tuff cone			0.91	0.011	
Providencia de Cuerunero	Tuff cone			0.29	0.005	
				Subtotal	**5.05**	**0.057**
				Total	**110.8**	

*This parameter corresponds to the base area of the volcanic structures. For phreatomagmatic volcanoes, this parameter corresponds to the surface covered by the tephra ring.

†For phreatomagmatic volcanoes, the estimated volume corresponds to the tephra ring. It is important to note that the values listed here are bulk volumes, involving all the material emitted by the eruptions. These values were not recalculated to dense rock equivalent.

§The eruption rate for the Miocene was taken from 8 Ma, which represents the oldest age determination for this epoch.